Doctor of Philosophy in Photonics

Diffuse optical monitoring of cerebral hemodynamics in experimental and clinical neurology

Igor Blanco

Supervisor: Professor Turgut Durduran

ICFO-The Institute of Photonic Sciences

Universitat Politècnica de Catalunya

Barcelona, 2014

Adicado a Pepi e Jorge

Acknowledgements

First of all, I want to acknowledge Prof. Turgut Durduran for guiding and supervising me along these last years and for giving me the opportunity to be part of the Medical Optics team. When looking back it seems very far away the day I joined the Medical Optics group and right now, I can only feel gratitude for all the wonderful people I have the privilege to work with: Alexia, Udo, Peyman, Johannes, Claudia, Juan Aguirre, Hari, Claus, Clara, Tanja, Jordi.. and many others.

At this point I would also like to thank for the help and support I have received from my collaborators in the biomedical projects described in this manuscript. In one side, the people at Idibaps: Anna Planas, Cristina Sola, Clara Castellví, Guadalupe Soria (gracias Lupe!) and Xavi Lopez with a special remark to Professor Carles Justicia with whom I shared many hours of animal experimentation. On the other side, the people from the Sleep and Stroke units at Hospital Sant Pau: Anna Mola, Mercedes Mayos, Ana Fortuna, Luca, Ariadna, Montse, Rosita, Raquel Delgado and Joan Martí.

Also, this work could not be possible without the help of many people at Icfo: Dmitri Petrov (in memoriam), Xavier Menino (ets un crack!), Rafa and Agnes, Mónica Montaña and Mónica Marro, Adri..

I would also like to express my gratitude to both David Artigas and Montserrat Calvo who lighted my path in the darkness moments.

Along these last four years I have made many friends.. the best crew a sailor

can find in Barcelona: Carles, Iñaki, Ricardo, Pelayo, Juan, Sybille, Marta, Pablo, Rodri, Taisuke, Valeria and a very very long etcetera.. thanks folks!.

Finalmente gostaríame enviarlle un agarimo ós amigos de toda a unha vida: Pabliño e Bea, Juancho e Raquel, Iosi e Rubén (Lobo), Stefano Palmisano e Arge, Moni e Ximi, Raul e Sergio, Marcus e Marta, Moises, Rafa... A maravillosa familia moañesa: meus tíos Roberto e Elena, Juan e Mari, Ana e Pepe, Lolo.. (e tódolos demais). Tamén a nova familia que fixen eiquí: Carlos e Elena, Neus e Vicent, María, Katia, Eli, Luiggi, Susi ... Mimadriña, fáiseme a lista interminable...

Pero sobre todo, a miña nai Pepi e o meu pai Jorge, o meu irmáns Saúl e Zule e o seu home Santi. E como non, o futuro deste país, os meus dous afillados Gael e Xabi (vaia dous!). E por último, e como non podía ser doutro xeito, o meu mais profundo agradecemento a persoa que me leva aguantando xa un tempo, o meu amoriño das silveiras, a miña Francina.

Abstract

The study of the brain using diffuse optical methods has progressed rapidly in the recent years. The possibility of studying the cerebral microvasculature in addition to the portability and low cost of these devices, opens a new door in the study of the cerebral pathophysiologies.

In this scenario, the study of the cerebral hemodynamics of ischemic patients might allow neurologists to improve the performance of the early medical treatments and therapies used up to date. In this thesis, I have conducted a pioneering study where cerebral autoregulation was studied in ischemic stroke patients during the early hours after the stroke.

Similarly, some other diseases can provoke impaired cerebral autoregulation in the long term. One of them is the obstructive sleep apnoea (OSA) syndrome which can provoke a risk increase of developing cardiovascular diseases and ischemic stroke. In this regards, I have carried out the largest to date study conducted with Diffuse Correlation Spectroscopy in patients with OSA and I have compared their hemodynamical response to an orthostatic challenge test with a control group of healthy subjects.

Finally, primary animal research is of great importance in the development of new therapies, medical strategies and in the validation of new drugs with the aim of reducing the high mortality and slow and costly recovery of ischemic patients. In consequence, many models of ischemia are reproduced in rodents where the cerebral hemodynamics are studied using expensive equipments such as

MRI scanners or by techniques that involve invasive approaches like for instance removing the scalp or thinning the skull which in turn cause a worsening in the living conditions of the animal.

In relation to this point, I have developed a fully non-invasive method to study the cerebral hemodynamics in rats that allows to proceed with longitudinal studies and which I hope will be useful in future biomedical research.

Resumen

El estudio del cerebro mediante métodos de óptica difusa ha progresado rápidamente en los últimos años. La posibilidad de estudiar la microvasculatura cerebral junto con la portabilidad y bajo coste de estos equipos abren una ventana de posibilidades para el estudio de fisiopatologías cerebrales. En este escenario, el estudio de la hemodinámica cerebral en pacientes isquémicos podría permitir a los neurólogos mejorar el rendimiento de los tratamientos médicos tempranos y de las terapias utilizadas hasta la fecha. En esta tesis he realizado un estudio pionero al respecto, estudiando por primera vez la hemodinámica cerebral de pacientes isquémicos durante las primeras horas después del infarto cerebral.

De igual manera, existen otro tipo de enfermedades que pueden desarrollar un empeoramiento a largo plazo de la autorregulación cerebral. Entre ellas destaca el síndrome de apnea obstructivo (SAO), debido al cual el empeoramiento de la hemodinámica cerebral provoca un aumento del riesgo directo de sufrir enfermedades cardiovasculares y un aumento del riesgo de infarto cerebral. Al respecto, he llevado a cabo el mayor estudio hasta la fecha con pacientes con SAO donde he estudiado su respuesta hemodinámica a un test ortostático y comparado estos resultados con los obtenidos en grupo de control de pacientes sanos.

Finalmente, la investigación primaria en animales es de vital importancia en el desarrollo de nuevas terapias y estrategias médicas así como en la validación de nuevos fármacos que reduzcan la alta mortalidad y la lenta y costosa recuperación

de los pacientes isquémicos. En consecuencia, numerosos modelos de isquemia son reproducidos en roedores donde se estudia la hemodinámica cerebral mediante caros equipos como los resonadores magnéticos o mediante técnicas que implican someter al animal a cierta cirugía en la que se le sustrae el cuero cabelludo o se le lima el cráneo. En relación con esto último, he desarrollado un método completamente no invasivo para estudiar la hemodinámica cerebral en ratas y que permite llevar a cabo estudios longitudinales, el cual espero sea utilidad en futuras investigaciones biomédicas.

Contents

List of Figures

List of Tables

Nomenclature

List of symbols

$\epsilon_i(\lambda)$	Extinction coefficient of the ith chromophore.
λ	Light wavelength.
$\left\langle \Delta r^2(\tau) \right\rangle$	Particle mean square displacement in time τ.
μ_a	Absorption coefficient (cm^{-1}).
μ_s	Scattering coefficient (cm^{-1}).
μ_s'	Reduced scattering coefficient.
ω	Intensity modulation frequency.
Φ	Fluence rate.
ρ	Source-detector distance.
τ	Correlation delay time.
c_i	Concentration of the ith chromophore.
D	Photon diffusion coefficient.
D_b	Brownian diffusion coefficient.
f	Frequency of the incident light.
l_{tr}	Transport mean free path.
$q = k_{out} - k_{in}$	Momentum transfer due to scattering event where k_{in} and k_{out} are the input and output field wavevectors.
v	Speed of light in tissue.

Y_t	Blood oxygen saturation.

List of acronyms

ACA	Anterior cerebral artery.
AHI	Apnoea-Hypopnoea Index.
ASL	Arterial spin labeled.
BFI	Blood flow index.
BMI	Body mass index.
BOLD	Blood oxygen level dependent method used in functional magnetic resonance imaging (fMRI).
CA	Cerebral autoregulation.
CAD	Coronary artery disease.
CBF	Cerebral blood flow.
CBFV	Cerebral blood flow velocity.
$\mathbf{CH_b}$	Deoxy-hemoglobin concentration.
$\mathbf{CH_bO_2}$	Oxy-hemoglobin concentration.
CPAP	Continuous positive air pressure.
CPP	Cerebral perfusion pressure.
CT	Computed tomography.
CT90	% of time during sleep where the $\mathbf{S_pO_2}$ is lower than 90%.
CVR	Cerebrovascular reactivity.
CW	Continuous-wave light source.
DCS	Diffuse correlation spectroscopy.

EEG	Electroencephalography.
FD	Frequency-domain light source.
fMRI	Functional magnetic resonance imaging.
HF	Heart failure.
HR	Heart rate.
ICA	Internal carotid artery.
IS	Ischemic stroke.
LDF	Laser doppler flowmetry.
LME	Linear mixed effects.
LSF	Laser speckle flowmetry.
MAP	Mean arterial pressure.
MCA	Middle cerebral artery.
MCAO	Middle cerebral artery occlusion.
MRI	Magnetic resonance imaging.
NIHSS	National Institutes of Health Stroke Scale.
NIRS	Near infrared spectroscopy.
ODI4%	Number of times where $S_{\mathbf{p}}O_{\mathbf{2}}$ decreases 4% due to an apnoea.
OISI	Optical intrinsic signal imaging.
OSA	Obstructive sleep apnoea.
PCA	Posterior cerebral artery.
PET	Positron emission tomography.
PSG	Polysomnography.
rCBF	Relative cerebral blood flow.

rTPA	Recombinant tissue plasminogen activator.
SNORM	Self-normalized relative cerebral blood flow.
SSPEs	Somatosensory evoked potentials.
S_pO_2	Arterial oxygen saturation.
TCD	Transcraneal doppler.
TD	Time-domain light source.
THC	Total hemoglobin concentration.
TIA	Transient ischemic attack.
XeCT	Xenon-enhanced computed tomography.

Thesis Objectives

Near-infrared diffuse correlation spectroscopy (DCS) is a non-invasive technique that allows to study the brain hemodynamics in human and animals in many clinical and medical scenarios.

Hypotheses

- Evoked functional activation in rats can be measured using a fully non-invasive longitudinal approach with diffuse correlation spectroscopy.
- The blood flow response to orthostatic challenge measured in ischemic stroke patients during the early hours after stroke is correlated to clinical outcome parameters such as the National Institutes of Health Stroke Scale or the modified Rankin Scale.
- Obstructive Sleep Apnoea patients classified in different groups according to the number of apnoeas/hypopnoeas per hour during sleep will show different cerebral blood flow responses to an orthostatic stress test.

Objectives

- To explore the feasibility of a fully non-invasive longitudinal diffuse correlation spectroscopy method using a particular anesthesia protocol to study the evoked functional activation in rats.

- To study the hemodynamics of ischemic stroke patients during the early hours after stroke using a portable diffuse correlation spectroscopy device.

- To study the hemodynamics of Obstructive Sleep Apnoea patients and to explore if groups of patients classified according to the number of apnoeas/hypopnoeas per hour during sleep show different cerebral blood flow responses to an orthostatic stress test and to find out if the cerebrovascular reactivity may correlate with key respiratory parameters.

1 Introduction

The understanding of brain function and its pathologies is one of the major challenges of medicine in 21st century. The impact of stroke in the society [1, 2], associated to growing ageing population in the West has provoked an increase of the public interest about the brain and the study of the processes involved on its functions. In this regards, clinical applications such as bedside brain function monitoring are expected to play a key role in a near future as portable fast diagnosis tools by means of reducing brain damage. This allows scenarios where the emergency squads start medical actions at the origin, prior to take the patient to the hospital with its consequent reduction in economical and social costs.

The brain is a complex organ that needs a regular supply of oxygen and nutrients through blood flow to guarantee its normal function. The study of the

mechanisms involved on this delivery are of great interest in the neuroscience community where cerebral microvasculature takes center stage. The cerebral autoregulation (CA), first described by Roy and Sherrington in 1890 [3], is the mechanism responsible of providing regular cerebral blood flow (CBF) when there is a change in the cerebral perfusion pressure (CPP) [4]. This process is controlled by the cerebrovascular reactivity (CVR) which regulates the diameter of the blood vessels in response to the increased CPP as illustrated on Figure 1.1.

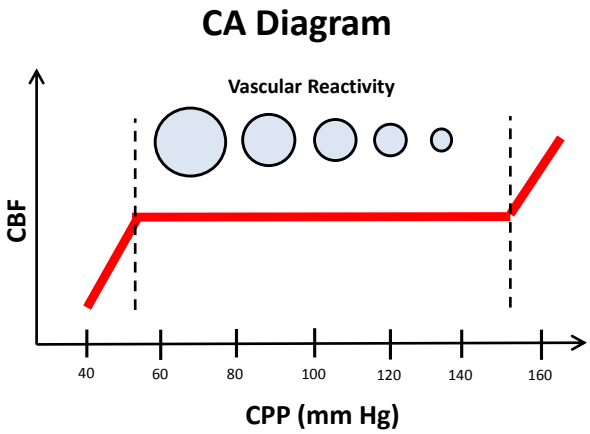

Figure 1.1: Diagram of cerebral autoregulation [5]: The cerebrovascular reactivity (CVR) is the mechanism that alters the diameter of the blood vessels in order to keep a constant cerebral blood flow (CBF) when there is an increase in the cerebral perfusion pressure (CPP)

There is a relation between impaired CA and certain neurological, cardiac and respiratory diseases [6–13] . In consequence, monitoring the neurovascularity of patients with impaired CA can be of great use for physiologists in terms of

studying the reasons that cause its unnormal functioning. This might open the gate to develop early detection tools and to explore ad-hoc treatments which, in both cases, might reduced the impact of the above mentioned diseases. Due to this reasons, many technologies were used to study the cerebral hemodynamics -hence CA- by means of monitoring the cerebral blood flow (CBF), the cerebral blood flow velocity (CBFV) or the tissue oxygenation.

Thereby, transcraneal doppler (TCD) [14,15] is an extended clinical tool that monitors CBFV but can only be used in large blood vessels [16] and its use is restricted to the thinner walls -insonation windows- of the skull [17].

CBF can be monitored at microvascular level through magnetic resonance imaging (MRI) [18] or computed tomography (CT) based techniques, such as arterial spin labeled perfusion magnetic resonance imaging (ASL-MRI) [19], Xenon-enhanced computed tomography (XeCT) [20] or positron emission tomography (PET) [21]. Unfortunately, these techniques involve expensive equipments with poor mobility and some of them use radioactive tracers.

Blood oxygen level dependent (BOLD) functional magnetic resonance imaging [22, 23] uses the presence of oxy- and deoxy-hemogloblin to study changes in the vascular reactivity induced by neuronal activity in three dimensional tomographic brain maps with moderate spatial resolution. However, its signal is difficult to interpret due to its low signal-to-noise ratio and complex statistical methods used. Also, this technique present similar issues in terms of economical costs and poor mobility.

Optical techniques are used to monitor cerebral hemodynamics by focusing on

the absorption and scattering properties of tissue. For instance, optical intrinsic signals imaging (OISI) [24–26] uses the reflectance of light to indicate active portions of the cortex but this method is limited to superficial measurements.

Near-infrared spectroscopy (NIRS) is based on light at some particular wavelengths being absorbed by certain chromophores like oxy- and deoxy-hemoglobin. As consequence, transcranial blood volume and blood oxygen saturation have been estimated. On the other hand, light scattering experiments obtain dynamic information of the medium by measuring the temporal fluctuations of the light intensity at the detectors. Among these, laser Doppler flowmetry (LDF) [27, 28] and laser speckle flowmetry (LSF) [29] have provided relatively low-cost alternatives but, as before, these methods are limited to superficial measurements. However, diffuse correlation spectroscopy (DCS) is a relatively low cost, portable technique with high temporal resolution that allows blood flow measurements in deep tissues [30–38].

1.1 Diffuse Optical Techniques

Jobsis [39] realized that in the near-infrared photons could travel deep into tissue due to the reduced absorption coefficients of water and hemoglobins. Within this 'physiological window' (Figure 1.2) that ranges from 650-900nm, the light transport is dominated by scattering rather than absorption and the photon transport can be approximated as a diffusive process. Here, the light absorption is caused by the presence of water, lipids, and particularly the oxy- and deoxy-hemoglobin among some other chromophores.

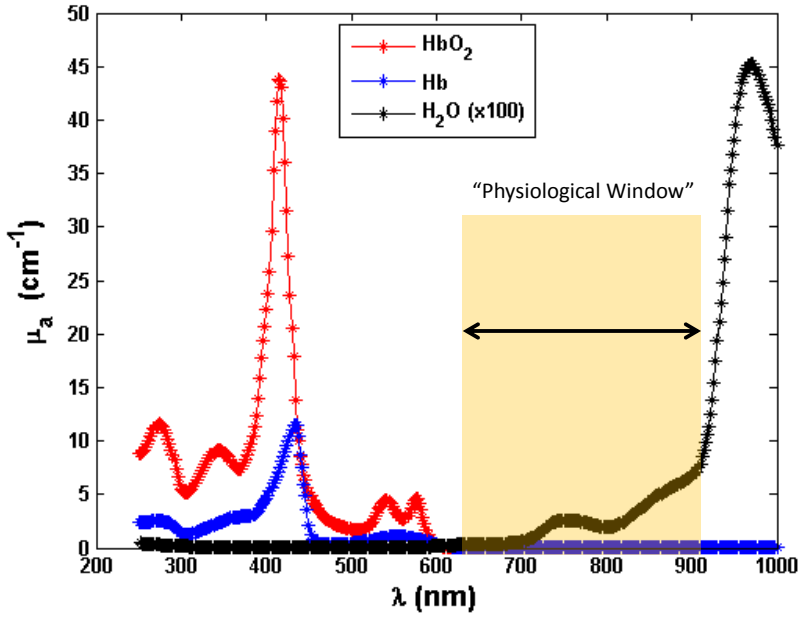

Figure 1.2: Absorption spectrum of tissue chromophores and location of the "Physiological Window" where absorption is relatively low.

Based on three different types of sources, near-infrared spectroscopy can be separated into continuous-wave (CW), frequency-domain (FD) and time-domain (TD) modalities where FD and TD allow to separate absorption from scattering process. On the other hand, diffuse correlation spectroscopy (DCS) allows non-invasive measurements of the blood flow in deep tissues through the interaction of the NIR light with the red blood cells and actually, this technology is able to reach the human brain transcranially [34, 35].

NIRS and DCS can be combined into an hybrid device which allows to

measure the CBF, the total hemoglobin concentration and the blood oxygen saturation.

1.2 Thesis Outline

I have centered this work on the study of the brain by means of developing DCS applications in rat and human *in vivo* tissues with the aim of studying the cerebral hemodynamics. This work has a clear medical orientation as it covers different scenarios where the CVR *might be* impaired like in patients with Obstructive Sleep Apnoea (OSA) syndrome to diseases where the CVR is impaired such as ischemic stroke. This last case is also the motivation for the study carried out with rats in this Thesis.

Accordingly, these challenges involved the utilization of both hybrid and single DCS devices, the creation of new optical probes or engineering solutions to avoid their displacement over long measurements among some other topics that will be described in detail in the following chapters.

Chapter 2 provides with the theoretical background that allows to study cerebral hemodynamics with diffuse correlation spectroscopy whereas Chapter 3 describes the instrumentation used by means of equipments, design of new probes and engineering solutions to the bedside clinical applications developed.

Chapter 4 describes the design of a non-invasive surface optical probe and the protocol used to study the rat brain hemodynamics by measuring the functional activation in the somatosensory area provoked by a set of electrical stimuli. The validation of this technique allows the neuroscience community to proceed with

longitudinal studies using a portable cheap device. Furthermore, it permits the researchers to study and to monitor the recovery of rat brain ischemia models through the use of new pharmacological drugs or rich environment therapies.

Chapter 5 studies the hemodynamics of ischemic stroke (IS) patients during the early hours after the stroke onset through an orthostatic stress challenge. The mean values of the relative cerebral blood flow (rCBF) for each patient at a given HOB angle and time stage are obtained and correlations of rCBF with other demographic and clinical parameters (includying recombinant tissue plasminogen activator (rtPA) treatments) are explored by using linear mixed effects (LME) models produced with R-Project statistical package. Also, I discuss the application of DCS as a bedside brain function clinical monitoring and its potential advantages in intensive care units.

Chapter 6 describes the effect of the Obstructive Sleep Apnoea syndrome on the microvascular cerebral blood flow. To that end, the cerebral vasoreactivity was studied in a large number (n=83) of subjects which were previously selected and grouped according to the apnoea-hypopnoea index (AHI) (number of apnoea and hypopnoea events/sleep hour) which is the parameter used to define the severity of this disease. The study also includes a control group of healthy subjects. This work focus on the response of these subjects to an orthostatic stress challenge. A complete analysis of this data is presented in this chapter by delivering the mean values of rCBF for each patient group at a given head-of-bed (HOB) angle and exploring the correlations of rCBF with other clinical and demographic parameters through LME models.

Chapter 7 summarizes the conclusions of this Thesis including a global discussion of the utility and convenience of DCS as a fast portable brain monitoring diagnose tool.

2 Theory

When shinning infrared light into tissue, the propagation of photons is mainly dominated by scattering rather than absorption. In this scenario, there are three important length scales to be considered. The first one is the *scattering length*, which is the typical distance traveled by a photon before it experiments a scattering event, and its reciprocal is the scattering coefficient μ_s (cm^{-1}). The second one is the *transport mean free path* or *random walk* (l_{tr}), which is the typical distance traveled by a photon before its direction is randomized. The reciprocal of this distance is the reduced scattering coefficient μ_s' (cm^{-1}). Finally, photons can also be absorbed in the medium and therefore the *absorption length* is the typical distance traveled by a photon before is absorbed, being its reciprocal the absorption coefficient μ_a (cm^{-1}) [34]. These coefficients are wavelength

dependent and they provide with the optical properties of the medium used to described the light propagation through the diffusion model. This method, also know as Diffuse Optical Spectroscopy (DOS) or Near-Infrared Spectroscopy (NIRS) allows to separate the effects of scattering from absorption.

There are three NIRS modalities based on three type of sources as illustrated in Figure 2.1. The first and simplest one is called *Continuous-Wave* (CW) and it consists in projecting continuous-wave light into a diffuse medium (tissue for instance) and to measure the attenuated outgoing light intensity [26,40–46]. This is the simplest approach but it provides with the lowest information per source detector pair and the absolute value of μ_a and μ_s' are difficult to determine.

The second type of source is the *Frequency-Domain* (FD) where a intensity modulated source produces a sinusoidal diffuse wave with angular frequency ω ($f = \frac{2\pi}{\omega}$ typically around 100 MHz). In this case, the absolute value of both the absorption and scattering coefficients can be obtained by analyzing the change in the amplitude and phase shift of this modulated outgoing light beam [47–51].

Finally, the *Time-Domain* (TD) or *Time-Resolved Spectroscopy* (TRS) uses light pulses containing a range of modulation frequencies. When coming out from tissue, these light pulses are attenuated and broadened due to the multiscattering events they experience and from the analysis of their shape the absolute values of μ_a and μ_s' can be determined [52–56].

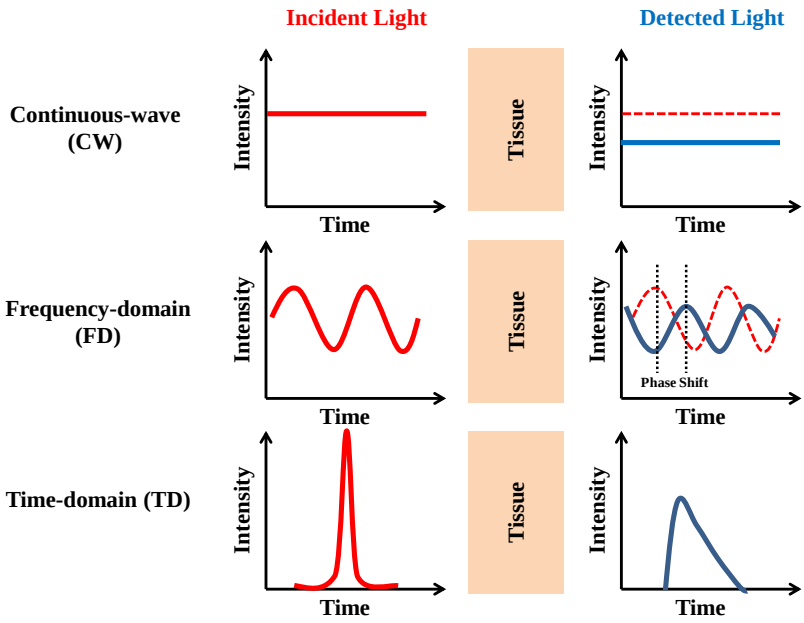

Figure 2.1: Three types of sources for NIRS. In red incoming light in tissue, in blue outgoing light from tissue. Top: Continuous-wave (CW) where attenuated signal of the light intensity is monitored. Middle: Frequency-domain (FD) where the amplitude and the phase shift of the output modulated light are monitored. Bottom: Time-domain (TD) where the broadening and the amplitude of the pulse are monitored

2.1 Photon Diffusion in Turbid Media

The light transport theory in a turbid media can be described through the radiation transport equation (RTE). Under some approximations, the RTE can be simplified to the photon diffusion equation [57, 58] where the photon fluence rate $\Phi(Wcm^{-2})$ obeys:

$$\nabla\cdot(D(r)\nabla\Phi(r,t)) - v\mu_a(r)\Phi(r,t) - \frac{\partial\Phi(r,t)}{\partial t} = -vS(r,t), \tag{2.1}$$

where:

$$D(r) = \frac{v}{3(\mu_s'(r) + \mu_a(r))}$$

D(r) is defined as the photon diffusion coefficient where v is the speed of the light in the medium.

The validity of the photon diffusion model lays in considering two assumptions [59]. The first one involves the radiance to be nearly isotropic and this condition is achieved when $\mu_s' >> \mu_a$ and the photon propagation distances are larger in comparison to the transport mean free path, l_{tr}. In this case, the source-detector distance must be larger than $3l_{tr}$ [58]. The second assumption implies that the time variations in the diffuse flux vector $\vec{J}$ are slow i.e this variations are negligible with respect to the vector itself.

2.2 Diffuse photon density waves (DPDW'S)

Since part of the experiments explained in this thesis were carried out using a frequency domain NIRS device, I will develop the following theoretical section from a frequency domain approach. In this case, we can consider a intensity modulated source that induces fluence rate disturbances which can be described as waves or *Diffuse Photon Density Waves* (DPDW) that oscillate at the same frequency ω as the source [60,61]. In this scenario, we can assume that the source term in Eq. (2.1) has 'dc' and 'ac' terms and can be expressed as:

$$S(r,t) = S_{dc}(r) + S_{ac}(r)e^{-i\omega t}$$

Correspondingly, the oscillating 'ac' term of the fluence Φ_{ac} can be expressed as:

$$\Phi_{ac}(r,t) = U(r)\cdot e^{-i\omega t} \tag{2.2}$$

By substituting this expression in Eq. (2.1) we obtain the diffusion equation with modulated source:

$$\nabla\cdot(D(r)\nabla U(r)) - (v\mu_a(r) - i\omega)U(r) = -vS_{ac}(r) \tag{2.3}$$

Depending on different geometries and distribution of optical properties, Eq. (2.3) can be solved either analytically or numerically. In the following section we consider one such simple geometry which is the infinite medium.

2.2.1 Photon diffusion in infinite, homogeneous turbid media

This is the simplest geometry and it is based on considering a single modulated point source at the origin. In this case, the intensity falls to zero at infinity because $S_{ac}(r) = S_{ac}\delta(r)$ and the solution for the fluence rate adopts the form of an overdamped spherical wave:

$$U(r) = \frac{vS_{ac}}{4\pi Dr} \cdot e^{-kr} \tag{2.4}$$

Where the complex wave vector $k = k_r + ik_i$ has real and imaginary parts, both dependent of the modulation frequency ω, the absorption coefficient μ_a and the reduced scattering coefficient μ_s' as in the form:

$$k_r = (\frac{v\mu_a}{2D})^{1/2}\left[(1 + [\frac{\omega}{v\mu_a}]^2) + 1\right]^{1/2} \tag{2.5}$$

$$k_i = (\frac{v\mu_a}{2D})^{1/2}\left[(1 + [\frac{\omega}{v\mu_a}]^2) - 1\right]^{1/2} \tag{2.6}$$

2.2.2 Photon diffusion in semi-infinite, homogeneous turbid media

Although the solution for the fluence rate derived from the infinite medium geometry provides with a description of the propagation of DPDW within the medium, most of experiments present an interface between tissue and air. In this scenario, tissue can be modeled as a semi-infinite medium and boundary

conditions can be used to solve the photon diffusion equation in the reflection geometry using the method of images [62]. In this case, the fluence rate at the interface adopts the form:

$$\Phi = z_b \hat{n} \cdot \nabla \Phi \tag{2.7}$$

This is known as the partial-flux boundary condition where, $\hat{n}$ is a vector normal to the tissue surface and:

$$z_b = \frac{2l_{tr}(1 + R_{eff})}{3(1 - R_{eff})}$$

where R_{eff} being the air-tissue effective reflection coefficient which adopts the form:

$$R_{eff} \approx -1.440n^2 + 0.710^{-1} + 0.668 + 0.00636n$$

and $n = n_{in}/n_{out}$ the index of refraction 'inside' and 'outside' ratio.

The second boundary condition comes from considering a negative source located at a distance $z = -(2z_b + l_{tr})$ that as a result will make the fluence rate equal to zero at a distance $z = -z_b$ outside the tissue as described in Figure 2.2.

This is called the extrapolated-zero boundary condition and it is expressed as:

$$\Phi(z = -z_b) = 0$$

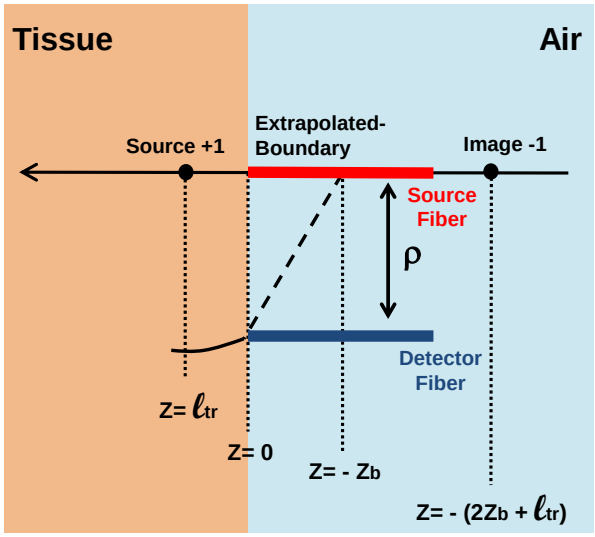

Figure 2.2: Semi infinite medium in the reflection geometry. By using the method of the images we can consider a negative source located at a distance $z = -(2z_b + l_{tr})$. As a result, the fluence rate will be equal to zero at a distance $z = -z_b$ outside the tissue.

In case of homogeneous media we can consider D(r) and $\mu_a(r)$ to be a constant and therefore Eq. (2.8) takes the form:

$$(\nabla^2 - k^2)U(r) = \frac{-v}{D} \cdot S_{ac}(r) \tag{2.8}$$

Where,

$$k^2 = \frac{(v\mu_a - iw)}{D}$$

.

The frequency domain Green's function $G_0(r, r_s)$ also satisfies the expression:

$$(\nabla^2 - k^2)G_0(r, r_s) = -\delta(r - r_s) \tag{2.9}$$

Thus, by calculating the Green's function on a given geometry we can solve the photon diffusion equation.

For the semi-infinite medium geometry the diffusion Green's function in the frequency domain adopts the form (in cylindrical coordinates being ρ the radius of the cylinder):

$$G_0([\rho, z], [\rho_s = 0, z_s = l_{tr}]) = \frac{1}{4\pi}\left[\frac{e^{-kr_1}}{r_1} - \frac{e^{-kr_b}}{r_b}\right] \tag{2.10}$$

Where:

$$r_1 = \sqrt{(z - l_{tr})^2 + \rho^2} \tag{2.11}$$

$$r_b = \sqrt{(z + 2z_b + l_{tr})^2 + \rho^2} \tag{2.12}$$

By then comparing Eq. (2.10) with the solution for the infinite medium in Eq. (2.4), it is straight forward that the fluence rate in the reflection mode over the tissue surface adopts the form:

$$U(\rho, z = o) = \frac{vS_0G_0([\rho, z = 0], [\rho_s = 0, z_s = l_{tr}])}{D} \tag{2.13}$$

In the limit when $\rho \gg (l_{tr} + 2z_b)$ the solution takes the form:

$$U(\rho, z = o) = \frac{A_0e^{-k_r\rho}}{\rho^2}e^{i(-k_i\rho+\theta_0)} = A(\rho)e^{i\theta(\rho)} \tag{2.14}$$

and the following expressions for the amplitude and phase can be obtained:

$$\ln(\rho^2 A(\rho)) = -k_r \rho + \ln A_0 \tag{2.15}$$

$$\theta(\rho) = -k_i \rho + \theta_0 \tag{2.16}$$

By measuring the outgoing amplitude and phase at different distances we can fit previous Eq. 2.15-2.16 to obtained k_i and k_r which in combination of Eq. 2.5-2.6 allow us to obtain the absorption and scattering coefficients at a given wavelength.

The absorption coefficient is related to the chromophores concentration through the following linear relation:

$$\mu_a(\lambda) = \sum_i \epsilon_i(\lambda) c_i, \tag{2.17}$$

where λ is the light wavelength, $\epsilon_i(\lambda)$ and c_i are respectively the extinction coefficient and the concentration of the ith chromophore.

By determining the absorption coefficient at different wavelengths we can obtain the concentration of important chromophores like the oxy- and deoxy-hemoglobin, water and lipids. In fact, the use of as much wavelengths as possible will improve the general output of the concentration of the chromophores. However, due to practical reasons, in this study we have focused on 690, 785 and 830nm as can be seen in the following chapter. Therefore, the concentration of oxy- and deoxy-hemoglobin (CH_bO_2 and CH_b) can be obtained from which the total hemoglobin concentration (also known as blood volume) can be derived:

$$THC = CH_b + CH_bO_2 \tag{2.18}$$

Similarly, the blood oxygen saturation Y_t can be estimated by using the expression:

$$Y_t = \left[\frac{CH_bO_2}{THC}\right] \times 100 \tag{2.19}$$

2.3 Diffuse Correlation Spectroscopy

When a laser beam is used to illuminate a rough surface, the light will be reflected in many directions. This reflected light will be composed by bright and dark spots called *speckles* as a result of the constructive and destructive interference cause by the different photon path lengths [63]. If instead illuminating a rough surface we shine the laser light into a turbid medium (like tissue for instance), the speckle pattern collected in a detector will fluctuate in time due to the motion of the scatterers. Diffuse Correlation Spectroscopy (DCS) [64, 65] was originated from Dynamic Light Scattering (DLS) [66] theory and uses the temporal fluctuations of near-infrared light to study the dynamics of a turbid medium like tissue.

There are two main regimes to take into account depending on whether photons experiment a single scattering event or if they propagate into the medium through multiple scattering experience.

2.3.1 Single scattering limit

In this first approach, we consider a long coherence laser source that shines light into a dilute solution of particles in suspension where photons scatters once or not at all as they travel through it. The scattered light is collected in a detector placed at an angle θ respect to the incident light beam as illustrated in Figure 2.3.

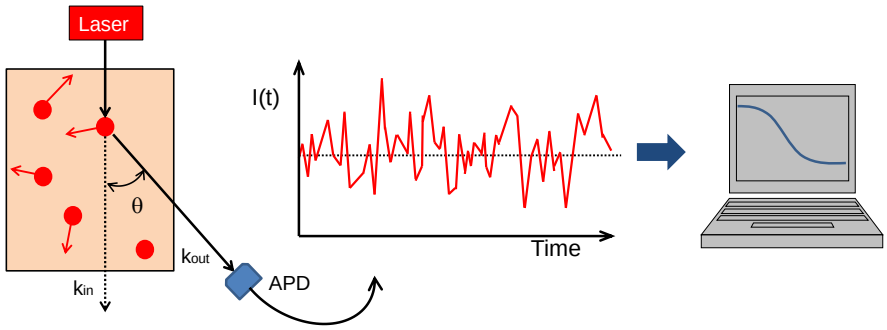

Figure 2.3: Schematic description of a single scattering experiment where the scattered light is collected in a detector placed at an angle θ respect to the incident light beam.

In the detector, the electric field is a superposition of all the scattered electric fields and takes the form:

$$E_T(t) = \hat{e}\, E_0\, F(\theta)\, e^{-iwt}\, e^{i(k_{out}R_d - k_{in}R_s)} \left(\sum_{i=1}^{N} e^{-iqr_i(t)} \right) \tag{2.20}$$

Where $\hat{e}$ is a unit vector that indicates the polarization direction of the scattered light, E_0 is the amplitude of the incident field, $F(\theta)$ is the scattering form factor and ω is the light angular frequency. Rs, Rd and r_i indicate the

positions of source, detector and ith scatterer respectively. The momentum transfer is represented by $q = k_{out} - k_{in}$ where k_{in} and k_{out} the input and output wavevectors.

If we consider independent, randomly positioned particles with uncorrelated random motion, the normalized electric field temporal autocorrelation (g_1) at the detector [66, 67] takes the form:

$$g_1(\tau) = \frac{\langle\ E(t)E^*(t+\tau)\rangle}{\langle\ |E(t)|^2\rangle} = e^{i\omega\tau}\ e^{-q^2\left\langle\Delta r^2(\tau)\right\rangle/6} \tag{2.21}$$

Where 'τ' is the correlation delay time, <> represents the *ensemble average* and $\left\langle\Delta r^2(\tau)\right\rangle$ the particle mean square displacement in time τ. Depending on the type of motions carried out by the scatterers, $\left\langle\Delta r^2(\tau)\right\rangle$ adopts different expressions:

- $\left\langle\Delta r^2(\tau)\right\rangle = 6D_b\tau$ for 'Brownian Motion'
- $\left\langle\Delta r^2(\tau)\right\rangle = \left\langle V^2\right\rangle\tau^2$ for 'Random Flow'

Where D_b is the particle diffusion coefficient and $\left\langle V^2\right\rangle$ is the second moment of the particle speed distribution.

However, experimentally we measured the normalized intensity temporal autocorrelation function (g_2) which takes the form:

$$g_2(\tau) = \frac{\langle\ I(t)I(t+\tau)\rangle}{\langle\ I(t)\rangle^2} \tag{2.22}$$

The normalized field autocorrelation function $g_1(\tau)$ is related to the normal-

ized intensity autocorrelation function $g_2(\tau)$ through the Siegert relation [68]:

$$g_2(\tau) = 1 + \beta|g_1(\tau)|^2 \tag{2.23}$$

where β is a parameter that depends on the number of speckles detected, the coherence length and the laser stability. The above mentioned Siegert relation is valid for stationary Gaussian sources as in the case described in this section where the medium converts the laser light into a Gaussian source. Also, the medium is ergodic as the time average is equivalent to the ensemble average in this case.

2.3.2 Multiple scattering limit

If in the previous example, we increase the concentration of scattering particles, photons will experience many scattering events before they exit the medium as illustrated in the reflection geometry example of Figure 2.4.

In this case, a photon reaches the detector located at a distance ρ after experiencing multiple scattering events and the accumulated phase of the electric field for this photon can be expressed as:

$$E(t)_{one\ path} = \hat{e}\ E_0\ e^{-iwt}\ e^{i(k_{N+1}\cdot R_d - k_1 R_s)} \prod_{j=1}^{N} F(\theta_j) \prod_{j=1}^{N} e^{-iq_j r_j(t)} \tag{2.24}$$

Similar to the single scattering limit case, $\mathrm{F}(\theta_j)$ is the form factor and θ_j the scattering angle for the j^{th} scattering event. N is the number of scattering

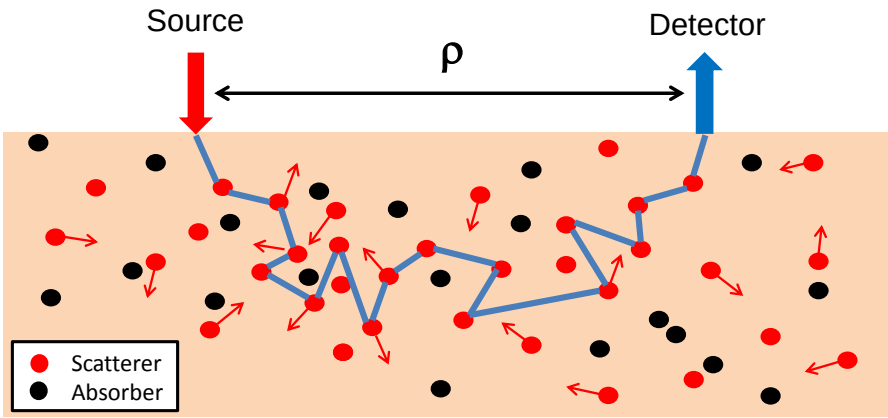

Figure 2.4: Example of the photon path during multi scattering events in the reflection geometry. A photon reaches the detector located at a distance ρ after experiencing multiple scattering events.

events along the photon path.

In the detector, the total scattered electric field will be the sum of all the fields due to all photon paths and can be expressed as:

$$E_T(t) = \sum^{All\ paths} E(t)_{one\ path} \tag{2.25}$$

If we assume that the individual photon paths are uncorrelated, the total temporal field autocorrelation function can be expressed in terms of the field autocorrelation for each individual photon path and therefore takes the form :

$$g_1(\tau) = \sum_{k=1}^{All\ paths} P_k \cdot g_1(\tau)_{k^{th}\ path} \tag{2.26}$$

where P_k is the probability of the k_{kth} photon path.

Following a similar derivation than Eq. 2.21 and considering an homogeneous highly scattering medium where scattering events are independent and scatterer displacements are uncorrelated, the temporal field autocorrelation for one photon path takes the form:

$$g_1(\tau)_{one\ path} = e^{i\omega\tau} e^{-\frac{1}{3}{k_0}^2 Y \left\langle \Delta r^2(\tau) \right\rangle} \tag{2.27}$$

and

$$Y = N \cdot (1 - < cos\theta >_N)$$

In highly scattering medium this parameter can be approximated to the number of random walks associated to a photon path and it takes the form:

$$Y = \frac{s}{l_{tr}} \tag{2.28}$$

where 's' is the total photon path length.

In the detector, the field autocorrelation function contains the contributions of all the photon paths and can be expressed as a function of the photon pathlength distribution P(s):

$$g_1(\tau) = e^{i\omega\tau} \int_0^{+\infty} P(s)\, e^{\frac{-s}{3l_{tr}}\, {k_0}^2 \left\langle \Delta r^2(\tau) \right\rangle} ds \tag{2.29}$$

2.3.3 Correlation diffusion equation

The correlation photon diffusion equation [30, 69] can be derived from the correlation transport equation (CTE) and takes the form:

$$\left[\nabla\cdot(D(r)\nabla) - v\mu_a(r) - \frac{1}{3}\mu_s' k_0^2 \left\langle \Delta r^2(\tau) \right\rangle\right] G_1(r,t) = -vS(r,t) \tag{2.30}$$

Where G_1 is the unnormalized electric field correlation function and $k_0 = 2\pi/\lambda$ is the wave vector of the incident CW light. The Green's function solution for Eq. (2.30) in the homogeneous semi-infinite medium geometry takes then the form:

$$G_1(\rho,z,\tau) = \frac{3\mu_s'}{4\pi}\left[\frac{exp(-K(\tau)r_1}{r_1} - \frac{exp(-K(\tau)r_b}{r_b}\right] \tag{2.31}$$

Where,

$$K(\tau) = \sqrt{3\mu_s'\mu_a + {\mu_s'}^2 k_0^2 \alpha \left\langle \Delta r^2(\tau) \right\rangle}$$

taking r_1 and r_b the form given in Eq. (2.11-2.12). The parameter α is the fraction of scattering events from moving scatterers (mainly red blood cells) as biological tissue contains also static or very low scatterers like organelles or mithocondria.

In the tissue surface ($z = 0$) the normalized temporal electric field correlation $g_1(\tau) = G_1(\rho,\tau)/G_1(\rho,0)$ will take the form:

$$g_1(\rho,\tau) = \frac{\left(\frac{exp(-K(\tau)r_1}{r_1} - \frac{exp(-K(\tau)r_b}{r_b}\right)}{\left(\frac{exp(-K(0)r_1}{r_1} - \frac{exp(-K(0)r_b}{r_b}\right)} \tag{2.32}$$

In a measurement we obtain the normalized temporal intensity autocorrelation $g_2(\tau)$ from which we can derived the normalized temporal electric field correlation $g_1(\tau)$ using the Siegert relation. Then by fitting the temporal decay of $g_1(\tau)$ for a given source detector separation we can obtain K^2. This is illustrated in the example of Figure 2.5.

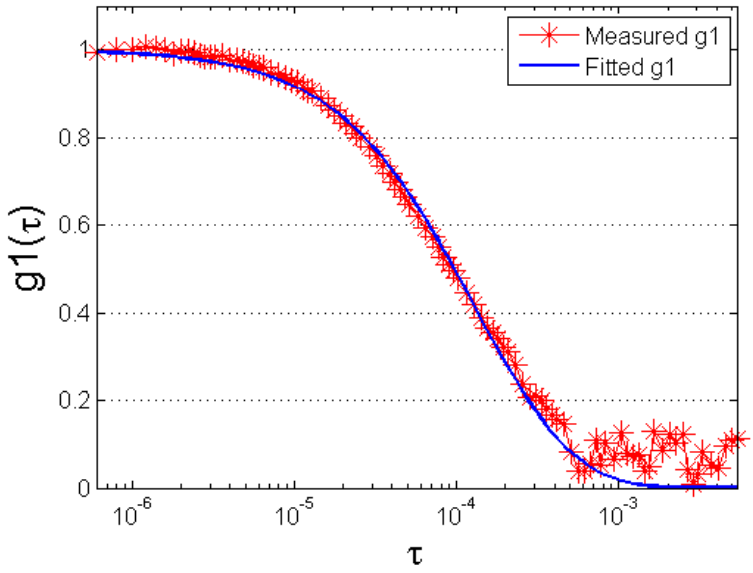

Figure 2.5: Example of g1 values (in red) measured in tissue versus the delay time τ. In blue, the fitting curve from which we obtain the $\left\langle \Delta r^2(\tau) \right\rangle$.

From this fitting, the $\left\langle \Delta r^2(\tau) \right\rangle$ is finally obtained which contains the dynamic

information of the medium.

Since DCS signal is obtained from the microvasculature of a tissue volume, a random flow model ($\left\langle \Delta r^2(\tau) \right\rangle = \left\langle V^2 \right\rangle \tau^2$) was adopted to fit the decay of the measured correlation curves. However, it was found [31, 32, 35] that Brownian model ($\left\langle \Delta r^2(\tau) \right\rangle = 6D_b\tau$) is more appropriate for such purpose being this model validated in a wide range of animal and human tissues like muscle, brain or tumors.

Although αD_b is not a measurement of the absolute blood flow, it is referred as 'Blood Flow Index' (BFI) as it correlates well with other blood flow modalities. Furthermore, the relative blood flow (rBF) is an index obtained by normalizing the blood flow index (BFI) with a given baseline value which reflects how the blood flow has change in % respect to the baseline values.

$$rBF = \left(\frac{BFI}{BFI_{\text{baseline}}} - 1\right) \times 100 \tag{2.33}$$

If the sampling tissue is brain, equation 2.33 uses *relative cerebral blood flow (rCBF)* instead of rBF. We will use this final parameter to describe the results obtained in the following chapters.

3

Instrumentation

In this thesis, I have used DCS and Frequency Domain NIRS devices to obtain values for the CBF and oxy- and deoxy-hemoglobin concentration respectively. Thus, depending on the needs of the experimental design, I have used single DCS devices (Chapters 4 and 5) or hybrid devices, result of combining both DCS and FD NIRS equipments (Chapter 6). In any case, since most of the research carried out on this thesis was done in hospital premises, all the set ups were adapted to be portable.

3.1 Diffuse Correlation Spectroscopy device

The schematic description of the functioning of the DCS device used is illustrated in Figure 3.1.

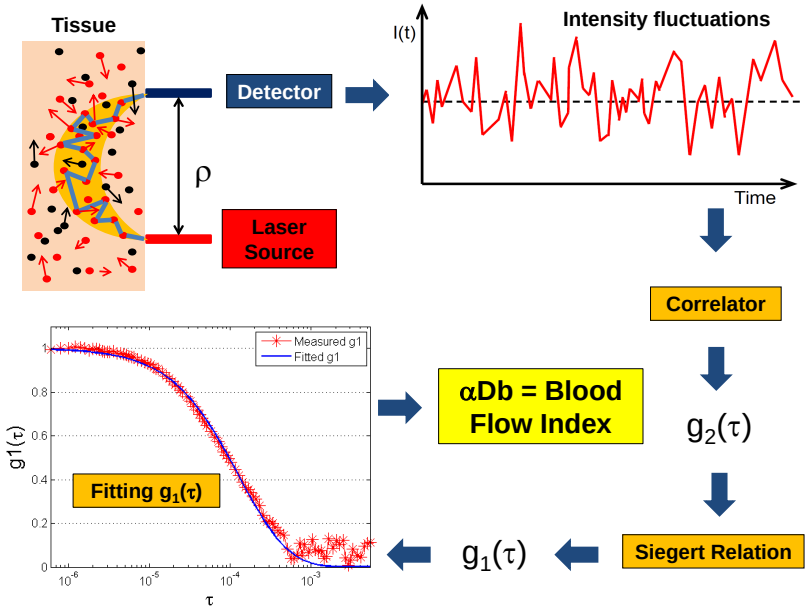

Figure 3.1: Schematic description of the functioning of DCS: Due to incident NIR laser light, photons experiment a set of scattering events that induce a phase change in the electric field of their waves. In the detector the light intensity oscillates in time. An autocorrelator uses the output of the detector to produce the normalized temporal intensity autocorrelation function (g_2). By using the Siegert relation, the electric field temporal autocorrelation function (g_1) is derived. By fitting g_1 the blood flow index (αDb) is finally extracted.

In the experiments I shined light into the tissue by using a long coherence laser source at 785nm (120mw, Crystalaser, Reno, Nevada, USA) through a

multimode fiber of $200\mu m$ diameter core. The light was collected using 8 single mode fibers of $5.8\mu m$ core diameter and sent into two arrays of 4 Excelitas Technologies (Dumberry, Vaudreuil, Canada) single-photon counting avalanche photodiodes (SPCM-AQ4C) conforming 8 (2x4) detectors. The output of each detector was used to build the normalized intensity autocorrelation function by using an 8 channel correlator (Correlator.com, Bridgewater, New Jersey, USA). Also, an optical switch was used in these studies when required.

Depending on the nature of the experiment carried out, different source detector geometries were used and therefore different optical probes were manufactured which will be explained in detail in the following sections of this chapter.

3.1.1 Rat Brain Probes

In this project, I have developed two similar optical probes based on the features of a rat skull of 6 months old illustrated on Figure 3.2. In both cases, the probe placement area was the (yellow) top flat part of the skull. The main reference point used was Bregma (the intersection of sagital and coronal sutures). The dimensions (11 x 11 mm) are in this case orientative as they change in time.

The first probe developed was an *implantable probe* and the second one a *surface probe* version which involved a brief alteration of its geometry as can be seen on Figure 3.3 where both geometries designs can be compared.

As it will be explained in detail in Chapter 4, the justification for this brief alteration comes from taking into account the thickness of the rat scalp (around 1mm), the fat accumulation and the natural growth of the animal. The reason of

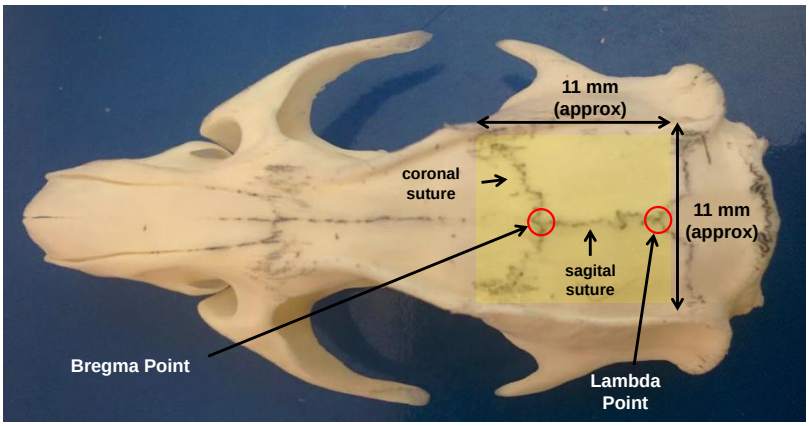

Figure 3.2: 6 months old rat skull with key landmarks (Bregma and Lambda points) and orientative dimensions. The probes placing area (yellow) is located on the top flat part of the skull.

having many source-detector pairs was to be able to monitor different volumes of the rat brain at different depths.

In both cases, I have used Bregma point (in red on Figure 3.3) as a reference point to properly placed the probes over the skull and the scalp respectively.

3.1.1.1 Implantable Probe

This probe consisted of two platforms with holes for fiber placement following the geometry described in the left side of Figure 3.3. The purpose of this geometry was to track different parts of the brain at different depths and locations.

The lower platform was implanted on the rat skull using Bregma point as a reference after removing the rat scalp. The optical fibers for both sources and

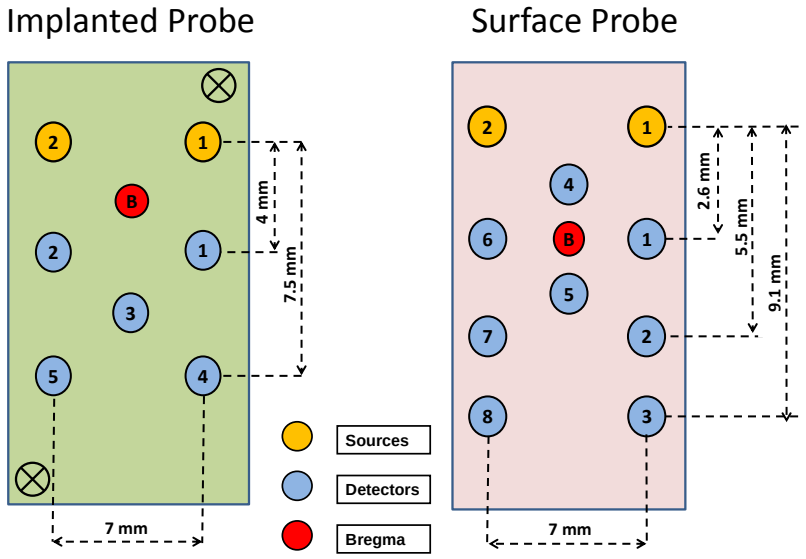

Figure 3.3: Comparison of implanted and surface probe geometries. The differences in the source-detector distances were motivated after taking into account the depth of the scalp, the fat accumulation and the natural growth of the animal.

detectors were located in the upper platform of the probe and fixed in their position with small screws. Finally both parts were put one to the other as shown in the diagram of Figure 3.4 becoming a single probe. At the end of each study session, the upper platform was removed leaving the lower platform in place.

This approach presents some advantages in terms of accuracy in positioning the probe in the correct place over the skull and it can stay on the rat head over long periods of time without changing its location. Also, it avoids the partial

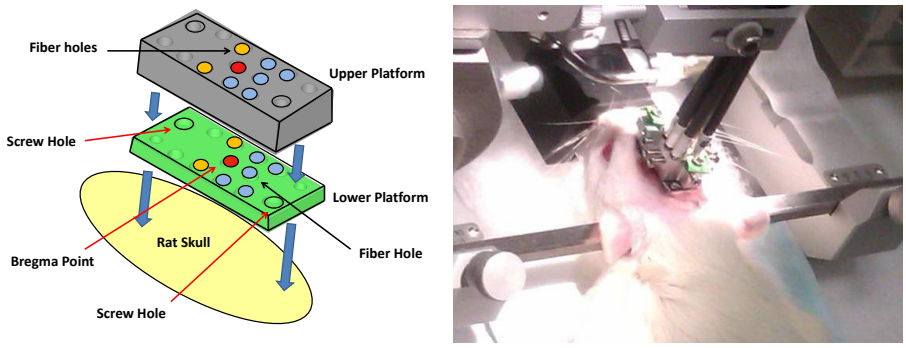

Figure 3.4: (Left) Description of the two stage platforms of the implantable probe and its placement on the skull. (Right) Picture of the implantable probe on rat during a measurement.

signal derived from the scalp and therefore reduces the signal to noise ratio. The lower implanted platform was made MRI compatible to allow its use alternatively during fMRI and DCS experiments.

On the other hand, the scalp must be removed to implant the probe and that derives into a surgical intervention [29, 70–76] with its inherent healing process which involves to often clean the fiber holes of the lower platform . Also, the living condition of the animals generally worsens as they are more vulnerable to suffer infections.

3.1.1.2 Surface Probe

The surface probe consisted of a single platform with holes for fiber placement which follow the geometry description of the right side of Figure 3.5. As before, the purpose of this geometry was to track different parts of the brain at different depths and locations.

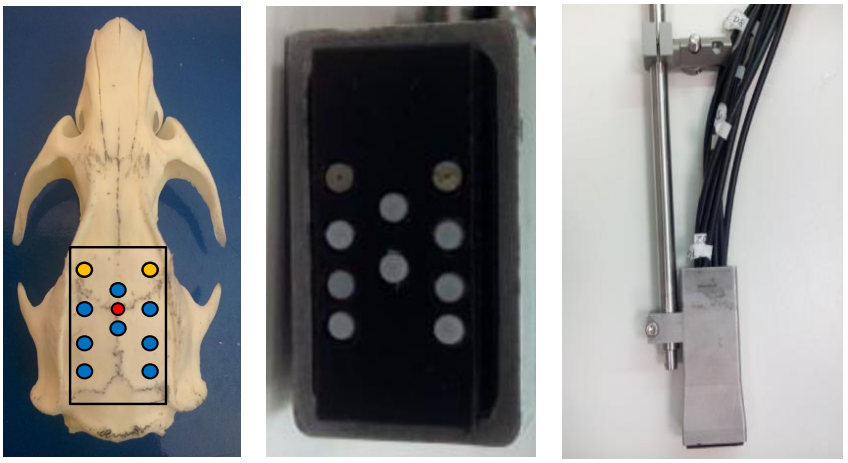

Figure 3.5: Left: Imaginary representation of the probe over the rat skull. Center: Overview of the surface probe. Right: Overview of the probe merged into the metallic shield.

This platform was merged with metallic cover shield with the purpose of avoiding light contamination and to integrate the probe into an estereotaxic arm which allowed us to move very precisely the probe in the space.

In comparison to the implanted probe, the surface approach is fully non-

invasive and therefore surgical interventions are not required. In this scenario, animals were simply shaved with an electric razor and depilatory cream to avoid side effects of the fur. Since I had no visual access to Bregma, the main difficulty laid on placing the probe over the scalp in the correct place. However, a set of steps were developed to enhance the accuracy of this process that will be explained in detail in Chapter 4.

3.1.2 Human Forehead Probe

Based on prior studies [33, 77], the optical probe developed for studying the hemodynamics of ischemic stroke patients was constructed with a flexible hypoallergenic material that allowed to be adapted to the shape of the forehead.

This probe was conformed by two symmetric sets of source-detector pairs at 2.5cm distance placed on both right and left frontal hemispheres as described on Figure 3.6. Due to the characteristics of this study, I have used custom made optical fibers with 90° bend tips. Each set of detectors collected the light into four avalanche photodiodes detectors to be averaged when processing the data.

[1]Human 3-D plot courtesy of Hemophotonics. S.L (http://www.hemophotonics.com/)

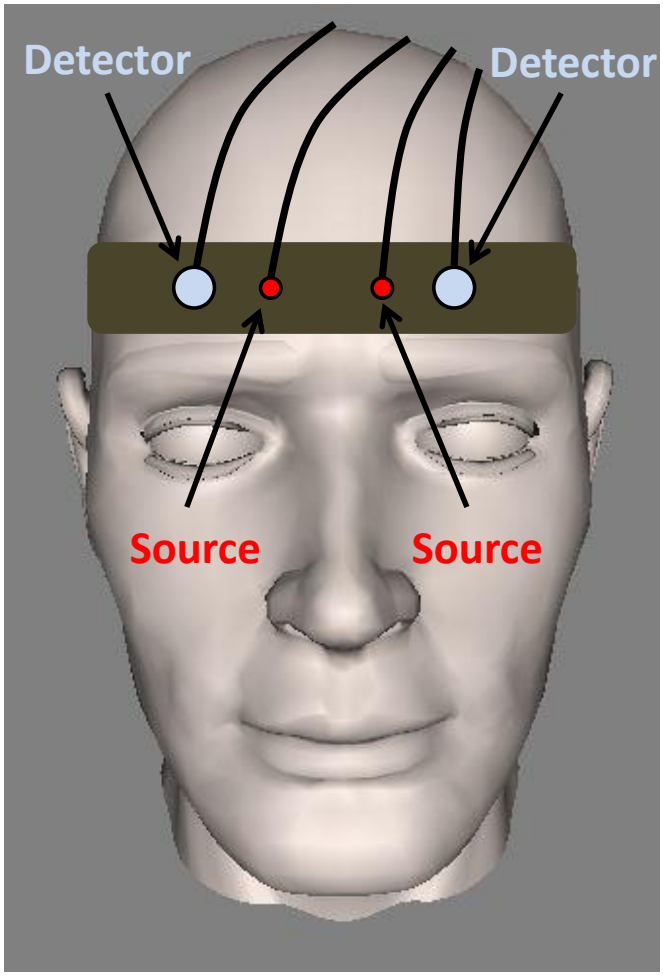

Figure 3.6: Sketch[1] of the human forehead probe use to study the hemodynamics of ischemic stroke patients. The probe was composed by two symmetric sets of source-detector pairs at 2.5cm distance placed on both right and left frontal hemispheres.

3.2 NIRS device

Figure 3.7 describes the functioning of a FD NIRS device where modulated light at 110Hz is shone into tissue at three different wavelengths. By measuring the change in amplitude and phase of the outgoing light at different source-detector distances both absorption and scattering coefficient can be determined.

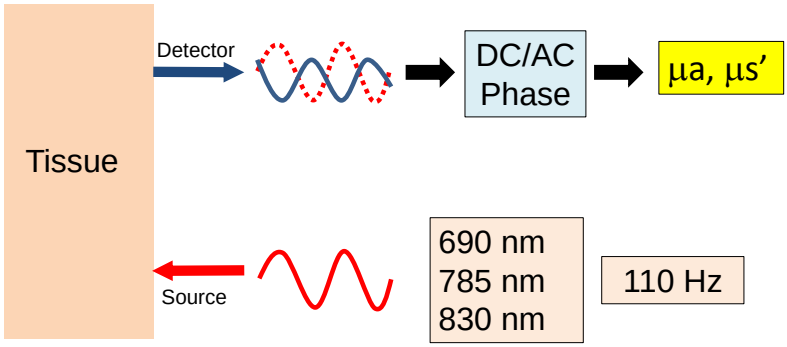

Figure 3.7: Schematic description of the functioning of a Frequency Domain NIRS device. A modulated (110Hz) light source (in red) is used to shine tissue using three different wavelengths alternatively (690, 785 and 830nm). The outgoing light (in blue) is collected in a detector at a given source-detector distance. By analyzing the intensity attenuation of this signal and its phase shift, the absorption (μ_a) and scattering (μ_s') coefficients can be determined.

For the experiments where I wanted to obtain the optical properties of the tissue, I have used a commercial FD NIRS device (Imagent, ISS, Illinois, USA) which was composed of 15 (5x3) laser sources organized in groups of 5 sources at three different wavelengths (690, 785 and 830nm respectively) and modulated

at 110Hz. The light was collected in two photomultipliers and by fitting the amplitude and the phase of the outgoing light, μa and μ_s' were calculated.

3.3 Hybrid Instrumentation

Measuring simultaneously the static and dynamical properties of the tissue can provide with very useful information about the blood flow and blood oxygenation. With this purpose, others in the past have built hybrid devices for many different purposes [31, 36, 78, 79].

In this study, I have utilized a portable set-up (Figure 3.8) composed by a DCS and a FD NIRS (ISS-Imagent). Both devices were designed to be portable allowing bedside monitoring and to work independently (controlled by independent computers) although they were interconnected when proceeding with a measurement. Accordingly, both measurements were synchronize and any event marked with DCS (like for instance a change in the head-of-bed) was also registered by the ISS-imagent device.

3.3.1 Sleep Study Probe

This optical probe was constructed with a flexible hypoallergenic material to be adapted to the shape of the forehead of the patients and was conformed by two sectors as shown in Figure 3.9a. The first one located over the right forehead of the patient was used for DCS measurements whereas the one in the left forehead was devoted to FD NIRS.

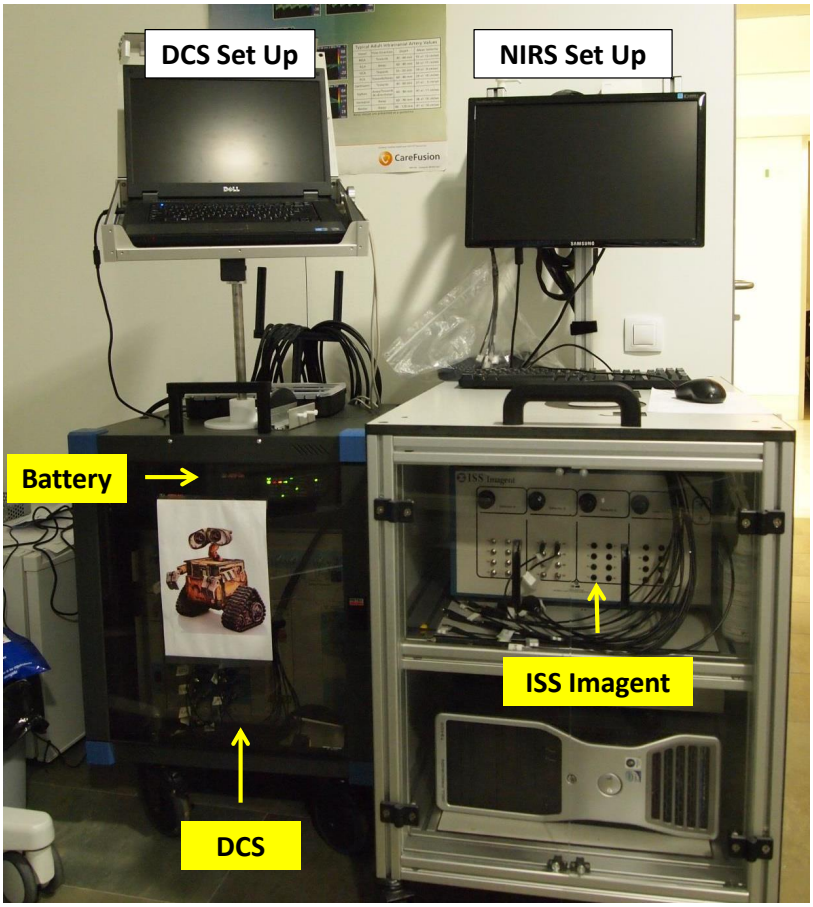

Figure 3.8: Picture of the hybrid portable set up. (Left) DCS device. (Right) ISS Imagen FD NIRS device.

The DCS part consisted in one laser source and two sets of detectors located at 1 cm and 2.5 cm far from the source as illustrated on the left side of Figure 3.9a. Each set of detectors collected the light into four avalanche photodiodes detectors to be averaged when processing the data.

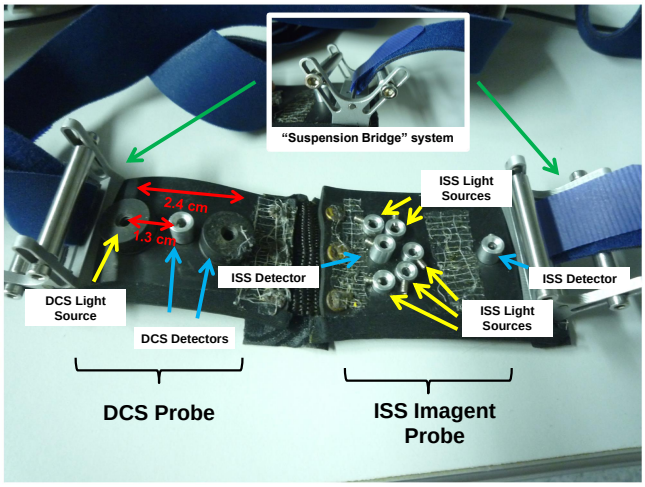

(a) View of the hybrid optical probe constructed with a flexible hypoallergenic material and composed by two sectors, one for the DCS probe (left) and the other for the NIRS one (right).

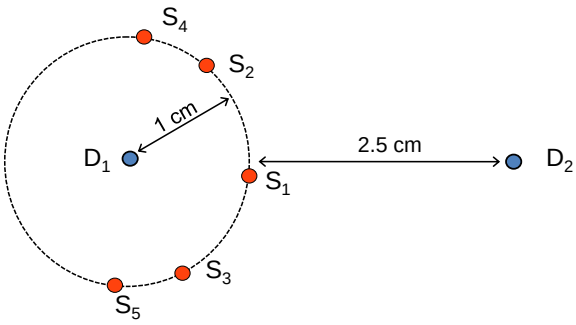

(b) Diagram of the self-calibrated NIRS probe. Sources in red are equidistant to detector one (in the left, in blue) but they present different distances to the second detector (in the right, in blue)

Figure 3.9: Description of the hybrid probe.

In the design of the NIRS probe (right side of Figure 3.9a) I took into account several factors that could lead to error in estimating μa and μ_s' like for instance the

poor contact between the fiber tips and the tissue or also the fiber imperfections. These factors are the so-called *coupling errors* [80] and can be expressed through *coupling coefficients* for both the sources and detectors fibers. I have used of a self calibration method [50] to obtain the relative values of all the coupling source coefficients using the sources equidistant to one detector as illustrated in Figure 3.9b. These coefficients were introduced in the measurements of the other detector from which μ_a and μ_s' were fitted by minimizing the χ^2 using nonlinear least square curve fitting.

4

Non-invasive monitoring of functional activation in rat brain with DCS

4.1 Introduction & motivation

Brain is a complex organ organized through interconnected areas responsible for different functions. Blood flow is delivered in the brain through three main vessels (i.e. 2 carotid arteries and the basilar artery) that leads blood to the circle of Willis where the main cerebral arteries branch out [81]. There are three main vascular territories that guarantee the blood flow delivery in the brain through the anterior cerebral artery (ACA), the middle cerebral artery (MCA) and the posterior cerebral artery (PCA). Among them, MCA takes center stage in the study of ischemic stroke as around 50% of them are produced when there is a

partial or total occlusion in the middle cerebral artery (MCAO) [82]. Depending on the severity of these type of strokes, the impact over a relatively large brain area can be huge, includying the motor and the somatosensory areas. This last one is of great interest in the neuroscience community for the study of stroke models, stroke recovery therapies and the design of new pharmacological drugs among some other reasons.

Neurovascular coupling is the relation between neuronal activity and cerebral blood flow increase in the microvasculature [83]. This is a complex mechanism not fully understood where neuronal activity implies energy consumption, producing a demand of oxygen and glucose which are carried out through the blood stream. The understanding of the neurovascular coupling and its alterations after cerebral pathophysiologies could provide important insights into the management of different pathological conditions such as ischemic stroke [84].

Electroencephalography (EEG) [85] techniques have been used to study the cerebral activity, i.e. the electrical activity, in both human and rodents but EEG signals can be difficult to interpret [86].

The blood oxygen level dependent (BOLD) [22] and arterial spin labeled (ASL) magnetic resonance imaging (MRI) methods have revolutionized the study of neurovascular coupling in humans as well as in experimental animals [19, 23, 87]. Unfortunately, the high costs of these equipments limits the access of the researchers to longitudinal studies.

Optical techniques such as laser Doppler flowmetry (LDF) [27, 28, 75, 76], optical intrinsic signals imaging (OISI) [24, 70, 71, 88, 89] and laser speckle flowmetry

(LSF) [29, 73, 74, 90] have provided relatively low-cost alternatives, albeit with some compromises, for the study of the neurovascular coupling. One main limitation of these methods is the fact that are limited to superficial measurements and therefore, in general, require thinning or removal of the skull.

Diffuse optical techniques such as near-infrared spectroscopy (NIRS) and diffuse correlation spectroscopy (DCS) allow non-invasive measurements of the cerebral hemodynamics in deep tissues and are even able to reach the human brain transcranially (through scalp, skull, etc..) [30–35, 91–93]. I am particularly interested in cerebral blood flow measurements in rodents where DCS can be utilized. Indeed, DCS and NIRS have been utilized in rodents transcranially [94] with the scalp retracted [79] and longitudinal functional activation has been demonstrated in mice [44] using a skull implantable fiber optical probe.

However, there are some limitations in this approach. Namely, the retraction of the scalp created some issues due to the healing of the tissue and repeatability is a concern due to the growing animal.

In the study of the neurovascular coupling in rodents, the paw (forepaw and hindpaw) electrical stimulation [95] is one of the most common external stimulus used to induced a functional activation in the somatosensory areas corresponding to forepaw or hindpaw (represented in orange and yellow respectively in Figure 4.1).

Within this context, α -chloralose has been extensively utilized as an anesthetic in rodents [74, 75, 96–99] as it preserves the neuronal activity and its hemodynamic response [100]. However, although is found to be an excellent

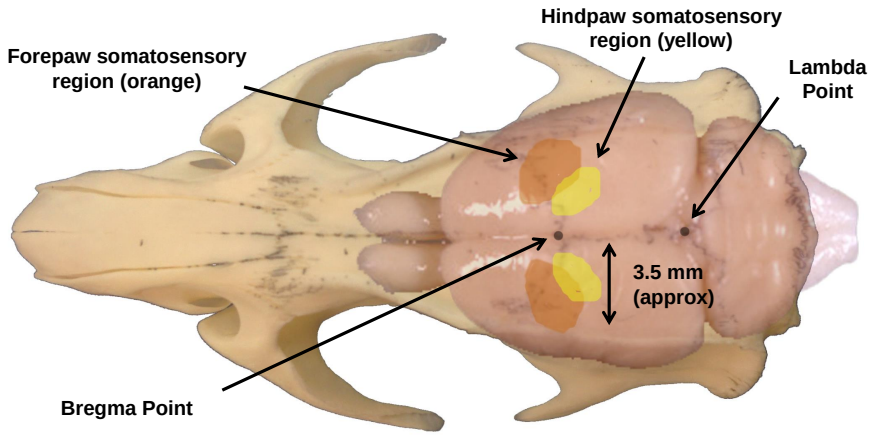

Figure 4.1: Areas of activation in the rat brain induced by forepaw stimulation (orange) and hindpaw stimulation (yellow).

sedative for specific studies, it is unsuitable in longitudinal studies [101].

Alternatively *Weber et al.* [102] developed a fully non invasive method for MRI based on the sedative medetomidine [103] and the monitoring of the animals during experimentation which allows to proceed with longitudinal studies [104–106].

The main objective of this study was to measure the evoked cerebral activity in a fully non invasive manner using this anesthesia protocol and to compare the findings with the results in the literature obtained with BOLD and optical techniques that required invasive methods (i.e removing the scalp and/or thinning the skull).

In this regards, I have developed two types of optical probes which were

already described in Chapter 3. The implantable MRI compatible probe was built with the aim of exploring the feasibility of measuring the evoked functional activation using this particular anesthesia whereas with the surface probe I took a step forward and I proceeded with fully non-invasive longitudinal measurements.

4.2 Methods

This study was performed in collaboration with Dr. Carles Justicia from the Department of Brain Ischemia and Neurodegeneration of the Institut d'Investigacions Biomèdiques August Pi i Sunyer (IDIBAPS), Barcelona, Spain. All the methods described in this section have been approved by the Ethical Committee of Animal Experimentation (CEEA) of the Generalitat de Catalunya and they were applied to all the animals involved on this study.

4.2.1 Anesthesia

Male Wistar rats with a body weight of 320 ± 50g in the beginning of the study were anesthetized with 4% isofluorane in $O_2 : N_2$ (30:70). After that, animals were placed in a stereotaxic frame with a face mask delivering the same gas mix with 3% isofluorane and a subcutaneous bolus of 0.05 mg/Kg of medetomidine (Domitor, Pfizer) was injected. Isoflurane was slowly discontinued over the course of the next 15 min at a rate of approximately 0.25% every 1 min starting 3 min after the bolus administration. Therefore, isoflurane is presumed to not be available at 15 min after the bolus administration. At this point, a continuous

subcutaneous infusion of medetomidine (1ml/h; 0.1 mg/Kg) was initiated for the whole duration of the experiment. The forehead of the animals was shaved using an electric razor and depilatory cream to avoid side effects in the optical signal produced by the fur. Two subdermal electrode needles were inserted in both forepaws for stimulation. The respiration rate (number of respiration per minute) was registered every 5 minutes and the body temperature was continuously monitored with a rectal probe and maintained around 37°C with in-house feedback controlled electrical blanket.

Around 30 minutes after the bolus injection, animals already washed out most of the isofluorane and they presented a stable condition with a respiration rate of approximately 50% compared with the initial respiration rate once the animal was anesthetized. The body temperature was around 37°C. At this point the stimulation protocol was initiated (described in next section). When the experiment was concluded the animal received an intraperitoneal injection (0.1mg/Kg) of atipamezole (Antisedan, Pzifer) to reverse the effect of the medetodimine.

4.2.2 Stimulation

I have used a stimulus paradigm which consisted in a rectangular constant current stimulus of 15 seconds followed by 45 seconds of recovery period. The 15 seconds stimulus was conformed by a train of pulses of 2mA and 300μs duration. Depending on the pulse rate used, each stimulus paradigm have the following features:

- 15 seconds stimulus duration at 3Hz pulse rate (45 pulses) followed by 45

second of recovery period.

- 15 seconds stimulus duration at 6Hz pulse rate (90 pulses) followed by 45 second of recovery period.

- 15 seconds stimulus duration at 9Hz pulse rate (135 pulses) followed by 45 second of recovery period.

Our protocol consisted in setting a pulse rate and to repeat 5 consecutive stimulus paradigms using the same pulse frequency. This set of 5 single stimulus periods conformed a train of stimuli of 5 minutes duration followed by 5 minutes of recovery period. These trains of stimuli were applied 3 times per paw alternatively as illustrated in Figure 4.2.

4.2.3 fMRI experiments

The fMRI experiments were conducted on a 7.0T BioSpec 70/30 horizontal scanner (Bruker BioSpin, Ettlingen, Germany), equipped with an actively shielded gradient system (400 mT/m, 12 cm inner diameter). The receiver coil was a 4-channel phased-array surface coil for the rat brain. For fMRI studies, coronal multislice spin-echo (SE) EPI images were acquired using the following parameters: TE/TR = 30/3000 ms; BW = 150 kHz; 5 consecutive slices of 2 mm thickness; Field-of-view = 2.56 x 2.56 cm^2; matrix of 64 x 64 pixels. Functional activation imaging was achieved with BOLD contrast MRI. Statistical parametric activation maps were constructed with the software STIMULATE [107]. Time course for each pixel was examined using a paired Student's t-test ($P < 0.01$).

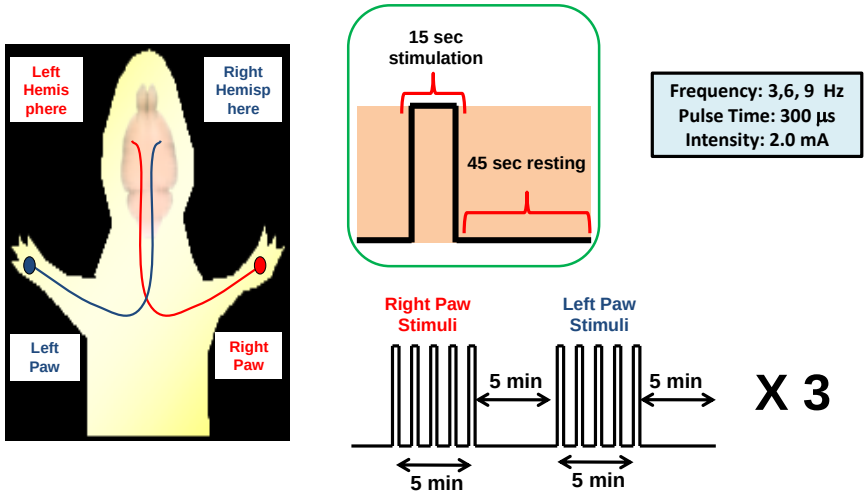

Figure 4.2: Diagram of the protocol followed to electrically stimulate the forepaw of the rat. Each stimulus paradigm consisted in 15 seconds stimulation followed by 45 seconds of recovery period. The stimulation was conformed by train of pulses of 2mA and 300μs duration. Different pulses rates of 3, 6 and 9 Hz were used depending on the experiment. 5 consecutive stimulus paradigms conformed a train of stimuli of 5 minutes duration followed by 5 minutes of recovery period. The trains of stimuli were applied 3 times per paw alternatively

4.2.4 Blood flow response from the optical signal

An optical switch was used to alternatively acquire data from both brain hemispheres. The averaging time for each single measurement was of 500ms which implies to have a temporal resolution of 1 sec per brain hemisphere.

The use of the implantable probe allowed to be very precise in measuring the correct region of interest. However, when I used the surface probe I had no visual access to Bregma and a set of steps were followed to properly placed the

probe over the rat scalp. This protocol is schematically explained on Figure 4.3 and it basically consisted in using a transparent plastic grid referenced to a set of landmarks (eyes, ears and nose) from which the location of Bregma point can be estimated. Distances in the plastic grid were modified according to the growth of the animal.

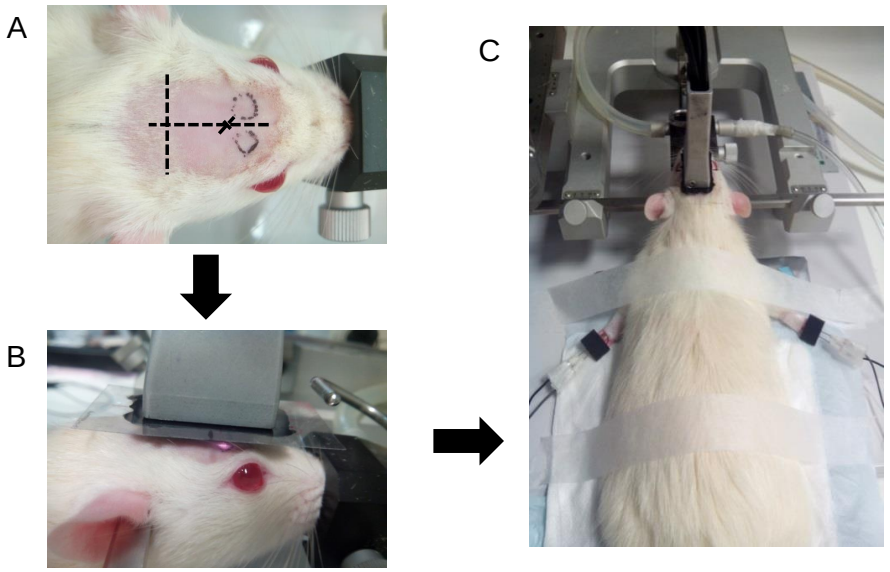

Figure 4.3: Description of the surface probe positioning protocol over the rat scalp

Two circles were plot (Figure 4.3-A) marking the projection of the laser beams over the scalp (Figure 4.3-B) to secure the correct positioning of the probe. By carefully monitoring this process, the probe was finally firmly placed over the scalp applying sufficient pressure to assure a good probe-scalp contact

as shown in Figure 4.3-C.

Due to the fact that animal physiology can change during the measurement, the blood flow response was calculated separately for each trains of stimuli. The relative cerebral blood flow (rCBF) was obtained by normalizing the blood flow index (BFI) of a given train of stimuli with a baseline obtained by averaging the means of the BFI corresponding to the 15 seconds prior to the start of the electrical discharge inside that train.

Characterization of the mean blood flow signal

The 15 (5x3) blood flow responses produced per paw per measurement were averaged. As a result, a final averaged rCBF signal was obtained which reflects the average blood flow response to electrical stimulation for the whole measurement.

In order to evaluate the strength of the averaged rCBF, I have followed the same protocol described in [75] to estimate its peak height i.e the maximum change in amplitude when compared to baseline values. This was performed by locating the maximum value of the signal and averaging the data from 1 sec prior to 1 sec posterior to the maximum amplitude.

In some occasions, the blood flow response to a given stimulus was weak and could not be distinguished from the noise levels which were observed to oscillate in a range of $\pm 10\%$ during the resting periods between trains of stimuli. Therefore, a selection criteria was introduced to differentiate the blood flow response from noise. This criteria establishes that the evoked functional activation is observed if there is a minimum of 15% in blood flow increase for all the stimulus *within*

at least one train of stimuli when compared to baseline values. All the averaged rCBF results described in the next section have been derived from measurements that accomplish the above mentioned criteria.

4.3 Results

4.3.1 BOLD results with stimulus pulses at different frequencies

All the individuals in this study were subjected to fMRI and anatomical imaging by MRI two weeks before proceeding with the optical measurements. The evoked response was evaluated with fMRI using stimulus pulses at a rates of 3, 6 and 9Hz which were randomly applied on each set of stimuli (the same frequency was used in the five consecutive stimulus that conformed a train of stimuli. After this, another frequency was selected).

The main plot of Figure 4.4 represents the averaged BOLD signals produced at the mentioned frequencies in the left brain hemisphere versus time. As we can see, the averaged signal produced at 9 Hz (in blue) presents the maximum amplitude closely followed by the signal produced at 6Hz (in green). When comparing these two signals it can be seen that the one produced at 6Hz decays slower during the stimulation time. Finally, the signal produced at 3Hz (in red) presents the lowest amplitude and also seems to decay slower than the 9Hz signal. The small plot in the right side is an example of the activation map produced by one of these stimulus.

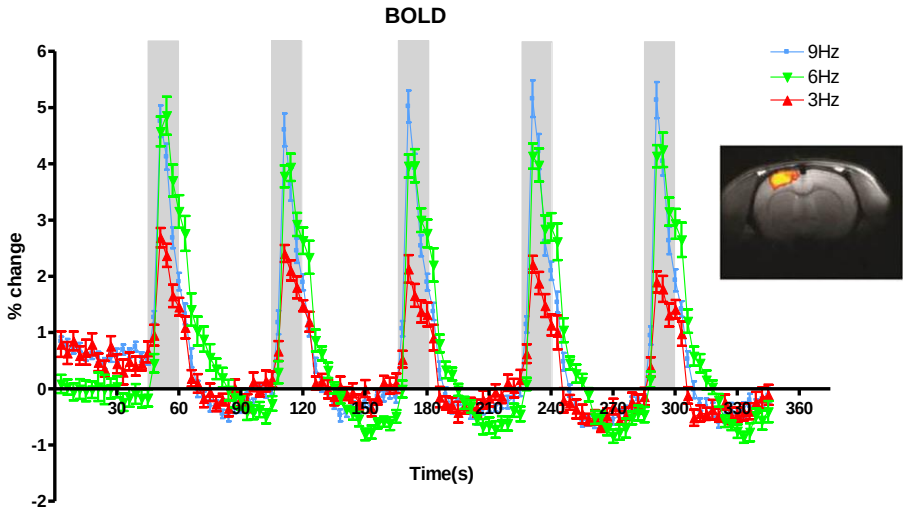

Figure 4.4: (Main) Example of BOLD signal produced at 3, 6 and 9 Hertz stimulation (in grey). (Right) Example of the activation map produced by one stimulus in the right forepaw.

4.3.2 Implantable Probe

Three rats were measured following the anesthesia and electrical protocol described previously. The evoked functional activation was obtained for all the specimens with stimulus of 3Hz pulse rate.

An example of these results can be seen in Figure 4.5 where the blood flow response to 3Hz stimulation is presented versus time. In this plot, we can seen how the average rCBF stays constant during the baseline period until the start of the stimulus. When that happens, the average rCBF experiments an increase of around 40% compared to baseline values and starts decreasing still during the

stimulus duration. When the stimulus is finished, the signal returns to baseline values. This result has features similar to the flow signals obtained in similar experiments described in the literature [97, 98]. This fact encouraged us to go a step further and to explore the feasibility of the surface probe.

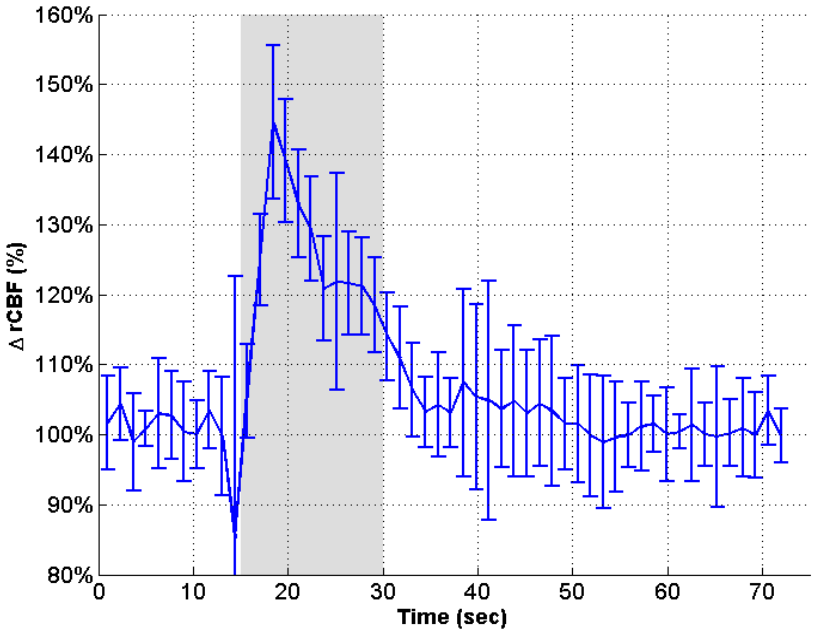

Figure 4.5: Example of the average rCBF (errorbars=std) versus time (sec) in the right hemisphere of one animal with the implantable probe at 3Hz electrical stimulation (in grey). The average rCBF stays constant during the baseline period until the start of the stimulus. When that happens, the average rCBF experiments an increase of around 40% compared to baseline values and starts decreasing still during the stimulus duration. When the stimulus is finished, the signal returns to baseline values

4.3.3 Surface Probe

In this section I present the results obtained with the surface probe in different sets of experiments according to the age of the animals and following the anesthesia, probe placement and electrical stimulation protocols described previously.

The first set of experiments involves measurements of 6 months old animals with a body weight of 320 ± 50g carried out during three consecutive weeks in the beginning of this study. In here, the pulse rate utilized for the electrical stimulation was of 9HZ. In the second set, animals of 18 moths old with a body weight of 580 ± 80g were measured during two consecutive weeks using 6Hz stimulus.

Finally, I will also show a representative longitudinal case of one animal which was included in both of the previous cohorts.

4.3.3.1 6 months old animals

All the animals presented in this section (n=5) were measured once per week during three consecutive weeks using stimulus of 9Hz pulse rate. The average blood flow response was obtained for all the specimens and the peak height was derived as explained previously. The values obtained for the peak heights in both hemispheres are represented in Figure 4.6. The results show intra- and inter-individual variability in the length of the bars (the strength of our signal).

For instance, the signal obtained in the left hemisphere of rat 5 measured in the second week presents a peak height of 44% and this value was obtained by averaging the 15 blood flow responses induced by the 15 electrical stimulations

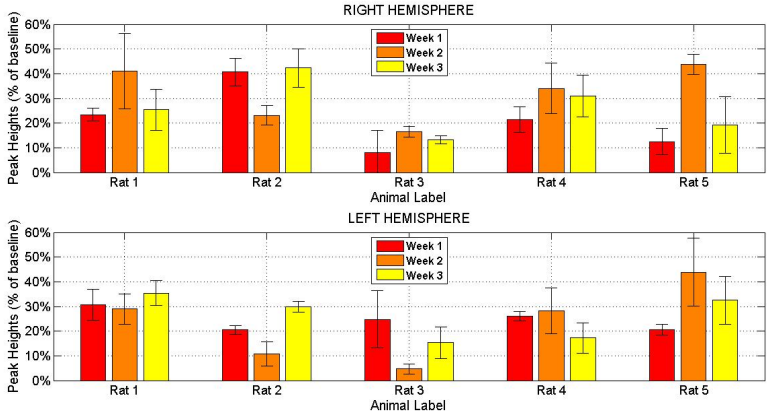

Figure 4.6: Right (Top) and left (Bottom) hemispheres peak heights versus animal label in the 6 months old group of animals measured over three consecutive weeks.

as illustrated in the left side of Figure 4.7.

In this example, the signal to noise ratio is good enough to identify all the blood flow responses and the final averaged rCBF signal obtained for this animal is illustrated in the example of Figure 4.8.

In compliance with the results obtained with the implantable probe, we can see that blood flow stays constant (around 100% in the figure) until the beginning of the electrical stimulation of 15 second duration (in grey). When the stimulus starts, the blood flow increases until it reaches its maximum value (52% increase compared to baseline values). Right after, still within the electrical stimulation, the flow signal starts decreasing smoothly conforming a *plateau* phase until the end of the stimulus. Finally, the blood flow returns to baseline values. The peak height parameter (44%) was obtained by averaging the data from 1 sec prior to

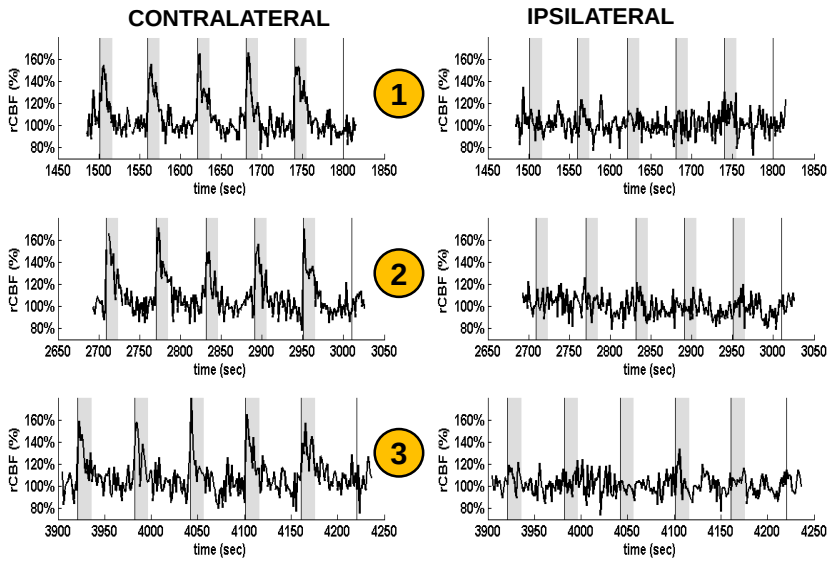

Figure 4.7: Example of the three contralateral rCBF trains of stimuli measured with the surface probe with good signal-to-noise ratio versus the ipsilateral response corresponding to rat 5 on the second week. The grey areas indicate the duration of the electrical stimuli (15 sec). Measurement started (time=0) 25 min after the bolus injection.

1 sec posterior to the maximum amplitude. As with the implantable probe, this signal has features similar to the flow signals obtained in the literature [97, 98].

On the other hand, when looking at the peak height of rat 3 in the same hemisphere and also measured during the same week, we can see that it presents a value 11%. The reason for this *low* value compared to the previous example is illustrated in the left side of Figure 4.9 where we can see the three rCBF trains of stimuli from which the peak height was derived.

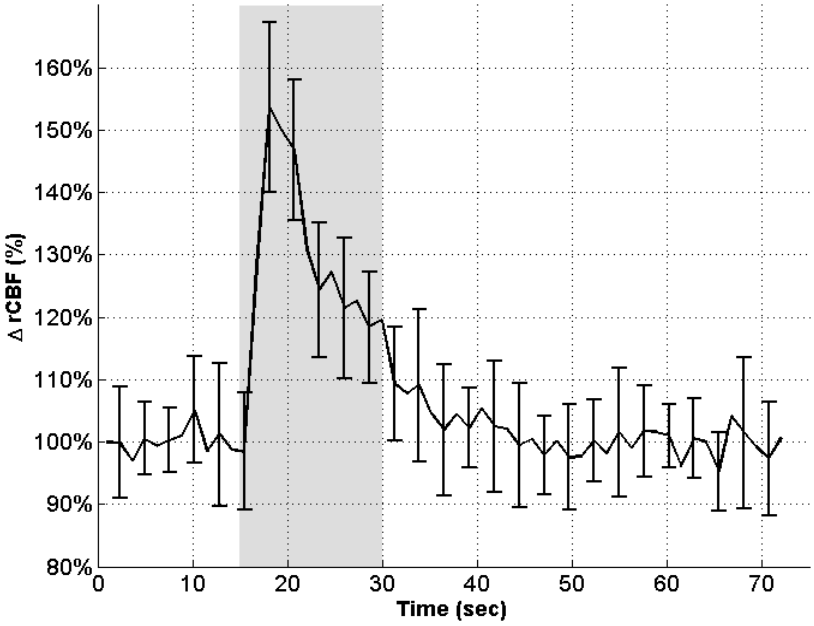

Figure 4.8: Example of the final averaged rCBF signal (errorbars=std, plotted every two points) versus time (sec) obtained from the contralateral trains of stimuli (left hemisphere) of rat 5 during the second week. The grey areas indicate the duration of the electrical stimuli (15 sec). The averaged rCBF stays constant (around 100% in the figure) until the beginning of the electrical stimulation. When the stimulus starts, the blood flow increases very fast until it reaches its maximum value (52% increase compared to baseline values). Right after, still within the electrical stimulation, the flow signal starts decreasing smoothly conforming a *plateau* phase until the end of the stimulus. Finally, the blood flow returns to baseline values. The peak height (44% in this case) is obtained by averaging the data from 1 sec prior to 1 sec posterior to the maximum amplitude.

In this case, the functional activation was observed only in the third train of stimuli and although the flow response accomplishes with the validity signal

criteria described previously, the peak height derived is relatively small (11%) compared to the previous example. The reason for this lays in the fact that the peak height is derived from the average of all the 15 blood flow responses, with independence if there was not flow response during the first two trains of stimuli.

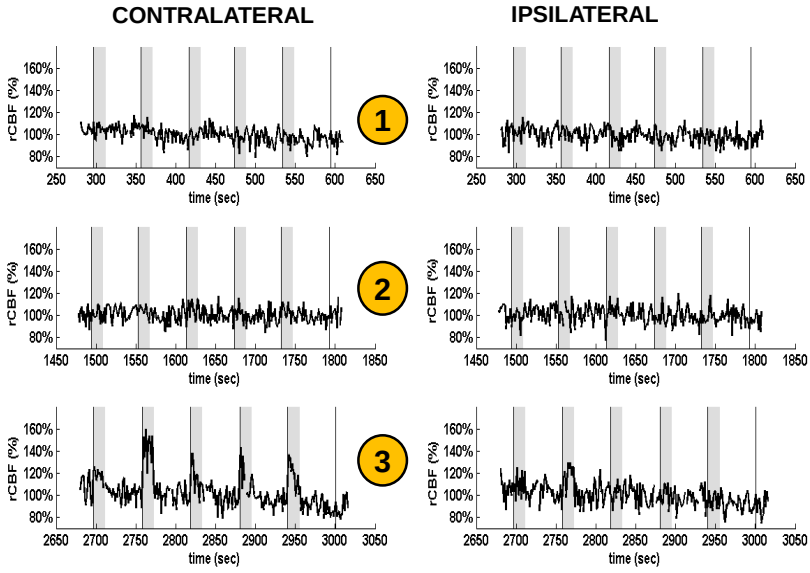

Figure 4.9: Example of contralateral rCBF trains of stimuli (left hemisphere) versus the ipsilateral response corresponding to rat 3 on the second week. Only the last train of stimuli induced a functional activation strong enough to be measured. The peak height derived is relatively small (11%) compared to the example derived from Figure 4.8 because it was built from the average of all the 15 blood flow responses with independence if the evoked functional activation was not observed in the first two trains of stimuli. Measurement started (time=0) 25 min after the bolus injection.

4.3.3.2 18 months old animals

All the animals presented in this section (n=7) were measured once per week during two consecutive weeks using 6Hz stimulation. The average blood flow response was obtained for all the animals and the peak height was derived in the same manner than the previous section. The values obtained for the peak heights in both hemispheres are represented in Figure 4.10. As before, the intra- and inter-individual variability shown in the results is caused by the same reasons explained previously.

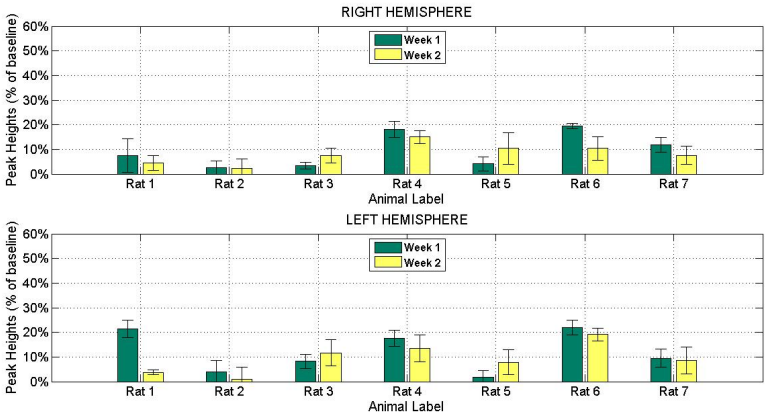

Figure 4.10: Right (Top) and left (Bottom) hemispheres peak heights versus animal label in the old group of animals over two different measurements.

4.3.3.3 Longitudinal study of a representative rat

In the next section I present a longitudinal case of one animal (rat 4) who was part of both cohorts of 6 and 18 months old experiments described previously.

The blood flow responses obtained with a year difference at 9Hz and 6Hz stimulus are compared in Figure 4.11.

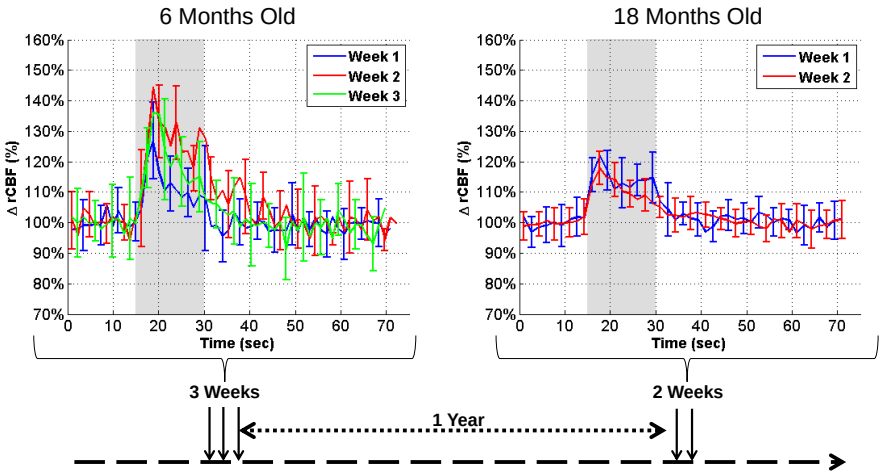

Figure 4.11: Left: Average rCBF signal in the right hemisphere of one animal during three consecutive weeks obtained at 9Hz stimulation frequency. Right: Average rCBF signal in the right hemisphere for the same animal measured one year later during two consecutive weeks obtained at 6Hz stimulation frequency.

In the left side of this plot we can see the blood flow responses to 9Hz stimulation obtained from the measurements carried out with the young rats. Although some differences in amplitude (within the errorbars), the three signals are in the same range and have similar shape. One year later, the same animal was measured during two consecutive weeks (right side of Figure 4.11) and the blood flow responses to 6Hz stimulation were similar in amplitude and shape.

As an overall, we can see that the blood flow responses obtained from both sets of experiments are very similar in terms of shape and amplitude although

this last one presents some attenuation for the older group of rats when compared to the young one.

Once again, all these signals have features similar to the flow signals obtained in the literature [97, 98].

4.4 Discussion

An initial evaluation of the evoked functional activation was carried out with fMRI which confirmed a normal physiological condition in all the animals presented on this study. The use of the implantable probe demonstrates that the evoked functional activation using this anesthesia protocol [102] can be measured with DCS. This approach was used in the past with a different anesthesia protocol [44, 79] and clearly presents some advantages like the low signal-to-noise ratio due to the absence of scalp or the possibility to visualize the skull to accurately place the probe over the right areas of interest. Also, the part of this probe which was fixed to the rat skull was made MRI compatible and therefore it allows to proceed with both optical and MRI experiments simultaneously.

However, the removal of the scalp made animals more sensitive to get infections and the fact that the probe was clamped to the skull might generate issues related to the animal growth. Furthermore, this issue is extended to optical techniques that involve the removal of the scalp or thinning the skull such as laser Doppler flowmetry (LDF) [27, 28, 75, 76], optical intrinsic signals imaging (OISI) [24, 70, 71, 88, 89] or laser speckle flowmetry (LSF) [29, 73, 74, 90]. In addition to this point, these techniques allow to proceed with superficial mea-

surements in contrast to the penetration depth of DCS that probes a relatively large tissue volume.

The surface probe eliminates the issues derived from surgical intervention and in combination with the absence of side effects in the anesthesia protocol used it guarantees a fully non-invasive approach which allows to proceed with longitudinal experiments [102, 104–106]. The results obtained with this probe present a stronger average rCBF signal in the young group of rats in response to 9Hz stimulation than the group of old rats with 6Hz stimulation. Also, the response to 9Hz is very similar to the response achieved at 3Hz stimulation. Regarding this point, one possibility is that the final signal obtained with the surface probe is weakened due to the partial volume effect [32, 108] of the rat scalp.

Within this context, the initial experiments carried out with 18 months old rats showed a very reduced response at 9Hz stimuli in contrast to stimulations induced at 6Hz stimulation which provided a clearer and stronger response. This response was also slower on its decay as shown on the fMRI results of Figure 4.4. For this reason, I utilized 6Hz as the stimulus frequency for the experiments with old rats. These differences between blood flow responses at different frequencies in the old population could be related to anatomical or physiological changes in the animal provoked by the elderly specimens (18 months old) and also could be linked to the differences in the peak heights when the young and the old populations are compared.

In relation to this point, the steps followed to place the surface probe over

the rat scalp involved using a plastic grid referenced to a set of landmarks that was designed based on an atlas [109]. One possibility is that the areas of interest (forepaw somatosensory regions) in the old rats stay out of the volume tracked by our probe. This could be caused by the growth of the animal which induces a *displacement* of our areas of interest [110] along the coronal direction.

Another factor to take into account comes from the fat accumulation on these old specimens which increases the width of the scalp and therefore it alters the penetration depth of the probe. Furthermore, dealing with such big animals presented some extra difficulties in terms of accommodating the animals in the stereotaxic frame and/or their tolerance to the anesthesia.

The results obtained with the surface probe in both populations did not show a 100% repeatability in the strength of the blood flow response but there is room for improvement. For instance, the method developed for probe positioning over the rat scalp can be implemented and new geometries involving a higher number of source-detector pairs can be built in future versions of this probe following the approach of *Boas el al.* in [99] or *Kawasima et al* in [111]. In relation to these points, it is important to highlight that the variability shown on Figs. 4.6 - 4.10 is also present in the results achieved by fMRI. Furthermore, similar variability was found within the somatosensory evoked potentials (SSEPs) derived from a forepaw stimulation in a previous study were fMRI and EEG signals were compared over weeks [112].

The nature of the anesthesia used in this study also plays a role in the quality of the results achieved. The neurovascular coupling is very sensitive

to anesthetics and sedatives [113–115] being reduced or suppress by many of them [113,115,116]. In consequence, animals present variability on their response to these substances and this inter individual variability may be exacerbated by several factors such as the stress, the age, the amount of fat in relation to body mass or the blood glucose among others.

Accordingly, by implementing the physiological conditions and therefore having a better control of the anesthetized animal we might be able to find out under which conditions the signal derived from the evoked functional activation can be maximized. An open possibility is that there is an *optimal temporal window for measurement* in terms of the physiological parameters under which the evoked blood flow response might be maximized. The existence of this window has not been confirmed yet and the features that characterizes it still remain unknown. However I am currently investigating on this direction.

4.5 Conclusion

The evoked functional activation in rats can be measured with both the implanted ans the surface probe using this particular anesthesia protocol that allows to proceed with longitudinal studies. The main advantage from the implantable approach comes from the relatively low signal-to-noise ratio caused by the absence of scalp and the accuracy in tracking the right regions of interest. Also, it permits to proceed with optical and MRI measurements simultaneously. However, its use involve exposing the animal to get infections after removing the scalp and the natural animal growth might also be an issue because part of

this probe is clamped into the rat skull. This fact suggest that the implantable approach might be more convenient for longitudinal studies of short duration (few weeks).

The surface probe eliminate this issues and permits to proceed with longer longitudinal studies (a year duration or longer eventually). This opens the possibility of studying chronic phases of neurodegenerative pathologies and possible recovery therapies.

5

Monitoring cerebral hemodynamics during early hours after stroke

5.1 Introduction & motivation

Stroke is the loss of brain function provoked by the interruption of blood flow supply in the brain which in the majority of cases is caused by an ischemia although it can also be produced by an hemorrhage.

In the case of ischemic stroke (IS) a thrombus (blood clot), an arterial embolus or a venous thrombosis partially or totally occlude a large cerebral artery impeding the regular blood flow supply. This lack of blood flow can also be produced by a cerebral hypoperfusion due to heart failure. In any case, the consequences of this interruption can be dramatic as they easily lead to long

term disabilities [117] or death.

Ischemic stroke is in fact one of the main causes of death [1, 2] in the West and the long term disabilities derived from it have a huge impact in terms of economical and human costs [118]. IS patients are often treated in specialized stroke units where their brains are closely monitored.

The National Institutes of Health Stroke Scale (NIHSS) [119] is an extended tool used to evaluate the impairment caused by stroke. This scale classifies the stroke severity into asymptomatic (0), minor (1-4), moderate (5-15), moderate to severe (16-20) and severe strokes (21-42). Neurologists also use the modified Rankin Scale [120] to estimate the degree of disability or dependence after stroke. This index ranges from 0 (no symptoms) to 6 (dead). In between, there are five levels from which disability is classified as no significant (1), slight (2), moderate (3), moderate-severe (4) and severe (5).

In order to reduce the damage derived from a IS, most of the medical interventions try to maximize the blood perfusion into the affected region. Some of this strategies involve intravenous hydration or withholding anti-hypertensive therapies. However, the blood perfusion depends on the cerebral perfusion pressure (CPP) [121] which is defined as the difference between the mean arterial pressure (MAP) and the intracranial pressure (ICP). Accordingly, another common medical practice to enhance the blood perfusion in IS patients is to lower the head-of-bed or keep the patient flat.

A rapid restoration of the blow flow has been proved to reduce brain damage [122] of IS patients. This fact makes timing to be also a key premise in most

of these clinical interventions. In relation to this point, the use in thrombolysis in the early hours after the stroke onset of recombinant tissue plasminogen activator (rtPA) has been found to improve the functional outcome of ischemic stroke patients [123].

Ischemic stroke patients are also classified depending on the time stage after the stroke onset [124]. For instance, patients within the first 6 hours after the stroke onset are referred as *hyper-acute* whereas the *acute* term is used in those patients between 6 and 48 hours after the stroke onset. The *subacute* stage covers a higher time period from the 48 hours up to 3 months and finally the *chronic* one is used in those patients after 3 months after the stroke onset.

Transcranial doppler (TCD) is the primary clinical modality for bedside monitoring of the cerebral hemodynamics in IS patients. However, TCD presents some limitations as its use is restricted to large vessels [16]. Furthermore, interpreting TCD results can be difficult sometimes as it works under the assumption that arteries keep a constant diameter [125]. In contrast, diffuse correlation spectroscopy (DCS) allows non-invasive transcranial (through scalp, skull, etc..) measurements of the cerebral hemodynamics [30–38].

The use of a head-of-bed (HOB) challenge alters the cerebral perfusion pressure and therefore induces changes in the cerebral blood blow. TCD has been used to monitor the effect of HOB challenge in the mean flow velocity (MFV) measured in occluded or partially recanalized middle cerebral artery (MCA) [126,127] and it was found an increase in the MFV when lowering the HOB angle.

On the other hand, the use of HOB in combination with DCS has been used

to study the cerebral hemodynamics in healthy patients and in scenarios where the cerebral autoregulation is impared, such as ischemic stroke or brain injured patients [33, 37, 38, 77].

For instance, *Edlow et al.* [38] studied the hemodynamics of a cohort of healthy subjects when lowering the HOB angle from 30° to 0° and estimated the induced mean (standard error) cerebral blood flow (CBF) change in 18% (±1.5%). Also, it was found that this change was independent from the age and the gender of the subjects.

Some other studies used the same protocol to monitor ischemic stroke patients during the acute stage. Thus, *Durduran et al.* [33] obtained a mean (standard error) CBF change of 30% (±7%) and 25% (±7%) in the ipsi and contra-infarct hemispheres when lowering the HOB angle from 30° to 0°. In contrast, *Favilla et al.* [77] estimated these changes in 17% (±4.6%) and 15% (±4.6%) in the ipsi and contra-infarct side using again the same HOB change.

In these two studies, the mean CBF changes obtained presented heterogenous distribution but this extended variability was not shown in healthy subjects [38] and it might reflect underlying pathophysiology [77]. Also, both studies presented a similar percentage (29%) of *paradoxical responders* (patients where the rCBF decreases when lowering the HOB) among their populations. Interestingly, the study carried out by *Favilla et al.* also included measurements of the MFV obtained through TCD from which these paradoxical responders could not be identified.

On the other hand, *Kim et al.* [37] used the same HOB protocol to study the

hemodynamics of a group of 10 brain-injured patients (subarachnoid hemorrhage, traumatic brain injury and arteriovenous malformation associated intracerebral hemorrhage) during the acute stage versus a control group of 10 healthy subjects. In compliance with the cohort of healthy subjects studied by *Edlow et al.* [38], the control group presented a mean (standard error) CBF change of 18% (±0.9%) when lowering the HOB angle from 30° to 0° whereas no change was found (0% ±2.8%) for the group of brain injured patients .

In this work I intend to take a step forward and to study the effect of a HOB challenge (described later) in a group of ischemic stroke patients within the first 12 hours after the stroke onset and to relate this with a set of medical parameters. The reason for focusing within this particular time stage was motivated by the fact that some early measurements (<6 hours) were missing for some patients. In order to facilitate the reading of this document, from now on I will refer as *hyper-acute* to the time stage within the first 12 hours after the stroke onset.

This study was developed based on the following hypothesis:

- The change in the head-of-bed angle causes a significant change in the rCBF for all the patients at all times and in both hemispheres.
- The change from 0° to 30° produces a decrease in the rCBF compared to the initial supine position.
- The rCBF dependence on the HOB angle is correlated to the subjects NIHSS at admission, 24 hours and at patient discharge.
- The rCBF dependence on the HOB angle is correlated to the modified

Rankin Scale as continuous variable or binary index measured three months after the stroke onset.

5.2 Methods

This study was performed in collaboration with Dr. Joan Martí and Dr. Raquel Delgado from the Stroke Unit of the Department of Neurology of Hospital de la Santa Creu i Sant Pau. All the methods described in this section have been approved by the Ethical Committee of Hospital de la Santa Creu i Sant Pau and written consent forms were provided from each patient surrogate.

5.2.1 Demographics

A total of 21 ischemic stroke patients were monitored in three different time stages as described in Table 6.1. The median of the age of the population was of 85 years old with an interquantile range of 20.5 years. Since I am interested in studying the blood flow response during the *hyper-acute* stage (<12 hours), I have focused on the 22 (6+16) measurements carried out within this time stage.

	<6 hours	>6 hours & < 12 hours	>12 hours
Measurements	6	16	20
Subjects	3	8	10

Table 5.1: Number of measurements and population before 6 hours, between 6 and 12 hours and after 12 hours after stroke onset.

The clinical status was evaluated in four time slots using the National Institutes of Health Stroke Scale (NIHSS). The first evaluation was carried out

when the patient arrived in the hospital, the second one was at 24 hours after the stroke onset, the third one at 48 hours after the stroke onset and the last one occurred at the patient discharge.

Most of the patients presented hypertension (90%) and half of them (48%) also presented high values of dyslipidemia or cholesterol. The incidence of diabetes melitus was of 24% and only the 19% of the population were active smokers. The 67% of the strokes occurred in the left brain hemisphere and a set of clinical variables was also included in the study such as *Thrombolisis* which is a categorical variable that indicates if the blocked artery has been recanalized (successful treatment), if it has not (unsuccessful treatment) or if this information is unknown.

Also, the condition of the *Internal Carotid Artery (ICA) Stenosis* was registered according to the following levels:

- 0 is referred to blockage of the ICA $< 50\%$, meaning normal artery condition.
- 1 is referred to blockage of the ICA $> 50\%$ and $< 70\%$.
- 2 is referred to blockage of the ICA $> 70\%$.
- 3 is referred to the complete occlusion of the ICA.
- 4 the ICA condition is unknown.

Another binary variable produced by the clinicians and defined as *Improvement* was included in the study. The criteria established by this variable states

that a given patient has improved its condition if there is a reduction in the NIHSS of 4 or more points 24h after the patient admission. The 24% of the patients in this study have been considered to have *improved* their condition according to this rule.

Finally, the modified Rankin Scale was also evaluated three months after the stroke onset and included in this study.

5.2.2 Blood flow response to orthostatic challenge

I aimed to study the hemodynamics of this group of IS patients by monitoring their blood flow response to the orthostatic challenge described in Figure 5.1. The optical probe used on these experiments has already been described in detail in Chapter 3.

The above mentioned challenge involved changing the HOB angle from an initial supine position to 30° and to return back to supine. This process was carried out on three time stages i.e 6 before hours, between 6 and 12 hours and after 12 hours of the stroke onset. I note here that not all subjects were measured at all three time points due to logistical reasons. The averaging time for each single measurement was of 2 sec and the data was collected for 10 minutes on each position.

The relative cerebral blood flow (rCBF) was obtained by normalizing the blood flow index (BFI) with the initial supine position.

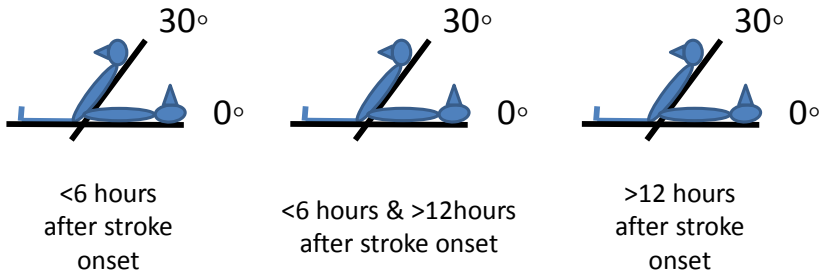

Figure 5.1: Orthostatic challenge used with AIS patients

5.2.3 Statistical analysis

I have used the R-Project GNU General Public License software (http://www.r-project.org) to build the statistical models. Thus, by fitting a linear mixed effects (LME) models (library "nlme" in R) [128], I explored the changes in the mean rCBF as a function of two factors. The first factor was the HOB angle and the second factor the remaining parameters described before. I used two-sided models and Type I error rate of 0.05. The level of the confidence intervals shown in the plots was of 95%.

5.3 Results

The CBF changes induced by the HOB challenge compared to the initial supine position in the ipsi-infarct (ipsi) and contra-infarct (contra) hemispheres were measured. The statistical analysis carried out with LME show no significant relation between the administration of the rTPA treatment, Thrombolisis or the

ICA Stenosis parameters and the blood flow response. With regards to the ICA Stenosis, the majority of the patients had a blockage of the ICA lower than 50% and therefore any dependence explored with this parameter lacks of statistical meaning.

The rCBF change induced at 30° for both hemispheres versus time after stroke (hours) is illustrated in Figure 5.2. The blue lines are fits to the data and the grey regions show the confidence intervals.

In the top part of this figure we can see that there is no dependency (p=0.808) between the rCBF and the time after stroke in the contra-infarct hemisphere. However, DCS was sensitive enough to identify five paradoxical responders (23% of total). The lower part of this plot shows the equivalent results found in the ipsi-infarct hemisphere. In here, the number of measurements with paradoxical response is up to six (27%) and there is a tendency (p=0.138) between the rCBF induced at 30° and the time after the stroke onset.

Some tendencies were also found between the rCBF in the ipsi-infarct hemisphere and the *Improvement* variable but we were not able to build any model due to the lack of strength in the statistics, provoked by the low number of patients who entered into this category (n=6). The high variability in the CBF change versus two groups of improved and non improved patients is illustrated in Figure 5.3. As we can see, the variable *Improvement* cannot be used as a factor to distinguish between both groups (p=0.558).

Similarly, no statistical significant correlations but tendencies were found when exploring the relation between the rCBF change and the NIHSS obtained

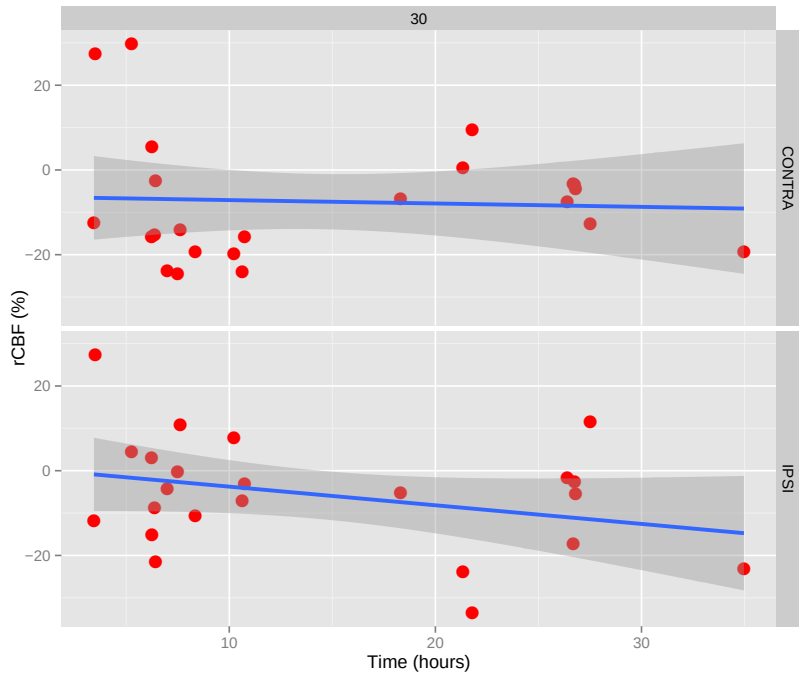

Figure 5.2: CBF changes in contra-infarct (Top) and ipsi-infarct (Bottom) hemispheres over time (hours after stroke onset) when head-of-bed position is increased to 30°. Both hemisphere present a similar percentage of paradoxical responders (23% and 27% respectively). There is no dependence on time after stroke in the contra-infarct hemisphere (p=0.808) where there is a the tendency (p=0.138) in the ipsi-infarct one. Blue lines are linear fits to the data and dark gray region are showing the confidence intervals.

at different time stages i.e (patient admission, 24 and 48 hours after the patient admission). This is illustrated in Figure 5.4 where we can see how the majority of the patients at hospital admission present a NIHSS index higher than 15. Due to the medical treatment, 24 hours later the NIHSS index gets reduced in some

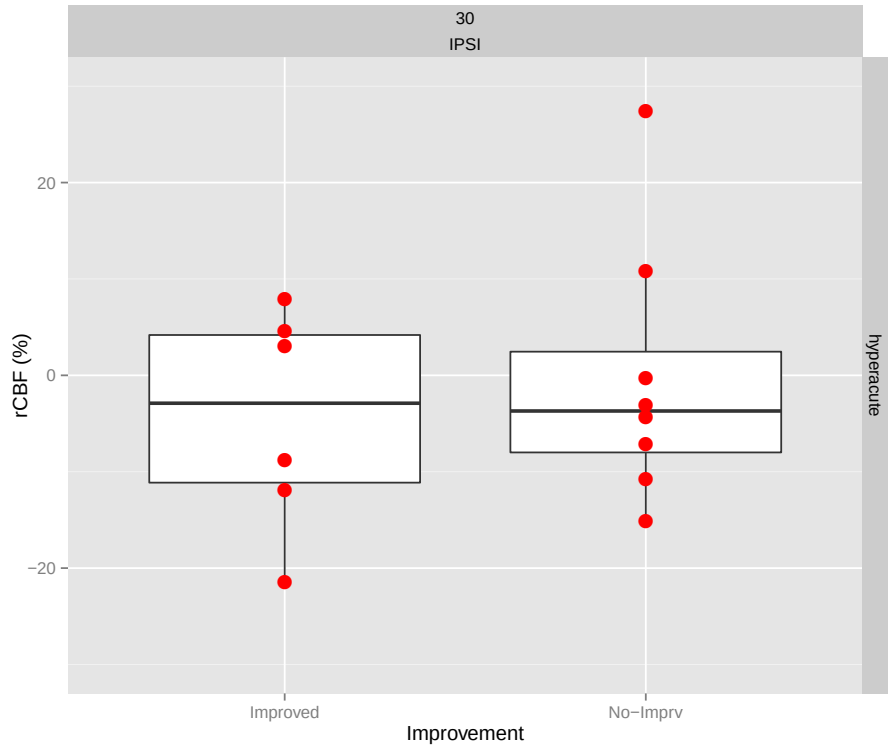

Figure 5.3: Boxplot of CBF changes at 30° in the ipsi-infarct (ipsi) hemisphere versus the Improvement parameter.

patients and it shows a more homogeneous distribution being this distribution very similar when obtained 48 hours after the patient admission. In these last two representations (middle and right plots of Figure 5.4) some trends (p=0.267; p=0.219) can be observed suggesting that patients with lower NIHSS have a higher (negative) CBF change in the ipsi-infarct hemisphere when moving the HOB from supine to 30 degrees.

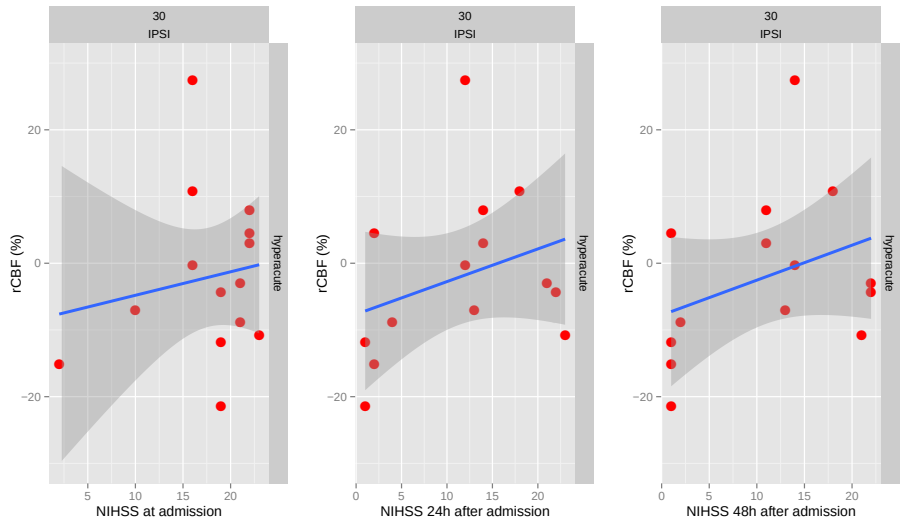

Figure 5.4: Left: CBF changes at 30° in the ipsi-infarct (ipsi) hemisphere versus NIHSS measured at the patient admission in hospital. Middle: CBF changes at 30° in the ipsi-infarct (ipsi) hemisphere versus NIHSS measured 24h after the patient admission.Right: CBF changes at 30° in the ipsi-infarct (ipsi) hemisphere versus NIHSS measured 48h after the patient admission. In all the plots,the blue line is the linear fit to the data and the dark gray region shows the confidence interval.

The NIHSS was also registered at the patient discharge. The rCBF change induced at 30° in the ipsi-infarct hemisphere versus three groups of NIHSS-based patients is represented in Figure 5.5. The first two groups were clustered according to lower/higher NIHSS than 10. The third one represented with the character x is related to those patients (n=4) who unfortunately passed away. Although this plot lacks of statistical significance, is interesting to see that three of the deceased patients did not shown any response to the HOB change and the

last one presented the strongest paradoxical response among the total population.

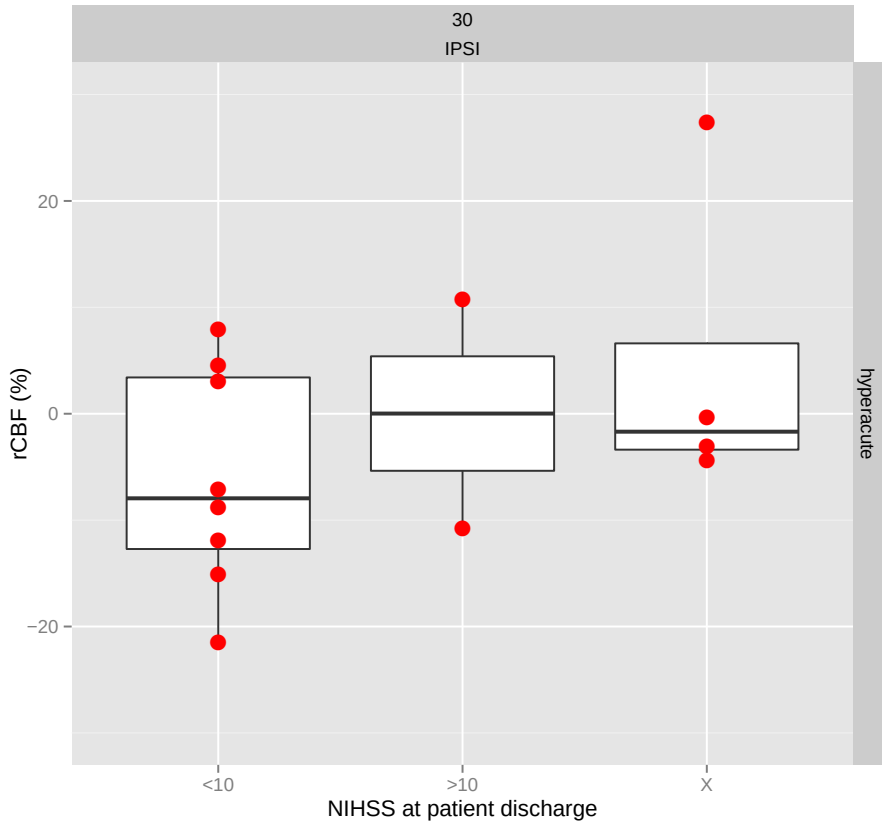

Figure 5.5: Boxplot of CBF changes at 30° in the ipsi-infarct (ipsi) hemisphere versus the NIHSS at discharge clustered in three groups. The first group contains the patients with NIHSS<10 whereas the second one is related to patients with NIHSS>10. The third one ("x") is related to deceased patients who did not survive. The patients within this group either did not show any response to the HOB change induced or they present the strongest paradoxical response.

On the other hand, statistical significant models were produced when explor-

ing the relation between the rCBF response to the orthostatic challenge during the hyper-acute stage versus the Rankin Scale obtained 3 moths after the stroke onset. The left plot of Figure 5.6 illustrates this change induced in the ipsi-infarct hemisphere at 30° versus the modified Rankin Scale as a continuous variable (p=0.012).

It can be seen that patients who present a higher change in the rCBF at 30° (negative values) during the hyper-acute stage also have better output (lower values of the modified Rankin Scale). The right plot of Figure 5.6 illustrates the same changes but considering the modified Rankin Scale as a binary index (p=0.002). As we can see, the paradoxical responders appear when the modified Rankin Scale is higher than 2. As before, patients who had a higher (negative) change in the ipsi-infarct hemisphere at 30° also presented a better output (modified Rankin Scale <=2) in contrast to the group of patients with modified Rankin Scale >2.

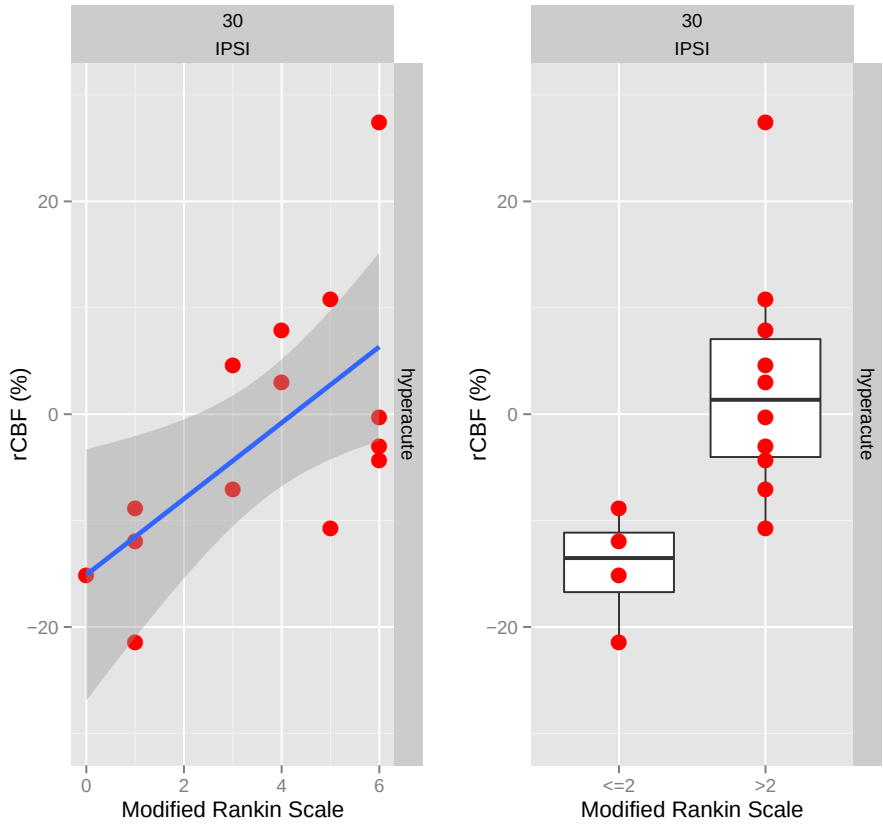

Figure 5.6: Left: CBF changes at 30° in the ipsi-infarct (ipsi) hemisphere versus Rankin Index as a continuous variable. The blue line is the linear fit to the data (p=0.012) and the dark gray region shows the confidence interval. Right: CBF changes at 30° in the ipsi-infarct (ipsi) hemisphere versus Rankin Index as a binary index (p=0.002).

5.4 Discussion

In this study, It was confirmed that the change in the head-of-bed has a significant effect on the rCBF response of ischemic stroke patients. The rCBF change compared to baseline values decreased in most of the patients when increased the HOB angle to 30°. However, in 24% of the measurements we found paradoxical responses in the contra-infarct hemisphere versus a 28% when considering the ipsi-infarct hemisphere. In any case, both percentages are in compliance with similar studies where the population of paradoxical responders was about 29% [33, 77].

I have explored the relation of the rCBF with many variables using linear mixed efffects (LME) models. No statistical findings revealed a dependence between the rCBF changes and the use of recombinant tissue plasminogen activator (rTPA) and the *Thrombolisis* and *ICA Stenosis* parameters. In this regards, the low number of patients which show reperfusion upon successful thrombolisis in large vessels might not be enough to find any dependence in the microvasculature. Similarly, since the majority of patients had a blockage of the ICA lower than 50%, any dependence explored with this parameter lacks of statistical meaning.

On the other hand, the results obtained when exploring the dependence between the rCBF induced at 30° measured in the ipsi-infarct hemisphere and the time after the stroke onset suggest some improvement in the cerebral vasculature in some patients which is reflected in the rCBF increase (negative values) with the time after the stroke onset.

Some tendencies were found between the rCBF in the ipsi-infarct hemisphere

and the *Improvement* variable (which is based on the NIHSS) for the 0° to 30° but we were not able to build any model due to the lack of strength in the statistics. Similarly, some other tendencies were found when exploring the relation between the rCBF induced at 30° and the NIHSS obtained at 24 and 48 hours after the stroke onset. This relation did not apply when considering the NIHSS values obtained at the patient admission as most of the NIHSS values are located around the same area (>15). Moreover, when exploring this relation at the patient discharge, no statistical significant results were obtained either. However, it was found that the small group of deceased patients did not show any blood flow response to the orthostatic challenge but one patient who show a strong paradoxical response. This finding seems to be related to the impairment of the cerebral hemodynamics on these patients and it is in compliance with previous results found in brain-injured patients [37] .

Finally, a statistical significant dependence was found between the CBF changes at 30° and the modified Rankin Scale measured three moths after the stroke onset. In this regards, the fact of have found statistical significant dependence using a *functional* scale (modified Rankin Scale) versus some tendencies when using instead a stroke scale (NIHSS) could be related to the fact that stroke scales only partly explain functional health [129]. This results suggest that by studying the hemodynamic response of ischemic stroke patients in the early hours after the stroke onset, we might be able to predict the patient output according to the modified Rankin Scale three months after the stroke onset.

5.5 Conclusion

The measurement of the rCBF response to an orthostatic challenge in the early hours after the stroke onset has reveal to provide promising information that can be used to predict the outcome of patients according to the functional modified Rankin Scale. DCS has proved again its capability in identifying paradoxical responders which might open the gate to *ad hoc* treatments by simply using the HOB in terms of maximizing the blood flow reperfusion into the infarcted area.

6

Cerebral hemodynamics of Obstructive Sleep Apnoea patients in response to orthostatic challenge

6.1 Introduction & motivation

The obstructive sleep apnoea (OSA) syndrome is characterized by the presence of total (apnoeas) or partial (hypopnoeas) collapse of the upper airway during sleep that affects 2-4% of the general population [130]. OSA syndrome symptoms include snoring, daytime sleepiness, morning headache, sexual dysfunction, mood and behavioral disorders, increased rate of traffic and occupational accidents and impaired quality of life [131]. The combination of these factors produce considerable economical costs which account for millions of dollars per year [132].

Each apnoea or hypopnoea event produce an episode of hypoxia-reoxygenation, increased autonomic activity and changes in intrapleural pressure. These mechanisms promote atherogenesis by different pathogenic pathways as oxidative stress, endothelial dysfunction [133, 134], hypercoagulability and metabolic disorder as insulin resistance [135].

These multi factorial processes are involved as pathogenic factors in the development to OSA syndrome as a cardiovascular risk factor with increased cardiovascular morbidity [136] such as hypertension, ischemic heart disease, stroke [7, 8, 137], arrhythmia, chronic heart failure and cardiovascular mortality especially in middle-aged population [11, 138–140]. OSA syndrome treatments cover medication, oral appliances and surgery among some other methods. However, the application of a *continuous positive airway pressure* (CPAP) therapy is of great use in improving the condition of OSA patients [141].

The diagnosis of this sleep disorder is performed by a sleep study (polysomnography or respiratory polygraphy). Among all the information derived from this type of study, there are a set of key parameters from which physiologists obtained the most important information in terms of diagnosing OSA syndrome (A full set of acronyms are included at the end of this chapter). They are basically the following:

- *The Mean Arterial Oxygen Saturation*, which is the mean value of SpO_2 over the night sleep.
- *The Minimum Arterial Oxygen Saturation*, which is the minimum value of SpO_2 over the night sleep.

- *CT90* which is defined as the percentage of time during the study where the SpO_2 was lower than 90%.

- *ODI4*%, the oxygen desaturation index at 4%. It is defined as the number of times per hour where the values registered for SpO_2 decrease 4% due to an apnoea.

In addition, the Epworth Sleepiness Scale [142] is an external parameter that can be helpful in diagnosing sleep disorders and basically consist in measuring the daytime sleepiness by using a questionnaire which is filled by the patient.

The severity of this syndrome is defined by the Apnoea-Hypopnoea Index (AHI) (number of apnoea and hypopnoeas events/sleep hour) from which OSA patients are classified as Severes (AHI$\geq$30), Moderates (15$\leq$AHI$<$30) and Milds (5$\leq$AHI$<$15). Patients with AHI$<$5 are considered as Healthy subjects or Non-OSA. Within this contex, the presence of an AHI$>$15 is associated with increased cardiovascular risk, with or without associated symptoms, and this risk is much higher for patients with an AHI$>$30 [143].

One of the hypotheses associated to the increased risk of strokes in OSA patients is related to impairments or alterations of cerebrovascular reactivity (CVR) [144] or cerebral autoregulation (CA) [10]. Cerebral vascular reactivity is an index of the capacity of the cerebral vessels to adapt to the metabolic demands of the brain and an autoregulation system to maintain a relatively constant blood flow during fluctuations in its perfusion pressure [145]. Since OSA patients present decreased cerebral autoregulation, they would have a lower compensating cerebral blood flow response to changes in pressure and this impairment of

cerebral autoregulation likely contributes to the increased incidence of stroke, as well as the poor outcome after stroke [12, 13].

Diffuse correlation spectroscopy (DCS) has been used to study the cerebral hemodynamics in humans [30–38]. In this regards, when studying of the cerebral autoregulation it is quite common to provoke a controlled change in the cerebral perfusion pressure to induce a change in the cerebral blood flow (CBF). For instance, the CBF response to bilateral thigh pressure cuff inflation/deflation protocol has been studied with DCS [36] and it was found that OSA patients present a significantly lower decrease in the CBF (-17%) when compared to a healthy control group (-26%).

Another common option to study the cerebral hemodynamics comes from the use of a head-of-bed (HOB) challenge. In this context, transcranial doppler (TCD) has been used to monitor the effect of HOB challenge in the mean flow velocity (MFV) [125–127, 146] but this technology presents some limitations as its use is restricted to large vessels [16] and the results derived from it must be interpreted carefully because TCD works under the assumption that arteries keep a constant diameter [125]. In contrast, DCS permits to study the cerebral microvasculature through a non-invasive transcranial (through scalp, skull, etc..) approach. The cerebral hemodynamics derived from a HOB challenge have been studied with DCS in both a cohort of healthy subjects [38] and different groups of patients with impaired cerebral autoregulation caused by neurological diseases such as ichemic stroke or brain-injured [33, 37, 77].

In these studies [33, 37, 77], measurements were initiated with the patient sit

at 30° angle and the change in the cerebral blood flow according to this initial position was obtained when lowering the HOB angle from 30° to 0° (supine position).

The mean (standard error) relative cerebral blood flow for the above mentioned HOB change was estimated in 18% (±1.5%) for the cohort of healthy subjects [38] and it was also found to be age and gender independent. It contrast, when studying ischemic stroke patients, *Durduran et al.* [33] obtained a mean (standard error) CBF change of 30% (±7%) and 25% (±7%) in the ipsi- and contra-infarct hemispheres whereas *Favilla et al.* [77] estimated these changes in 17% (±4.6%) and 15% (±4.6%) in the ipsi- and contra-infarct respectively. The heterogeneous distribution in the CBF change present in these last two studies is suggested that might reflect underlying pathophysiology [77] in contrast to the study of healthy subjects [38] where this extended variability was not shown. Furthermore, both cohorts of ischemic stroke patients had similar percentages (around 29%) of *paradoxical responders* (patients where the rCBF decreases when lowering the HOB or the other way around) being those patients undetectable through TCD measurements [77].

Kim et al. [37] also compared the hemodynamic responses of one group of 10 brain-injured patients (subarachnoid hemorrhage, traumatic brain injury and arteriovenous malformation associated intracerebral hemorrhage) versus a control group of 10 healthy subjects using the same HOB protocol. No change was found (0% ±2.8%) for the group of brain injured patients whereas the control group presented a mean (standard error) CBF change of 18% (±0.9%) being

this results in compliance with the cohort of healthy subjects studied by *Edlow et al.* [38].

Since OSA patients might present impaired cerebral autoregulation, I intend to study the hemodynamic response to an orthosthatic challenge of a group of OSA patients and to compare their cerebral hemodynamics with a control group of healthy subjects. Furthermore, this study was developed to explore if AHI-based groups of OSA patients show different cerebral blood flow responses and to find out if the CVR may correlate with key respiratory parameters.

Thus, the objectives of this study can be summarized as follows:

- To explore if AHI based groups of OSA patients show different responses to an orthostatic stress test.
- To study the CA of the OSA patients versus the Non-OSA along the orthostatic challenge.
- To study possible correlations between the blood flow responses and a set of respiratory parameters.

On the other hand, the oxy- and deoxy-hemoglobin concentrations were also obtained during the orthostatic test -hence the design of the probe described in Chapter 3- but this part of the study is still in preparation. Furthermore, this study was part of a more extended project on which the hemodynamics of the severe OSA patients were studied during a *Splitted Night* where patients sleep half of the night without any treatment whilst a CPAP treatment is applied in the second part. This is the reason why the optical probe had to be CPAP

compatible. This study (also in preparation) consisted in a polysomnography (PSG) in combination with blood flow measurements obtained with DCS carried out to monitor how effective the CPAP treatment was in OSA patients.

As an overall, these studies also give us the opportunity to explore the feasibility of DCS as a diagnostic tool in a cohort of patients which might have different levels of impaired cerebral autoregulation.

6.2 Methods

This study was performed in collaboration with MD. Mercedes Mayo, MD. Ana Fortuna and Dr. Anna Mola from the Sleep Unit of the Department of Respiratory Medicine of Hospital de la Santa Creu i Sant Pau, Barcelona, Spain. All the methods described in this section have been approved by the Ethical Committee of Hospital de la Santa Creu i Sant Pau and written consent forms were provided from each patient. The OSA patients enrolled in this study were derived from the Sleep Unit after successfully passing through an exclusion criteria which covered the following points:

- Patients older than 80 years old.
- Patients which received a previous CPAP treatment.
- Patient with chronic obstructive pulmonary disease (COPD)
- Patients with neuromuscular diseases.
- Patients with previous Ischemic Stroke.

- Patient who refuse to participate in the study.

6.2.1 Sample size and demographics

A cohort of 83 patients (63.9% Males) conformed the population of this study. Table 6.1 reflects the distribution of patients according to the AHI classification.

	Non-OSA	Mild	Moderate	Severe
Population	14 (16.9%)	29 (34.9%)	12 (14.5%)	28 (33.7%)

Table 6.1: Number and percentage of patients splitted by AHI group

Some patients presented hypertension (24%), dyslipidemia or cholesterol (18%) and diabetes melitus (14%). The 51.5% of the population were conformed by non-smokers whilst the 33% and 15.5% of them were former and active smokers. The body mass index (BMI) showed a distribution 36.1% of overweighted ($25 \leq BMI < 29.99$) and 24.1%, 9.6% and 7.2% of obese mild ($30 \leq BMI < 34.99$), obese moderate ($35 \leq BMI < 39.99$) and obese morbid ($BMI \geq 40$) patients respectively.

The 3.6% of the patients (n=3) presented asthma and one subject had a previous transient ischemic attack (TIA). The remaining patients did not present other respiratory or neuro pathology (chronic obstructive pulmonary disease, ischemic stroke and others diseases). Cardiopathologies (coronary artery disease (CAD), heart failure (HF) and other diseases) were not relevant on 95.2% of the population.

The median and interquantile range (IQR) was obtained for the BMI, AHI, age and Epworth Sleepiness Scale as shown in Table 6.2. A similar description

related to the respiratory variables can be found on Table 6.3 which shows how the severe group is affected by parameters such as the CT90 (16.2% of the time with SpO_2 lower than 90% during sleep) or the ODI4% (63.5 occurrences where SpO_2 drops 4% due to an apnoea per hour sleep). These values are reduced for the remaining groups. Thus, the moderate group presents a 1.4% for the CT90 and 15.2 occurrences for the ODI4% whereas the mild group has a 0% for the CT90 and 5.7 occurrences for the ODI%. Finally, the control group of Non-OSA patients presents a 0% for the CT90 and 1 occurrence for the ODI%.

	Total	Severe	Moderate	Mild	Non-OSA
BMI (Kg/m^2)	28.5 (8)	32.6 (5.6)	26 (4.4)	28.2 (7.1)	23.5 (3.5)
AHI (Apnoeas/hour)	14.3 (39.8)	73.5 (37.9)	19 (2)	9.4 (4.9)	2 (2.9)
Age (Years)	54 (13.5)	58 (10.2)	52.5 (14.2)	54 (12)	52.5 (15.5)
Epworth (a.u.)	10 (8)	11.5 (7.2)	10 (7)	12 (7)	7 (4)

Table 6.2: Demographics of patients (median and IQR in brackets) splitted by AHI group

	Total	Severe	Moderate	Mild	Non-OSA
Mean SpO_2 (%)	94 (3)	93 (3)	95 (2)	95 (2)	95.5 (1)
Min SpO_2 (%)	86 (13)	76 (10.5)	84 (8)	88 (5)	91.5 (3)
CT90 (%)	0.4 (10.6)	16.2 (16.7)	1.4 (3.1)	0 (0.3)	0 (0)
ODI4% (occurrences)	11.1 (38.1)	63.5 (32.6)	15.2 (9.7)	5.7 (6.9)	1 (2.4)

Table 6.3: Respiratory parameters of patients (median and IQR in brackets) splitted by AHI group

6.2.2 Blood flow response to orthostatic challenge

In this study I have utilized a modified version of the orthostatic challenge used to monitor the hemodynamics of acute ischemic stroke patients [33, 77].

This protocol involved changing the head-of-bed (HOB) angle in the following sequence: 0° to 30° to 0° to 20° to -8° to 0°. The angle corresponding to 30° involves tilting only the back of the bed while the 20° tilts the whole bed as illustrated Figure 6.1.

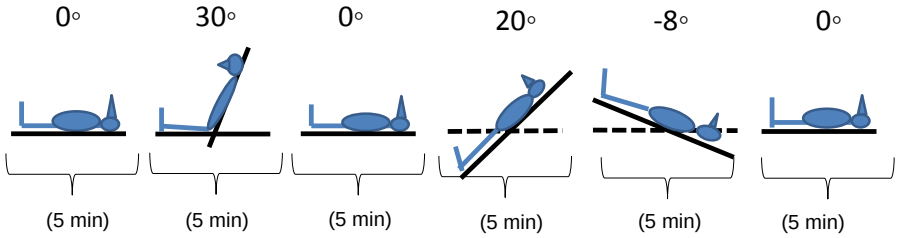

Figure 6.1: Diagram of the orthostatic challenge employed in this study.

In order to initiate the experiment with stable CBF values, patients remained in a comfortable supine position for 15 minutes prior to start the measurement. During the experiment, patients stayed for 5 minutes at each HOB position.

The relative cerebral blood flow (rCBF) was obtained by normalizing the blood flow index (BFI) obtained for each HOB angle with the mean BFI corresponding to the initial supine position.

I was also interested in exploring the absolute change in the CBF any time I move the patient along the orthostatic challenge by looking at a new parameter called *Self Normalized rCBF* (SNORM rCBF) by normalizing all the BFI values for a given angle with the mean BFI value that corresponds to the previous HOB position.

In both cases, the rCBF and the SNORM rCBF were averaged for each HOB

stretch but the values obtained during the initial and the last minute on each HOB position were discarded to avoid transient effects. In consequence both parameters presented a unique mean value per HOB angle.

In some occasions patients sneezed or coughed accidentally provoking alterations in the BFI measurements. A filtering process was therefore applied to get rid of any value of the rCBF or the SNORM rCBF higher than twice the standard deviation on each averaging stretch.

I also monitored the mean arterial pressure (MAP), the arterial oxygen saturation by pulse oximetry (SpO_2) and the heart rate (HR) in 25 patients at each head of bed position. The MAP was registered in the middle of each HOB position whilst the SpO_2 and HR were measured one minute after locating the patient on a given position and one minute prior to change it and then both values were averaged.

6.2.3 Adapted Instrumentation

I have utilized a portable set-up described in Chapter 3. I note that I have used a probe designed for a sleep study in a subset of the population since we desire the ability to compare the results. The hybrid probe developed had to be located over the patient's forehead as shown on Figure 6.2 in a manner that was not affected by the movement of the patient and allowing to place some other sensors like electrodes, microphones or any medical hardware related to the use of a polysomnography.

Also, the probe had to allow the implant/removal of a *continuous positive*

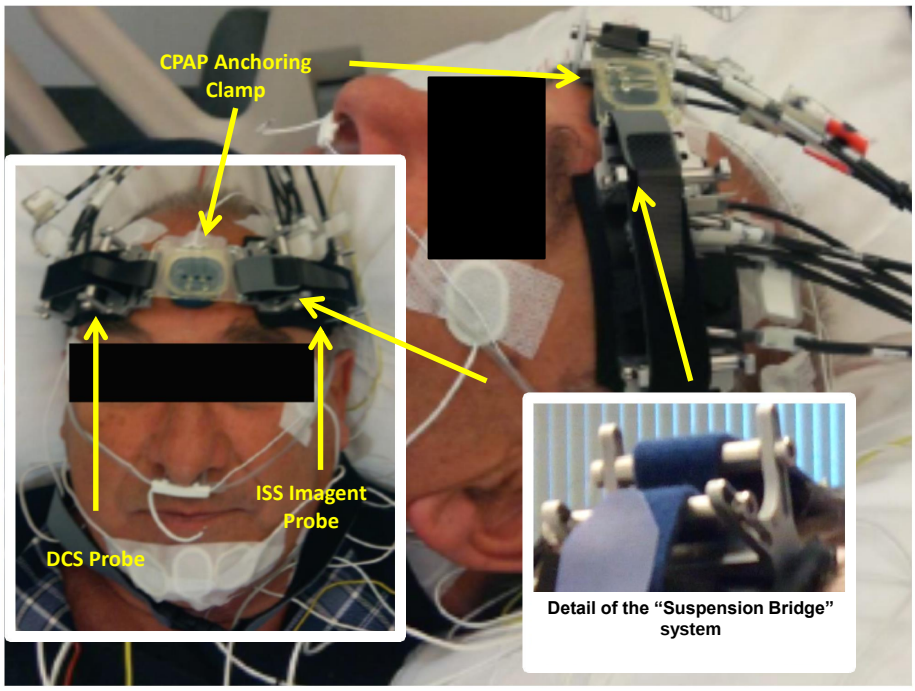

Figure 6.2: Overview of the hybrid probe on the patient's forehead during a polysomnography.

air pressure (CPAP) mask when necessary with the minimum impact possible on the optical measurement. This problem was solved by utilizing the straps of the CPAP mask on an adjusting system based on the forces developed on the structure of a *suspension bridge*. The key part of the system were two metallic pieces shown in bottom right side of Figure 6.2. The system worked in a way that the stronger the CPAP straps were tighten up, the stronger the probe was attached, adapting its form to the shape of the patient forehead.

6.2.4 Statistical analysis

As in chapter 5, I have used the R-Project GNU General Public License software (http://www.r-project.org) to build two types of statistical models. In the first one, by fitting a linear mixed effects (LME) models (library "nlme" in R) [128], I explored the changes in the mean rCBF and mean SNORM rCBF as a function of two factors. The first factor was the HOB angle and the second factor the remaining clinical and respiratory parameters. On the second type, I proceed in the same way but focusing on the 0° to 30° change and therefore excluding the HOB angle as a factor from the models. In both cases, I used two-sided models and Type I error rate of 0.05. The level of the confidence intervals shown in the plots was of 95%. Also, Pearson product-moment correlation coefficients were obtained to explore linear correlations between two variables and paired T-Test were used to determine if two sets of data were significantly different from each other.

6.3 Results

6.3.1 Mean arterial pressure, arterial oxygen saturation and heart rate during the orthostatic challenge

The results obtained for the mean arterial pressure (MAP), the arterial oxygen saturation (SpO_2) and the heart rate (HR) for all the HOB angles can be visualized on Figure 6.3. A paired T-Test was carried out to find out if changes on the MAP, SpO_2 and HR along the orthostatic challenge were statistically

different from the first supine position. As it can be seen on Table 6.4, MAP has a statistically significant *change* when the head is elevated at 30° and 20° respect to the initial supine position whereas the SpO_2 has the same significance at 30° only (although the pvalue corresponding at 20° is quite close to 0.05).

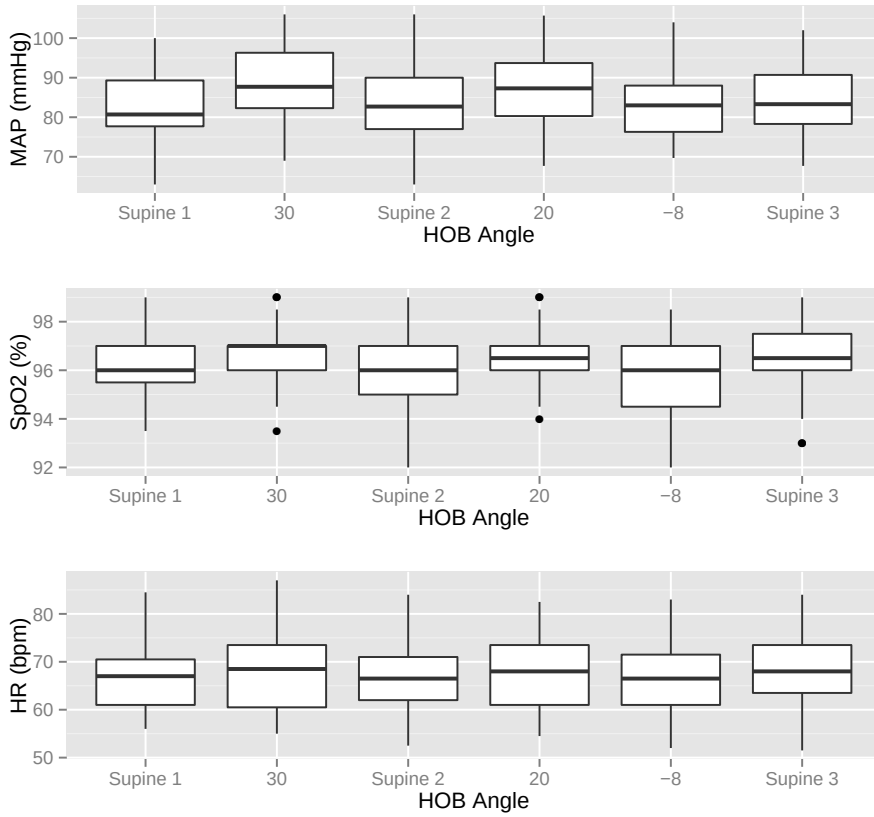

Figure 6.3: Top: Distribution of the mean arterial pressure (MAP) values at each HOB angle. Middle:Distribution of the arterial oxygen saturation (SpO_2) values at each HOB angle. Bottom: Distribution of the heart rate (HR) values at each HOB angle.

	ΔMAP (mmHg)	ΔSpO_2 (%)	ΔHR (bpm)
Supine 1 vs 30°	-5.30 (< 0.001*)	-0.54 (0.006*)	-0.74 (0.396)
Supine 1 vs Supine 2	-1.08 (0.089)	-0.04 (0.863)	0.88 (0.230)
Supine 1 vs 20°	-3.26 (< 0.001*)	-0.42 (0.054)	-0.06 (0.948)
Supine 1 vs −8°	-0.52 (0.495)	0.3 (0.181)	1.18 (0.206)
Supine 1 vs Supine 3	-1.16 (0.273)	-0.042 (0.129)	0.4 (0.735)

Table 6.4: Changes (pvalues) in the mean arterial pressure (MAP), the arterial oxygen saturation (SpO_2) and the heart rate (HR) of 25 patients when comparing HOB angles. The MAP has a statistically significant change when the head is elevated at 30° and 20° respect to the initial supine position whereas the SpO_2 has the same significance at 30° only (although the pvalue corresponding at 20° is quite close to 0.05). Both parameters do not change significantly when patients are put back in supine positions or at −8°. The heart rate does not change significantly along the orthostatic test when compare to the initial supine position

As expected, both parameters do not change significantly when patients are put back in supine positions or at −8°. Finally, the heart rate does not change significantly along the orthostatic test when compare to the initial supine position.

6.3.2 Blood flow response along the orthostatic challenge

The results obtained per group and HOB angle for the rCBF and SNORM rCBF are contained on Tables 6.5-6.6.

These results show *homogeneity* among the blood flow responses of all the groups at the initial 0° to 30° change. However, this homogeneity is broken for the remaining HOB angles. This is illustrated in Figure 6.4. As we can see, the CBF response is similar for the groups in the initial HOB change. After that, the blood flow response for the OSA groups clearly diverge when compared to

	TOTAL	SEVERE	MODERATE	MILD	NON-OSA
0° to 30°	-17.1 (1.1)	-16.2 (2)	-17.7 (2.3)	-17.5 (1.8)	-17.3 (2.7)
30° to 0°	4.5 (1.4)	7.5 (2.5)	8.1 (3.6)	4.4 (2.5)	-4.4 (2.5)
0° to 20°	-10.2 (1.7)	-6.1 (3)	-9.3 (4)	-11.6 (2.5)	-16.5 (4.5)
20° to -8°	14.9 (2.2)	17.5 (3.7)	21.3 (4.5)	17.4 (4.1)	-0.7 (4.5)
-8° to 0°	11.2 (2.1)	16 (3.7)	19.1 (4.8)	11.5 (3.2)	-5.6 (4.3)

Table 6.5: rCBF values (in %): Mean and Standard Error of the Mean (SEM) per patient type and HOB angle. The mean blood flow responses of all the groups at the initial 0° to 30° change presents *homogeneous* values (-17.1%, -16.2%, -17.7%, -17.5% and -17.3%). This *homogeneity* is broken for the remaining HOB changes.

	TOTAL	SEVERE	MODERATE	MILD	NON-OSA
0° to 30°	-17.1 (1.1)	-16.2 (2)	-17.7 (2.3)	-17.5 (1.8)	-17.3 (2.7)
30° to 0°	27 (2)	29.6 (3.6)	31.3 (2.3)	27.9 (3.9)	16.4 (2.9)
0° to 20°	-14.1 (1.1)	-12.8 (1.6)	-16.3 (2)	-15 (1.9)	-12.8 (4)
20° to -8°	29.1 (1.9)	26.5 (3.3)	34.7 (3.2)	33.5 (3.3)	20.4 (4.1)
-8° to 0°	-3 (0.7)	-1.2 (1.2)	-1.9 (1.5)	-4.4 (1.4)	-4.9 (0.9)

Table 6.6: Self-Normalized rCBF values (in %): Mean and Standard Error of the Mean (SEM) per patient type and HOB angle. The absolute change in the blood flow response present similar range within the first HOB change. After that, the SNORM rCBF values starts diverging, particularly when comparing the OSA versus the Non-OSA populations.

the control group of healthy subjects. For instance, when we look at the second and third supine positions we can see how distribution of rCBF values is mostly located in the positive Y axis. In contrast, the distribution obtained for the healthy control group is closer to zero and most of its distribution is located in the negative Y axis.

This effect is more clear when looking at the absolute CBF change (SNORM rCBF) versus the reordered HOB angles going from positive to negative angles. This is illustrated in Figure 6.5. As we can see, changes of similar magnitude in

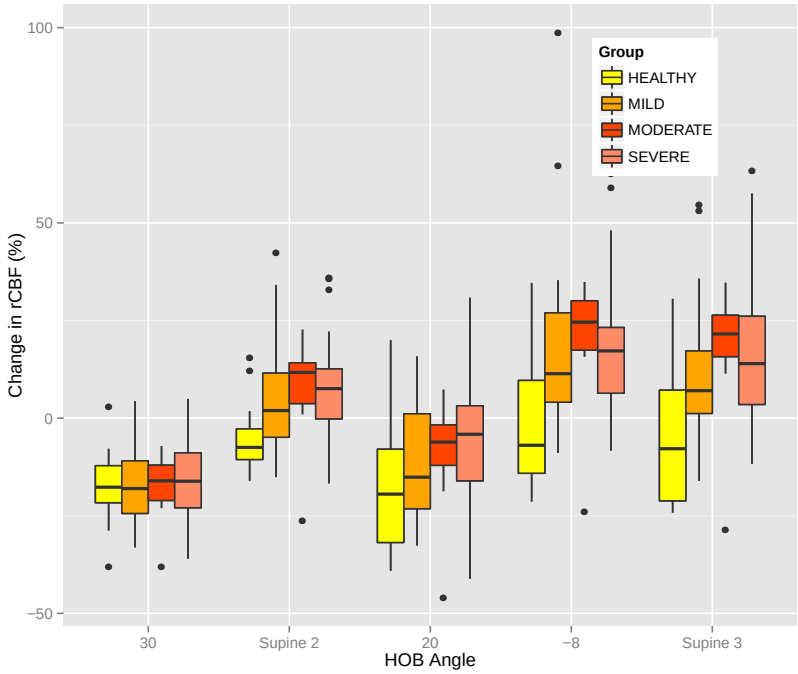

Figure 6.4: Distribution of the blood flow responses per group obtained along the orthostatic challenge when normalized with the initial supine position. The initial 0° to 30° change induce a similar response in all the groups. Right after, the blood flow responses for the OSA groups clearly diverge when compared to the control group of healthy subjects.

the HOB (30°,−30° and −28°) seem to produce different blood flow responses for the different groups. Thus, the blood flow change in absolute value for the OSA groups seems to be higher at −30° and −28° when compared to the 30° change. In contrast, the flow response obtained for the control group at −30° and −28° seems to be in compliance with the initial change of 30°.

The results obtained in Table 6.7 confirmed that these changes at −30° and

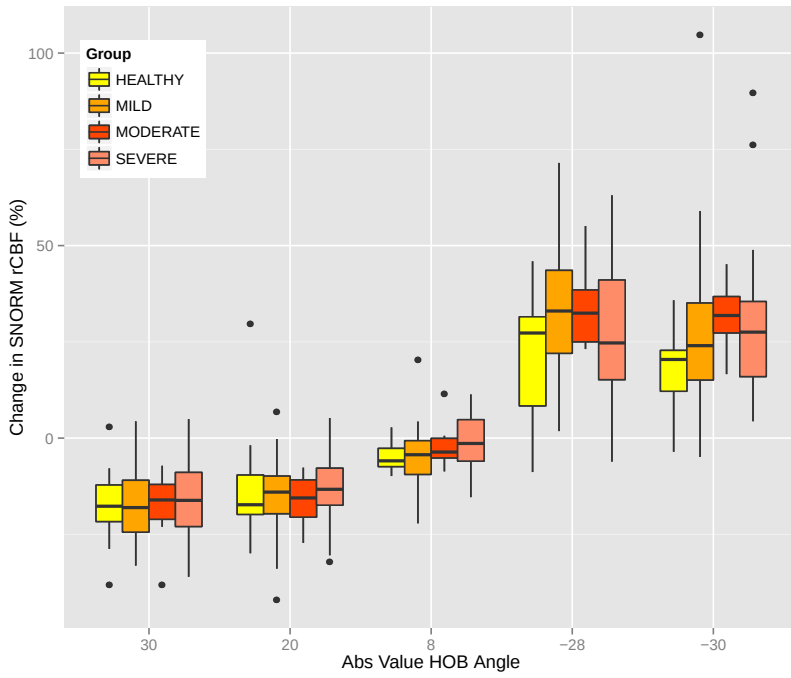

Figure 6.5: Self-Normalized rCBF boxplot for all different groups versus HOB angles. Changes of similar magnitude in the HOB (30°,−30° and −28°) produce different blood flow responses for the OSA and Non-OSA groups. These changes are higher for the OSA groups at −30° and −28° when compared to the 30° change. In contrast, the flow response obtained for the control group at −30° and −28° is in compliance with the initial change of 30°.

−28° were statistically different than the initial change induced at 30° for all the OSA groups. In contrast, these changes were the *same* for the control group of healthy subjects.

The *increase* in the Self-Normalized rCBF when moving along the HOB angles axis for all the OSA groups illustrated previously on Figure 6.5 have

	30° vs -30°	30° vs -28°	-30° vs -28°
Total	< 0.001*	< 0.001*	0.286
Severe	< 0.001*	0.001*	0.405
Moderate	0.003*	< 0.001*	0.355
Mild	0.003*	< 0.001*	0.133
Non-OSA	0.704	0.414	0.192

Table 6.7: T-test pvalues comparing the Self-Normalized rCBF for the HOB angles at 30°,-30° and -28°. In the OSA groups, the changes induced at -30° and -28° are statistically different than the initial change induced at 30°. In contrast, these changes are the *same* for the control group of healthy subjects.

encouraged us to explore if there is any dependence between that increase and the HOB angle that might be correlated with all the parameters and groups involved on this study.

For that purpose, I have produced a linear fitting with the Self-Normalized rCBF per patient versus the ordered HOB angles and added the slope of these fitting as a new parameter called *Slope*. This concept is illustrated in Figure 6.6. The top part of this graph shows the boxplot values for the Self-Normalized rCBF versus the ordered HOB angles whereas the bottom part illustrates the concept of the *Slope* by showing some linear fittings for all the groups of patients.

6.3.3 Exploring the dependence of the blood flow response on the clinical and respiratory parameters

I have initially explored any possible dependence between the rCBF and the remaining parameters by using Pearson's correlation coefficient tests. Several models were created by exploring the dataset as a global and also by clustering

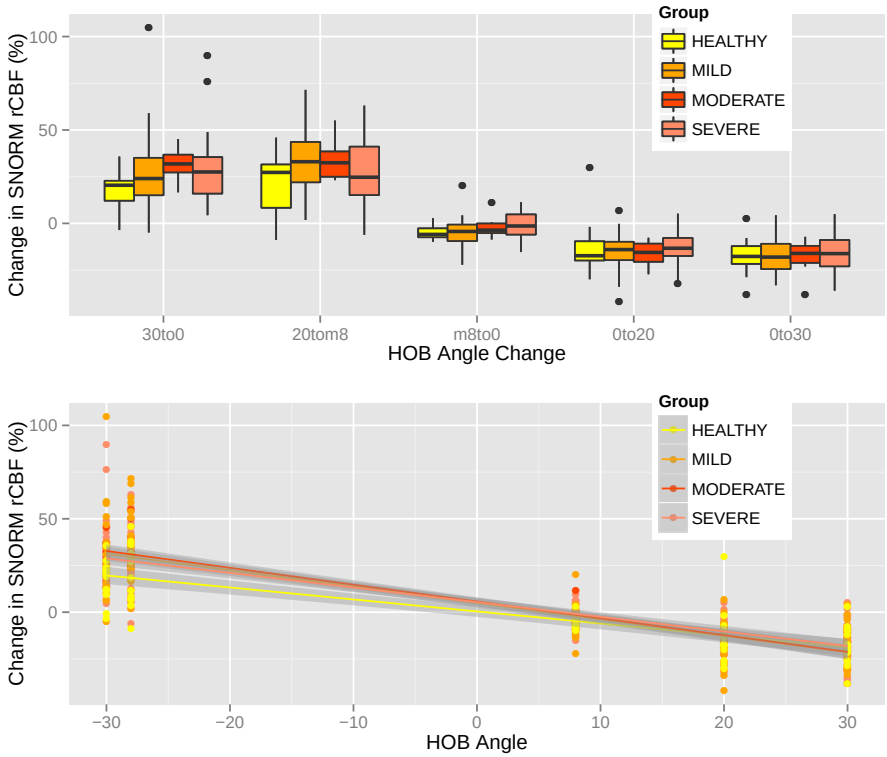

Figure 6.6: Top: Self-Normalized rCBF boxplots versus the ordered HOB angles. Bottom: Example of slopes produced when fitting the Self-Normalized rCBF versus the HOB angles.

it according to the patient AHI-based groups or the HOB change applied but no relation was found on these initial tests.

A more sophisticated approach was carried out through linear mixed effects (LME) models and the following relations were found:

- There is a statistically significant dependence ($p<0.001$) of the rCBF with

the HOB angle as fixed effect when no classification is applied to the patients in terms of the Apnoea-Hypopnoea Index (Severe, Moderate, Milds and Non-OSA) i.e considering all the groups as one.

- The previous relation breaks (p=0.074) when the group classification of patients based on the Apnoea-Hypopnoea Index is included. This finding reveals that although there is a clear effect of the flow response provoked by the HOB changes, we cannot distinguish this effect among the AHI-based groups.

- There is a statistically significant dependence (p=0.002) between rCBF and the HOB angle in addition to the Mean Oxygen saturation as fixed effects.

- There is a statistically significant dependence (p=0.001) between rCBF and the HOB angle in addition to the Body Mass Index as fixed effects.

6.3.3.1 Mean Oxygen Saturation and Body Mass Index

As previously mentioned, I have researched through LME the effect in the blood flow response of the HOB change in addition to the mean oxygen saturation on one side and the Body Mass Index on the other side as fixed effects. Statistically significant dependencies were found for these two model produced, when considering all the groups together along the orthostatic test. This relation implies that rCBF decreases whenever the Mean Oxygen Saturation increases as illustrated in Figure 6.7.

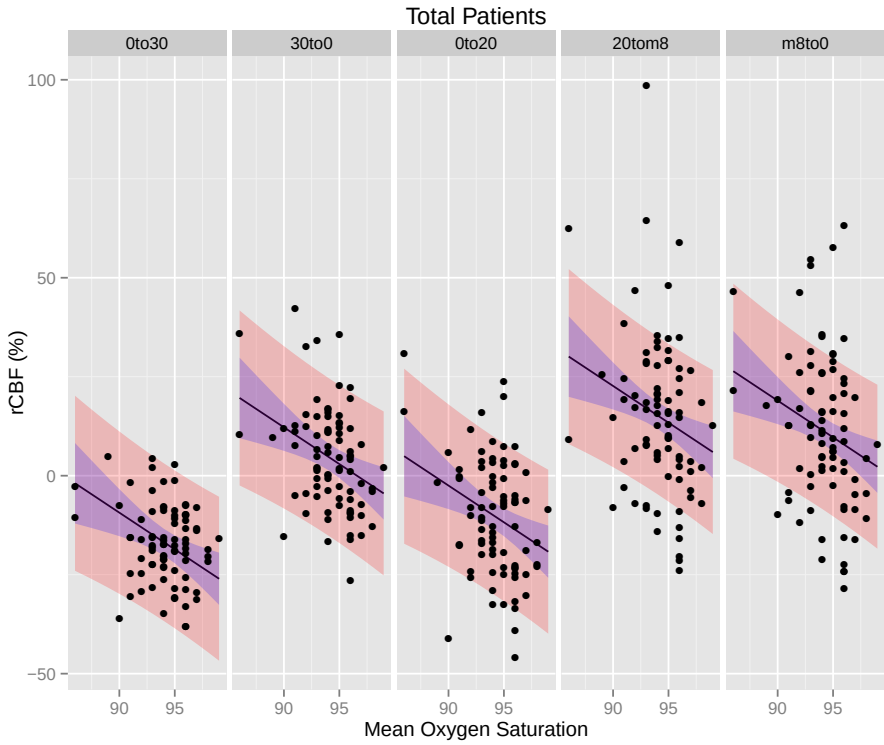

Figure 6.7: rCBF versus Mean Oxygen Saturation for all the HOB angles and all the groups. The blue area represents the confidence intervals for the model whereas the pink one covers the area ± twice the standard deviation.

As we can see, the flow response is higher in the 0° to 30° change for those patients who present better (higher) values in the mean oxygen saturation in contrast to the low flow response for those subjects who present worst (lower) values in the mean oxygen saturation. When looking at the 30° to 0° instead, the patients with better values of mean oxygen saturation seem to recover easier

to baseline. However, as we move along the orthostatic test, the rCBF values diverge and interpretation of any trend must be done with caution.

This dependency was also found when considering only the Mild group as illustrated in Figure 6.8.

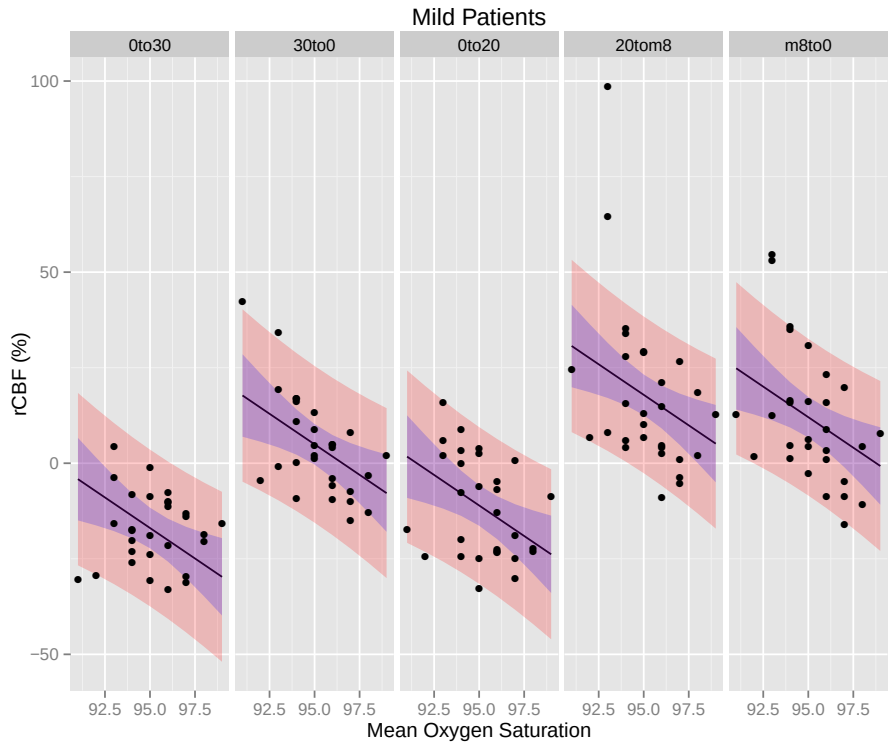

Figure 6.8: rCBF versus Mean Oxygen Saturation for all the HOB angles and Mild group. The blue area represents the confidence intervals for the model whereas the pink one covers the area ± twice the standard deviation.

As before, patients who have better levels of the mean oxygen saturation

seem to perform better.

A similar type of dependency appears with the rCBF and HOB angle plus the Body Mass Index when considering again all the groups together along the orthostatic test. This is illustrated in Figure 6.9 where we can see how the rCBF decreases whenever the Body Mass Index increases in the 0° to 30° change.

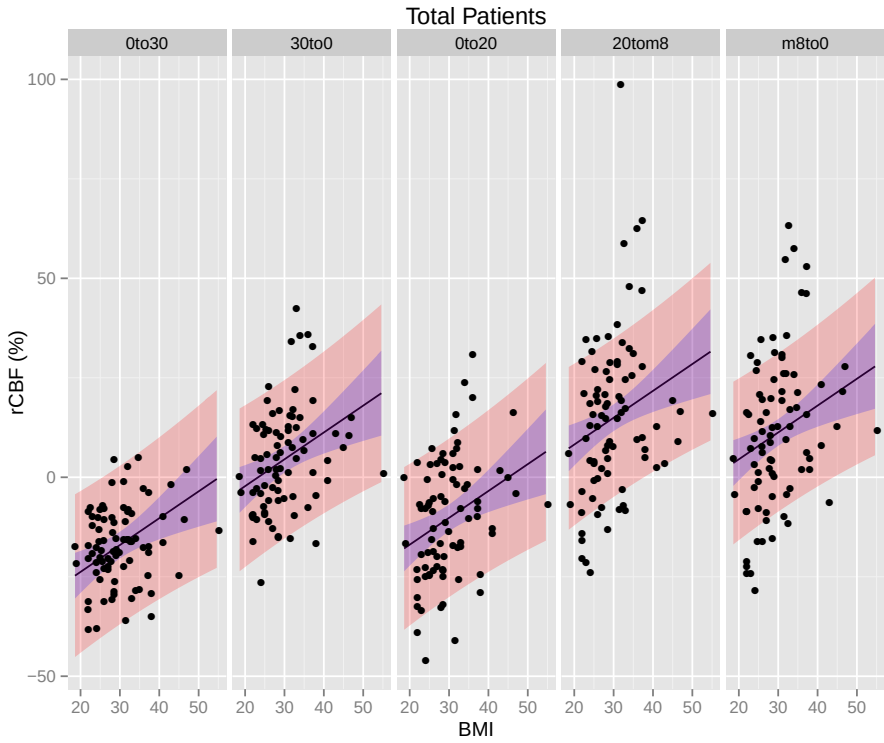

Figure 6.9: rCBF versus BMI for all the HOB angles and all the groups. The blue area represents the confidence intervals for the model whereas the pink one covers the area ± twice the standard deviation.

This dependency also stands for the Mild group as shown in Figure 6.10. As with the previous example, the rCBF values diverge whenever we move along the orthostatic test and the interpretation of trends must be done carefully.

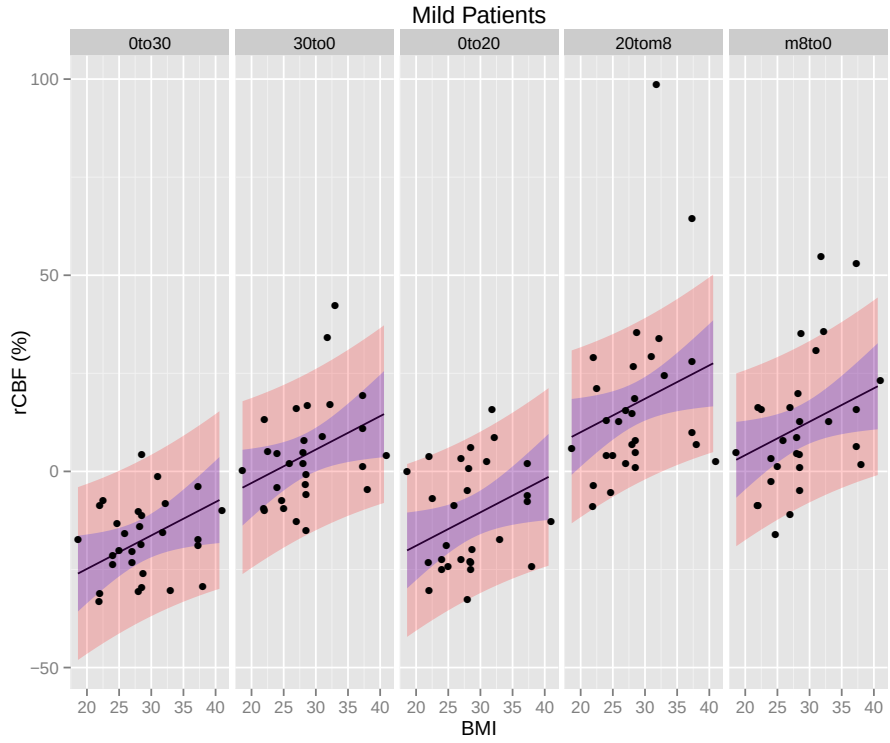

Figure 6.10: rCBF versus BMI for all the HOB angles and Mild group. The blue area represents the confidence intervals for the model whereas the pink one covers the area ± twice the standard deviation.

In relation to these last two LME models, the blood flow response is lower in patients who present poorer values of the Mean SpO_2 in the 0° to 30°, 30°

to 0° and 0° to 20° changes. A similar relation (but opposite tendency) applies to those patients with higher BMI where their flow response is also lower for those changes. In both models, the further HOB changes are more variable and therefore interpretation becomes more difficult. In this regards, we must take into account the short range of both Mean SpO_2 and BMI variables that weakens the strength of the models.

6.3.4 Exploring the rCBF at the 0° to 30° HOB change

The rCBF presents a more *homogeneous* distribution in the at 0° to 30° change and therefore I have focused on this HOB change to explore its dependence (if any) with a set of fixed key factors: The AHI, the Mean SpO_2, the CT90, the ODI4% and the BMI. The population of *paradoxical responders* (patients where the rCBF increases when changing the HOB from 0° to 30°) was very low (4.8%) in contrast to previous studies carried out with ischemic stroke patients [33, 77] where this population was quite significant (around 29%). Since the *reverse effect* in the blood flow response of the paradoxical responders is quite strong, I have followed the criteria used by *Favilla et. al* [77] to avoid *confounding effects* and excluded these patients from the statistical analysis.

The results of these models can be checked on table 6.8.

The *NA* text remarks the prior discussed point of the low range of the parameters involved. This restriction particularly applies to the Non-OSA, Mild and Moderate groups. As consequence, I have focused the modeling on the Severe group and all the groups together (Total).

	Non-OSA	Mild	Moderate	Severe	Total
AHI	NA	NA	NA	0.123	0.571
Mean SpO_2	NA	NA	NA	0.091	0.26
CT90	NA	NA	NA	0.291	0.418
ODI4%	NA	NA	NA	0.265	0.873
BMI	NA	NA	NA	0.606	0.219

Table 6.8: P-Values for LME with rCBF as a fixed factor. NA=Not Applicable

In these results, no statistical significant dependences were found between the rCBF produced for the 0° to 30° change and any of the previous mentioned parameters. This can be visualized on Figure 6.11 where the values of the rCBF versus those parameters are shown for the severe population.

In these plots, a tendency can be seen in the representation of the flow response versus the Mean SpO_2. In compliance with the results achieved when considering the total orthostatic challenge, this relation implies that the blood flow response is stronger for those patients that present better oxygen saturation values. However, the large errorbars inherent to the nature of the data and the short range of the Mean SpO_2 produce poor statistics. In fact, this trend would disappear if we remove the two patients with oxygen saturation values lower than 87.5. A similar thing occurs when exploring the relation with the rCBF and the remaining parameters. For instance, in the case of the BMI or the CT90, the trends found suggest that patients with higher BMI or CT90 values would present worst blood flow response in contrast to the ODI4% where patients with worst respiratory condition (higher values of ODI4%) would present better blood flow response.

This evidence is eventually more clear when we explore the dependence of

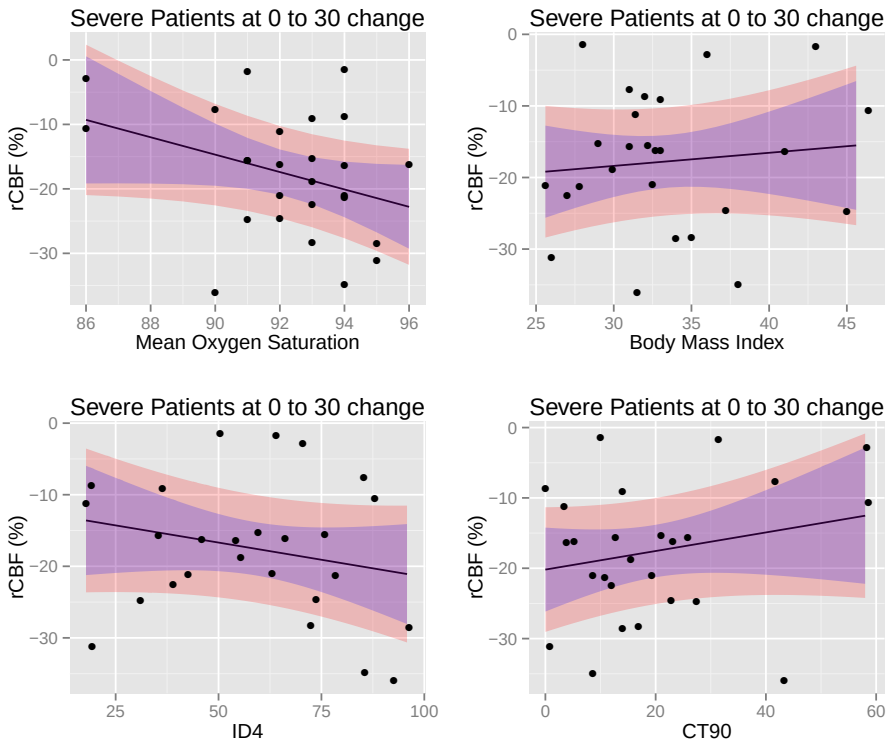

Figure 6.11: Exploring the rCBF at 0 to 30 versus a set of key respiratory parameters for the Severe Group. The blue areas represents the confidence intervals for the models whereas the pink ones cover the area ± twice the standard deviation.

the blood flow response and the Apnoea-Hypopnoea Index even when the data range was extended to the total population. This is illustrated in Figure 6.12 where we can see that there is no relation between these two parameters. The first thing to consider in this case is the nature of this index in terms of the data range. For instance, patients were recruited according to the severity of the OSA

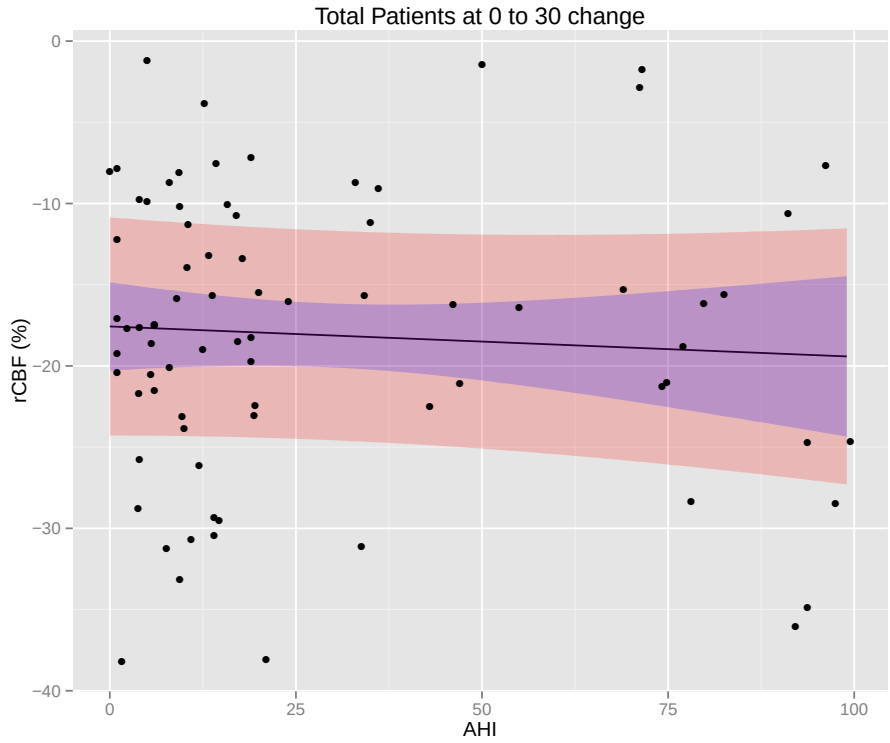

Figure 6.12: Exploring the rCBF versus the AHI for all the groups. The blue areas represents the confidence intervals for the models whereas the pink ones cover the area ± twice the standard deviation.

syndrome. In consequence, we have groups which present similar percentages of population like for instance the Mild (34.9%) and Severe (33.7%) but they cover different ranges of the AHI index. In the case of the Mild group, all these patients are located in a range of 15 points whereas the Severe group is disperse in a range of 70 points. Furthermore, the blood flow responses show high variability

along the whole AHI range but it is particularly interesting that this variability stands for low AHI ranges (< 15) where we would have expected that patients will show higher CBF changes in comparision to the flow responses obtained for patients with very high AHI (> 75).

6.3.5 Exploring The Slope

In this section I have proceeded in a similar manner but using the Slope instead, which by definition involves the whole orthostatic challenge. For the same reasons explained in the previous section, any patient presenting *paradoxical response* in the 0° to 30° change was excluded from the models produced. The results of these models can be check on table 6.9.

	Non-OSA	Mild	Moderate	Severe	Total
AHI	NA	NA	NA	0.183	0.449
Mean SpO_2	NA	NA	NA	0.102	0.658
CT90	NA	NA	NA	0.331	0.594
ODI4%	NA	NA	NA	0.279	0.671
BMI	NA	NA	NA	0.651	0.86

Table 6.9: P-Values for LME with Slope as a fixed factor. NA=Not Applicable.

Again, the *NA* text remarks the prior discussed point of the low range of the parameters involved, being this restriction applied to the Non-OSA, Mild and Moderate groups. As with the rCBF exploration at the 0° to 30° change, no relation was found between the Slope derived from the orthostatic test on the Severe and the Total population with any of the parameters involved.

This can be visualized on Figure 6.13 where the values of the Slope versus

those parameters are shown for the severe population.

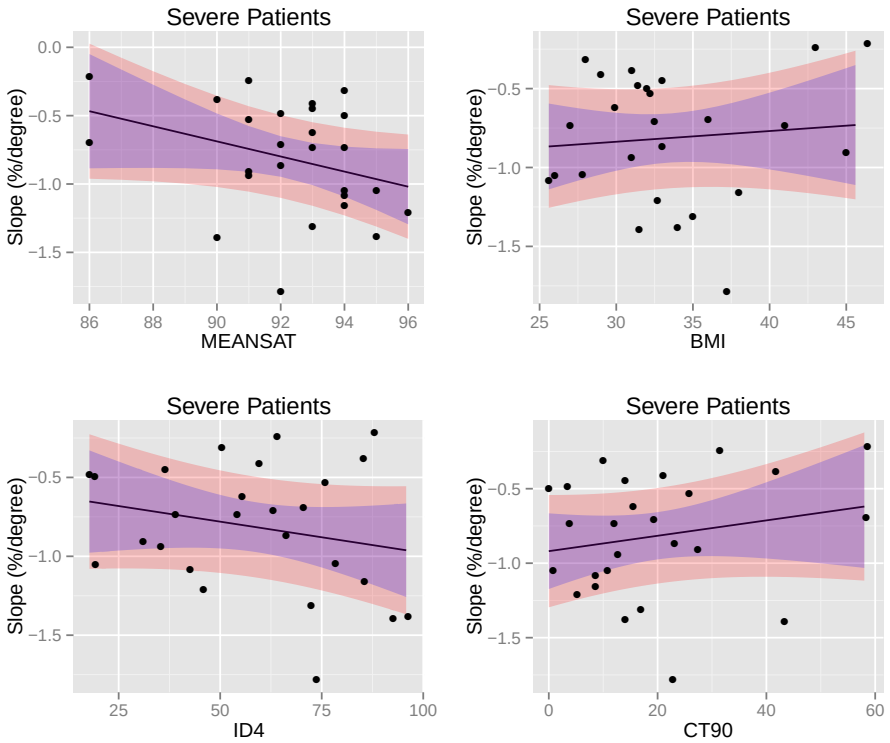

Figure 6.13: Exploring the Slope versus a set of key respiratory parameters for the Severe Group. The blue areas represents the confidence intervals for the models whereas the pink ones cover the area ± twice the standard deviation.

In these plots, similar tendencies were obtained than those when considering the rCBF induced at the 0° to 30° change. For instance, in compliance with previous results, there is a clear trend where the Slope present higher (negative) values for those patients who have better oxygen saturation values. However, the

statistics for this model are poor due to the the large errorbars and the short range of the Mean SpO_2. As before, this trend would disappear if we remove the previously mentioned two patients with oxygen saturation values lower than 87.5. The results obtained for the BMI, ODI4% and CT90 present similar trends than those obtained for the rCBF induced at the 0° to 30° change.

Similarly, no relation was found either between Slope and the Apnoea-Hypopnoea Index when the data range was extended to the total population as illustrated in Figure 6.14. As before, this model lacks of statistical significance due to the same issues related to the AHI range. However, the rCBF variability is lower for low AHI ranges (< 15) and surprisingly patients with very low AHI present low Slope values which means that their global blood flow change along the orthostatic challenge is low.

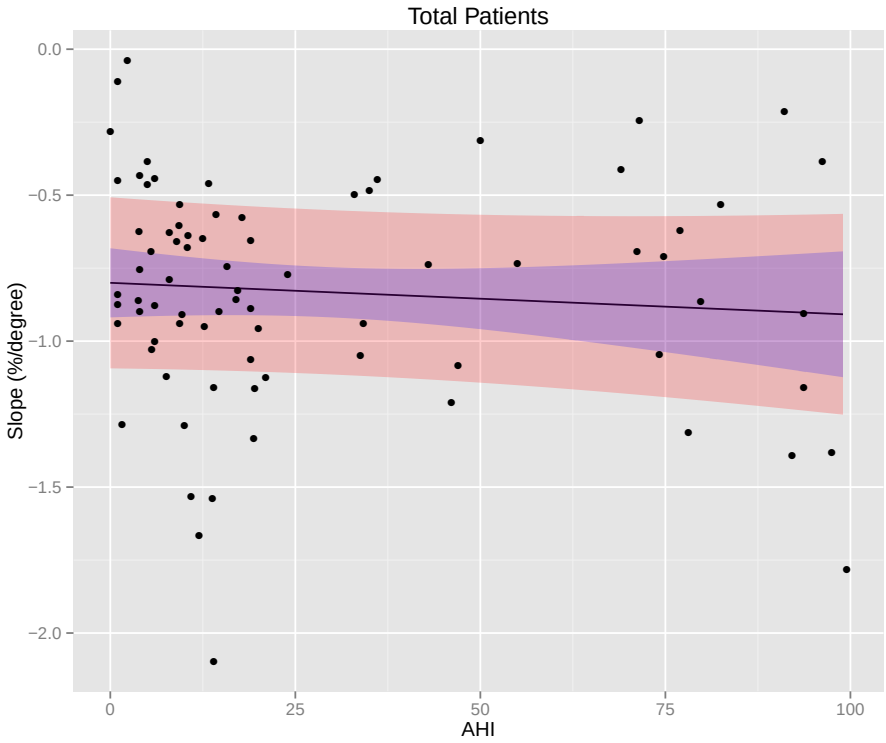

Figure 6.14: Exploring the Slope versus the AHI for all the groups. The blue areas represents the confidence intervals for the models whereas the pink ones cover the area ± twice the standard deviation.

6.4 Discussion

I have used an orthostatic challenge test to study the cerebral hemodynamics of cohort of OSA patients (n=69) and a control group of healthy subjects (n=14). In compliance with previous studies [33,37,38,77], DCS was able to distinguish the hemodynamical response induced by the HOB change although we were not able to distinguish between AHI-based groups of patients.

The values obtained for blood flow response to the initial 0° to 30° change represented in Table 6.5 are very similar to those achieved by *Edlow et al.* from a cohort of healthy subjects [38]. In this regards, the Apnoea-Hypopnoea Index has been validated to classify the severeness of the OSA syndrome and many works relate increase cardiovascular risk in patients with AHI>30 [143]. However, the AHI classification might not be enough to find *hidden* impaired cerebral autoregulation in OSA patients.

In this regards, endothelium plays an important role in the cerebral autoregulation mechanisms by regulating the resting tone of the vessels through the release of the potent vasoactive factors such as nitric oxide [147]. In the case of OSA patients, it was found that they present abnormal endothelium -dependent and independent vasodilation [148,149] and increased sympathetic nerve activity that leads to increased vasoconstriction [150–152]. This mechanism provokes an increased of the vascular oxidative stress that alters the vascular tone regulation of the brain [153]. Also, an increase of intravascular pressure induces a vasoconstriction through a myogenic response that alters the vessel resistance adjustments [154] and leads to alterations in the cerebral autoregulation [155].

The paradoxical responses were a significant finding in severely injured subjects [33, 77] but this study did not present a large population (4.8%). The reasons that causes this paradoxical responses still remain nowadays unclear but could be related to high intracranial pressure (ICP) or heart failure [156, 157].

On the other hand, when looking at the mean values of rCBF and SNORM rCBF on Tables 6.5-6.6 it was found that the control group of healthy subjects presented some differences when comparing to the OSA patients. For instance, they seem to *easily recover* the rCBF baseline values when returning from 30° or −8° to the supine positions. This is reflected on the rCBF values for those angles (-4.4% ±2.5% and -5.6% ±4.3% respectively) and it is also in compliance with the fact that the control group of healthy subjects is the only one where the SNORM rCBF values at 0° to 30° and 30° to 0° are very similar in terms of absolute value (17.3% ±2.7% versus 16.4% ±2.9%). In contrast, the rCBF values obtained for the OSA groups when returning from 30° or −8° to the supine positions are of 4.4% ±2.5% and 11.5% ±3.2% for the Milds, 8.1% ±3.6% and 19.1% ±4.8% for the Moderates and 7.5% ±2.5% and 16% ±3.7% for the Severes. Similarly, we can see that the absolute value of the SNORM rCBF differs in the OSA groups for the 0° to 30° and 30° to 0° changes. These values are of 17.5% ±1.8% and 27.9% ±3.9% for the Milds, 17.7% ±2.3% and 31.3% ±2.3% for the Moderates and 16.2% ±2% and 29.6% ±3.6% for the Severes.

Furthermore, results obtained from a paired t-test and summarized in Table 6.7 demonstrates that HOB changes of similar magnitude (around ±30°) produce different blood flow responses in absolute value in the OSA population

when compared to the control group. These changes are higher for the OSA groups at -30° and -28° when compared to 30° whereas the flow response obtained for the control group is the same for all these three angles of 30°, -30° and -28°.

One possibility that could explain these results is that OSA patients might need longer period of time than the 5 minutes they stayed on each position to stabilize their hemodynamical response. In compliance with this result, a previous study carried out during wakefulness show that OSA patients present impaired compensatory response to an orthostatic challenge [10]. This impairment was reflected in the significantly slower rate of recovery of the cerebral blood flow velocity (CBFV) and MAP versus a control group of healthy patients.

The blood flow response was also found to be dependent on the Mean SpO_2 and BMI for the total orthostatic challenge. However, this statistical finding needs to be considered cautiously as the short range of both Mean SpO_2 and BMI variables might have weakened the strength of these models. In relation to this point, we must also take into consideration that the sleep parameters used in this study were measured only *once* and *at night* whilst the DCS measurements were carried out during the day. In relation to this point, the impairment in the cerebrovascular reactivity provoked by the apneic events during sleep is maintained during daytime [158] although reduced when compared to early morning measurements.

The combination of DCS and HOB seems to be a good test but it has only been validated in studies carried out with severed injured patients [33, 37, 77].

One possibility that could explain why OSA groups present similar blood flow responses and therefore we cannot distinguish between them is that the test is not sensitive enough in milder cases than severe injured patients. This sensitivity could be improved by using a stronger and faster body positioning challenge (full reversal). In this regards, for technical reasons the bed manipulation performed in this study was done manually and slowly (around 15 second for the 0° to 30° change). Another alternative is to use a leg cuff release protocol [36]. However, the strong dilation in the artery endothelium induced by this protocol can increase the coronary risk factors [159]. Also, changes in the cerebral blood flow could be induced by acetazolamide [160] which is mildly invasive although its use can produce side effects [161] such as headache, nausea or general malaise.

As an overall, the blood flow responses obtained in this study suggest that through a carefully conducted study on recovery dynamics we might be able to reveal better discriminatory capabilities. In any case, the method used in this study appears suitable given the large population studied, yet the correct protocol in a future study is to be defined.

6.5 Conclusion

I have studied the cerebral hemodynamics of 83 patients in response to an orthostatic challenge. From the results obtained we were able to distinguish the hemodynamical response induced by the HOB change although were not able to differentiate between AHI-based groups of patients. In order to succeed at this levels, more patients per group would be needed to recruit for a future study.

This study also shows that healthy subjects seem to have higher capacity to recover to the CBF values when returning to the supine position in contrast to those classified as OSA patients. In this regards, I have explored possible correlations between the blood flow response to the orthostatic challenge versus a set of key respiratory parameters and particularly the Apnoea-Hypopnoea Index used to classified OSA patients according to the severity of this syndrome. The lack of relations found suggest that this index might not be appropriated to identify impaired cerebral autoregulation. This fact suggest that DCS could play a role as a diagnose tool for evaluating the CVR future clinical trials.

Table 6.10: List of acronyms

AIS	Acute ischemic stroke
AHI	Apnoea-Hypopnoea Index
BMI	Body mass index
CA	Cerebral autoregulation
CPAP	Continuous positive air pressure
CT90	% of time during the study where the SpO_2 was lower than 90%
CVR	Cerebrovascular reactivity
ODI4%	# of times/hour where the SpO_2 decreases 4% due to an apnoea
OSA	Obstructive sleep apnoea
$\mathbf{S_pO_2}$	Arterial oxygen saturation
PSG	Polysomnography

7
Conclusions

Several biomedical applications based on diffuse optical techniques have been described along this manuscript. In all these scenarios I had to face different challenges such as developing new optical probes through a fully non-invasive approach, engineering solutions to secure the correct probe positioning over the rat scalp and human heads or developing new protocols to secure the optical measurement in small rat brain areas. In these regards, I would like to thank my collaborators at the Stroke and Sleep units of Hospital de la Santa Creu i Sant Pau and the Department of Brain Ischemia and Neurodegeneration, Institute for Biomedical Research (IIBB), Spanish Research Council (CSIC), Institut d'Investigacions Biomèdiques August Pi i Sunyer (IDIBAPS) from whom I learned a lot about animal and human physiology and from where I got con-

tinuous feedback and support along these years.

The results obtained in this thesis reflect the great potential of this technology to obtain information about the hemodynamics of humans and rodents through a fully non-invasive manner. This fact plus some extra features like for instance its low cost and/or portability makes it very attractive in biological and medical studies.

Also, this technology has been capable to be used simultaneously with medical sensors (such as polysomnography and/or transcraneal doppler) and has also the potential to be used simultaneously with MRI. This fact opens the door to proceed with multi-disciplinary experiments in future studies.

As a summary, here they are the main conclusions of this Thesis.

Non-invasive monitoring of functional activation in rat brain with DCS

In this study, I have described the performance of both an implanted and surface probes which allow to measure the functional activation in rats in a fully non invasive manner. The main advantage from the implantable probe comes from the relatively low signal-to-noise ratio caused by the absence of scalp and the accuracy in tracking the right regions of interest. Also, it allows to proceed with optical and MRI measurements simultaneously.

The surface probe eliminates the minimal surgery needed for the use of the implantable probe and the risk of infections derived from it, allowing to proceed with longer longitudinal studies (a year duration or longer eventually). This fact

opens the possibility of studying chronic phases of neurodegenerative pathologies and possible recovery therapies.

Monitoring cerebral hemodynamics during early hours after stroke

In this chapter, I have studied the blood flow response to an orthostatic challenge during the early hours after the stroke onset. The results obtained have revealed to provide promising information to predict the outcome of ischemic stroke patients according to the functional modified Rankin Scale.

This finding could be of great use to improve the medical diagnose and might open the gate to *ad hoc* treatments by simply using a head-of-bed challenge in the early hours after the stroke onset.

Once more, diffuse correlation spectroscopy has proved its capability to identify paradoxical responders and therefore to provide neurologist with relevant information about the cerebral hemodynamics of ischemic stroke patients.

Cerebral hemodynamics of Obstructive Sleep Apnoea patients in response to orthostatic challenge

In this last chapter, I have monitored the cerebral hemodynamics of a large cohort (n=69) of Obstructive Sleep Apnoea (OSA) patients and compared their blood flow responses to an orthostatic challenge with a control group of healthy subjects (n=14). The hemodynamical responses induced by the head-of-bed (HOB) challenge were successfully measured by DCS although we were not able

to distinguish between groups of patients clustered according to the Apnoea-Hypopnoea Index (AHI).

The results obtained also show that healthy subjects seem to have a higher capacity to recover to initial cerebral blood flow values when altering the HOB from supine to 30 and return back to supine position. The fact that the blood flow response to the orthostatic challenge is not dependent on the AHI suggests that this index might not be appropriated to identify impaired cerebrovascular reactivity or cerebral autoregulation.

As an overall, the blood flow responses to an orthostatic challenge suggest that through a carefully conducted study on recovery dynamics we might be able to reveal better discriminatory capabilities and therefore to produce more sophisticated models about cerebral hemodynamics and respiratory parameters. In relation to this point, DCS could play a role as a diagnose tool for evaluating the cerebrovascular reactivity in future clinical trials.

Bibliography

[1] Alan D Lopez, Colin D Mathers, Majid Ezzati, Dean T Jamison, and Christopher JL Murray. Global and regional burden of disease and risk factors, 2001: systematic analysis of population health data. *The Lancet*, 367(9524):1747–1757, 2006. (see pp. 1 and 70)

[2] Valery L Feigin, Carlene MM Lawes, Derrick A Bennett, and Craig S Anderson. Stroke epidemiology: a review of population-based studies of incidence, prevalence, and case-fatality in the late 20th century. *The Lancet Neurology*, 2(1):43–53, 2003. (see pp. 1 and 70)

[3] Charles Smart Roy and CS Sherrington. On the regulation of the blood-supply of the brain. *The Journal of physiology*, 11(1-2):85, 1890. (see p. 2)

[4] OB Paulson, S Strandgaard, and L Edvinsson. Cerebral autoregulation. *Cerebrovascular and brain metabolism reviews*, 2(2):161–192, 1989. (see p.

2)

[5] Eric C Peterson, Zhengfeng Wang, and Gavin Britz. Regulation of cerebral blood flow. *International journal of vascular medicine*, 2011, 2011. (see p. 2)

[6] Niels A Lassen. Control of cerebral circulation in health and disease. *Circulation research*, 34(6):749–760, 1974. (see p. 2)

[7] Markku Partinen and Heikki Palomaki. Snoring and cerebral infarction. *The Lancet*, 326(8468):1325–1326, 1985. (see pp. 2 and 90)

[8] H Palomäki. Snoring and the risk of ischemic brain infarction. *Stroke*, 22(8):1021–1025, 1991. (see pp. 2 and 90)

[9] H Klar Yaggi, John Concato, Walter N Kernan, Judith H Lichtman, Lawrence M Brass, and Vahid Mohsenin. Obstructive sleep apnea as a risk factor for stroke and death. *New England Journal of Medicine*, 353(19):2034–2041, 2005. (see p. 2)

[10] Fred Urbano, Francoise Roux, Joseph Schindler, and Vahid Mohsenin. Impaired cerebral autoregulation in obstructive sleep apnea. *Journal of Applied Physiology*, 105(6):1852–1857, 2008. (see pp. 2, 91, and 124)

[11] WT McNicholas, MR Bonsignore, et al. Sleep apnoea as an independent risk factor for cardiovascular disease: current evidence, basic mechanisms and research priorities. *European Respiratory Journal*, 29(1):156–178, 2007. (see pp. 2 and 90)

[12] EM Bålfors and Karl A Franklin. Impairment of cerebral perfusion during obstructive sleep apneas. *American journal of respiratory and critical care medicine*, 150(6):1587–1591, 1994. (see pp. 2 and 92)

[13] David J Durgan and Robert M Bryan. Cerebrovascular consequences of obstructive sleep apnea. *Journal of the American Heart Association*, 1(4), 2012. (see pp. 2 and 92)

[14] Rune Aaslid, Thomas-Marc Markwalder, and Helge Nornes. Noninvasive transcranial doppler ultrasound recording of flow velocity in basal cerebral arteries. *Journal of neurosurgery*, 57(6):769–774, 1982. (see p. 3)

[15] Fin Stolze Larsen, Karsten Skovgaard Olsen, Bent Adel Hansen, Olaf B Paulson, and Gitte Moos Knudsen. Transcranial doppler is valid for determination of the lower limit of cerebral blood flow autoregulation. *Stroke*, 25(10):1985–1988, 1994. (see p. 3)

[16] CC Bishop, S Powell, D Rutt, et al. Transcranial doppler measurement of middle cerebral artery blood flow velocity: a validation study. *Stroke*, 17(5):913–915, 1986. (see pp. 3, 71, and 92)

[17] Marinella Marinoni, Andrea Ginanneschi, Paolo Forleo, and Luigi Amaducci. Technical limits in transcranial doppler recording: Inadquate acoustic windows. *Ultrasound in medicine & biology*, 23(8):1275–1277, 1997. (see p. 3)

[18] Anna M Planas. Noninvasive brain imaging in small animal stroke models: Mri and pet. In *Rodent Models of Stroke*, pages 139–165. Springer, 2010. (see p. 3)

[19] Ronald L Wolf and John A Detre. Clinical neuroimaging using arterial spin-labeled perfusion magnetic resonance imaging. *Neurotherapeutics*, 4(3):346–359, 2007. (see pp. 3 and 44)

[20] BP Drayer, SK Wolfson, OM Reinmuth, M Dujovny, M Boehnke, and EE Cook. Xenon enhanced ct for analysis of cerebral integrity, perfusion, and blood flow. *Stroke*, 9(2):123–130, 1978. (see p. 3)

[21] Harry T Chugani, Michael E Phelps, and John C Mazziotta. Positron emission tomography study of human brain functional development. *Annals of neurology*, 22(4):487–497, 1987. (see p. 3)

[22] Seiji Ogawa, TM Lee, AR Kay, and DW Tank. Brain magnetic resonance imaging with contrast dependent on blood oxygenation. *Proceedings of the National Academy of Sciences*, 87(24):9868–9872, 1990. (see pp. 3 and 44)

[23] S Ogawa, RS Menon, DW Tank, SG Kim, H Merkle, JM Ellermann, and K Ugurbil. Functional brain mapping by blood oxygenation level-dependent contrast magnetic resonance imaging. a comparison of signal characteristics with a biophysical model. *Biophysical Journal*, 64(3):803, 1993. (see pp. 3 and 44)

[24] TAGA Bonhoeffer and A Grinvald. Optical imaging based on intrinsic signals: the methodology. *Brain mapping: The methods*, pages 55–97, 1996. (see pp. 4, 44, and 63)

[25] Elizabeth MC Hillman. Optical brain imaging in vivo: techniques and applications from animal to man. *Journal of biomedical optics*, 12(5):051402–051402, 2007. (see p. 4)

[26] Janos Luckl, Wesley Baker, Zheng-Hui Sun, Turgut Durduran, Arjun G Yodh, and Joel H Greenberg. The biological effect of contralateral forepaw stimulation in rat focal cerebral ischemia: a multispectral optical imaging study. *Frontiers in neuroenergetics*, 2, 2010. (see pp. 4 and 10)

[27] P Ake Oberg. Laser-doppler flowmetry. *Critical reviews in biomedical engineering*, 18(2):125–163, 1989. (see pp. 4, 44, and 63)

[28] Gert E Nilsson, Torsten Tenland, and P Ake Oberg. Evaluation of a laser doppler flowmeter for measurement of tissue blood flow. *Biomedical Engineering, IEEE Transactions on*, (10):597–604, 1980. (see pp. 4, 44, and 63)

[29] Andrew K Dunn, Hayrunnisa Bolay, Michael A Moskowitz, and David A Boas. Dynamic imaging of cerebral blood flow using laser speckle. *Journal of Cerebral Blood Flow & Metabolism*, 21(3):195–201, 2001. (see pp. 4, 34, 45, and 63)

[30] David A Boas. *Diffuse photon probes of structural and dynamical properties of turbid media: theory and biomedical applications.* PhD thesis, University of Pennsylvania, 1996. (see pp. 4, 25, 45, 71, and 92)

[31] Turgut Durduran. *Non-invasive measurements of tissue hemodynamics with hybrid diffuse optical methods.* PhD thesis, University of Pennsylvania, 2004. (see pp. 4, 27, 39, 45, 71, and 92)

[32] Turgut Durduran, Guoqiang Yu, Mark G Burnett, John A Detre, Joel H Greenberg, Jiongjiong Wang, Chao Zhou, and Arjun G Yodh. Diffuse optical measurement of blood flow, blood oxygenation, and metabolism in a human brain during sensorimotor cortex activation. *Optics letters*, 29(15):1766–1768, 2004. (see pp. 4, 27, 45, 64, 71, and 92)

[33] Turgut Durduran, Chao Zhou, Brian L Edlow, Guoqiang Yu, Regine Choe, Meeri N Kim, Brett L Cucchiara, Mary E Putt, Qaisar Shah, Scott E Kasner, et al. Transcranial optical monitoring of cerebrovascular hemodynamics in acute stroke patients. *Optics express*, 17(5):3884, 2009. (see pp. 4, 36, 45, 71, 72, 85, 92, 93, 97, 114, 122, 123, and 124)

[34] T. Durduran, R. Choe, WB Baker, and AG Yodh. Diffuse optics for tissue monitoring and tomography. *Reports on Progress in Physics*, 73:076701, 2010. (see pp. 4, 5, 9, 45, 71, and 92)

[35] Turgut Durduran and Arjun G Yodh. Diffuse correlation spectroscopy for non-invasive, micro-vascular cerebral blood flow measurement. *NeuroImage*, 2013. (see pp. 4, 5, 27, 45, 71, and 92)

[36] Ran Cheng. Noninvasive near-infrared diffuse optical monitoring of cerebral hemodynamics and autoregulation. 2013. (see pp. 4, 39, 71, 92, and 125)

[37] Meeri N Kim, Brian L Edlow, Turgut Durduran, Suzanne Frangos, Rickson C Mesquita, Joshua M Levine, Joel H Greenberg, Arjun G Yodh, and John A Detre. Continuous optical monitoring of cerebral hemodynamics during head-of-bed manipulation in brain-injured adults. *Neurocritical care*, pages 1–11, 2013. (see pp. 4, 71, 72, 86, 92, 93, and 122)

[38] Brian L Edlow, Meeri N Kim, Turgut Durduran, Chao Zhou, Mary E Putt, Arjun G Yodh, Joel H Greenberg, and John A Detre. The effects of healthy aging on cerebral hemodynamic responses to posture change. *Physiological measurement*, 31(4):477, 2010. (see pp. 4, 71, 72, 73, 92, 93, 94, and 122)

[39] Frans F Jobsis. Noninvasive, infrared monitoring of cerebral and myocardial oxygen sufficiency and circulatory parameters. *Science*, 198(4323):1264–1267, 1977. (see p. 4)

[40] Peyman Zirak, Raquel Delgado-Mederos, Lavinia Dinia, David Carrera, Joan Martí-Fàbregas, and Turgut Durduran. Transcranial diffuse optical monitoring of microvascular cerebral hemodynamics after thrombolysis in ischemic stroke. *Journal of biomedical optics*, 19(1):018002–018002, 2014. (see p. 10)

[41] A Siegel, JJ Marota, and David Boas. Design and evaluation of a continuous-wave diffuse optical tomography system. *Optics Express*, 4(8):287–298, 1999. (see p. 10)

[42] S Nioka, Q Luo, and B Chance. Human brain functional imaging with reflectance cws. In *Oxygen Transport to Tissue Xix*, pages 237–242. Springer, 1997. (see p. 10)

[43] Felix Scholkmann, Stefan Kleiser, Andreas Jaakko Metz, Raphael Zimmermann, Juan Mata Pavia, Ursula Wolf, and Martin Wolf. A review on continuous wave functional near-infrared spectroscopy and imaging instrumentation and methodology. *Neuroimage*, 85:6–27, 2014. (see p. 10)

[44] Yu Shang, Lei Chen, Michal Toborek, and Guoqiang Yu. Diffuse optical monitoring of repeated cerebral ischemia in mice. *Optics express*, 19(21):20301–20315, 2011. (see pp. 10, 45, and 63)

[45] Rickson C Mesquita, Nicolas Skuli, Meeri N Kim, Jiaming Liang, Steve Schenkel, Amar J Majmundar, M Celeste Simon, and Arjun G Yodh. Hemodynamic and metabolic diffuse optical monitoring in a mouse model of hindlimb ischemia. *Biomedical optics express*, 1(4):1173–1187, 2010. (see p. 10)

[46] Rickson C Mesquita, Turgut Durduran, Guoqiang Yu, Erin M Buckley, Meeri N Kim, Chao Zhou, Regine Choe, Ulas Sunar, and Arjun G Yodh. Direct measurement of tissue blood flow and metabolism with diffuse optics.

Philosophical Transactions of the Royal Society A: Mathematical, Physical and Engineering Sciences, 369(1955):4390–4406, 2011. No cited.

[47] Brian W Pogue and Michael S Patterson. Frequency-domain optical absorption spectroscopy of finite tissue volumes using diffusion theory. *Physics in medicine and biology*, 39(7):1157, 1994. (see p. 10)

[48] Michael S Patterson, J David Moulton, Brian C Wilson, Klaus W Berndt, and Joseph R Lakowicz. Frequency-domain reflectance for the determination of the scattering and absorption properties of tissue. *Applied optics*, 30(31):4474–4476, 1991. (see p. 10)

[49] Ulas Sunar, Harry Quon, Turgut Durduran, Jun Zhang, Chao Zhou, Alex Kilger, Shoko Nioka, Arjun G Yodh, Britton Chance, Robert Lustig, et al. Noninvasive diffuse optical measurement of blood flow and blood oxygenation for monitoring radiation therapy in patients with head and neck tumors: a pilot study. *Journal of biomedical optics*, 11(6):064021–064021, 2006. (see p. 10)

[50] Parisa Farzam, Peyman Zirak, Tiziano Binzoni, and Turgut Durduran. Pulsatile and steady-state hemodynamics of the human patella bone by diffuse optical spectroscopy. *Physiological measurement*, 34(8):839, 2013. (see pp. 10 and 42)

[51] Rickson C Mesquita, Mary Putt, Malavika Chandra, Guoqiang Yu, Xiaoman Xing, Sung Wan Han, Gwen Lech, Yu Shang, Turgut Durduran,

Chao Zhou, et al. Diffuse optical characterization of an exercising patient group with peripheral artery disease. *Journal of biomedical optics*, 18(5):057007–057007, 2013. (see p. 10)

[52] Britton Chance, Shoko Nioka, Jane Kent, Kevin McCully, Michael Fountain, Robert Greenfeld, and Gary Holtom. Time-resolved spectroscopy of hemoglobin and myoglobin in resting and ischemic muscle. *Analytical biochemistry*, 174(2):698–707, 1988. (see p. 10)

[53] Marco Ferrari, Qingnong Wei, Luca Carraresi, Roberto A De Blasi, and Giovanni Zaccanti. Time-resolved spectroscopy of the human forearm. *Journal of Photochemistry and Photobiology B: Biology*, 16(2):141–153, 1992. (see p. 10)

[54] Steven L Jacques. Time resolved propagation of ultrashort laser pulses within turbid tissues. *Applied optics*, 28(12):2223–2229, 1989. (see p. 10)

[55] Michael S Patterson, Britton Chance, and Brian C Wilson. Time resolved reflectance and transmittance for the non-invasive measurement of tissue optical properties. *Applied optics*, 28(12):2331–2336, 1989. (see p. 10)

[56] Paola Taroni, Antonio Pifferi, Alessandro Torricelli, Daniela Comelli, and Rinaldo Cubeddu. In vivo absorption and scattering spectroscopy of biological tissues. *Photochemical & Photobiological Sciences*, 2(2):124–129, 2003. (see p. 10)

[57] K Furutsu. Diffusion equation derived from space-time transport equation. *JOSA*, 70(4):360–366, 1980. (see p. 12)

[58] Akira Ishimaru. *Wave propagation and scattering in random media*, volume 2. Academic press New York, 1978. (see p. 12)

[59] Daniele Contini, Fabrizio Martelli, and Giovanni Zaccanti. Photon migration through a turbid slab described by a model based on diffusion approximation. i. theory. *Applied optics*, 36(19):4587–4599, 1997. (see p. 12)

[60] Arjun Yodh and Britton Chance. Spectroscopy and imaging with diffusing light. *Physics Today*, 48(3):34–41, 1995. (see p. 13)

[61] Maureen A O'Leary. *Imaging with diffuse photon density waves*. PhD thesis, University of Pennsylvania, 1996. (see p. 13)

[62] John David Jackson and John D Jackson. *Classical electrodynamics*, volume 3. Wiley New York etc., 1962. (see p. 15)

[63] Joseph W Goodman. *Speckle phenomena in optics: theory and applications*, volume 1. 2007. (see p. 19)

[64] G Maret and PE Wolf. Multiple light scattering from disordered media. the effect of brownian motion of scatterers. *Zeitschrift für Physik B Condensed Matter*, 65(4):409–413, 1987. (see p. 19)

[65] DJ Pine, DA Weitz, PM Chaikin, and E Herbolzheimer. Diffusing wave spectroscopy. *Physical Review Letters*, 60(12):1134, 1988. (see p. 19)

[66] Bruce J Berne and Robert Pecora. *Dynamic light scattering: with applications to chemistry, biology, and physics*. Courier Dover Publications, 2000. (see pp. 19 and 21)

[67] B Chu. Laser light scattering: basic principles and practice (2nd), 1991. (see p. 21)

[68] P-A Lemieux and DJ Durian. Investigating non-gaussian scattering processes by using¡ i¿ n¡/i¿ th-order intensity correlation functions. *JOSA A*, 16(7):1651–1664, 1999. (see p. 22)

[69] DA Boas, LE Campbell, and AG Yodh. Scattering and imaging with diffusing temporal field correlations. *Physical review letters*, 75(9):1855, 1995. (see p. 25)

[70] Anna Devor, Sava Sakadžić, Vivek J Srinivasan, Mohammad A Yaseen, Krystal Nizar, Payam A Saisan, Peifang Tian, Anders M Dale, Sergei A Vinogradov, Maria Angela Franceschini, et al. Frontiers in optical imaging of cerebral blood flow and metabolism. *Journal of Cerebral Blood Flow & Metabolism*, 32(7):1259–1276, 2012. (see pp. 34, 44, and 63)

[71] Koichiro Sakaguchi, Tomoya Tachibana, Shunsuke Furukawa, Takushige Katsura, Kyoko Yamazaki, Hideo Kawaguchi, Atsushi Maki, and Eiji Okada. Experimental prediction of the wavelength-dependent path-length factor for optical intrinsic signal analysis. *Applied optics*, 46(14):2769–2777, 2007. (see pp. 34, 44, and 63)

[72] Syed Mohammad Shams Kazmi, Ashwin B Parthasarthy, Nelly E Song, Theresa A Jones, and Andrew K Dunn. Chronic imaging of cortical blood flow using multi-exposure speckle imaging. *Journal of Cerebral Blood Flow & Metabolism*, 33(6):798–808, 2013. (see p. 34)

[73] Cenk Ayata, Andrew K Dunn, Yasemin Gursoy-Özdemir, Zhihong Huang, David A Boas, and Michael A Moskowitz. Laser speckle flowmetry for the study of cerebrovascular physiology in normal and ischemic mouse cortex. *Journal of Cerebral Blood Flow & Metabolism*, 24(7):744–755, 2004. (see pp. 34, 45, and 63)

[74] Turgut Durduran, Mark G Burnett, Guoqiang Yu, Chao Zhou, Daisuke Furuya, Arjun G Yodh, John A Detre, and Joel H Greenberg. Spatiotemporal quantification of cerebral blood flow during functional activation in rat somatosensory cortex using laser-speckle flowmetry. *Journal of Cerebral Blood Flow & Metabolism*, 24(5):518–525, 2004. (see pp. 34, 45, and 63)

[75] Beau M Ances, John A Detre, Kazushi Takahashi, and Joel H Greenberg. Transcranial laser doppler mapping of activation flow coupling of the rat somatosensory cortex. *Neuroscience letters*, 257(1):25–28, 1998. (see pp. 34, 44, 45, 52, and 63)

[76] T Dalkara, K Irikura, Z Huang, N Panahian, and MA Moskowitz. Cerebrovascular responses under controlled and monitored physiological conditions in the anesthetized mouse. *Journal of Cerebral Blood Flow & Metabolism*, 15(4):631–638, 1995. (see pp. 34, 44, and 63)

[77] Christopher G Favilla, Rickson C Mesquita, Michael Mullen, Turgut Durduran, Xiangping Lu, Meeri N Kim, David L Minkoff, Scott E Kasner, Joel H Greenberg, Arjun G Yodh, et al. Optical bedside monitoring of cerebral blood flow in acute ischemic stroke patients during head-of-bed manipulation. *Stroke*, 45(5):1269–1274, 2014. (see pp. 36, 72, 85, 92, 93, 97, 114, 122, 123, and 124)

[78] Peyman Zirak, Raquel Delgado-Mederos, Joan Martí-Fàbregas, and Turgut Durduran. Effects of acetazolamide on the micro-and macro-vascular cerebral hemodynamics: a diffuse optical and transcranial doppler ultrasound study. *Biomedical optics express*, 1(5):1443–1459, 2010. (see p. 39)

[79] Cecil Cheung, Joseph P Culver, Kasushi Takahashi, Joel H Greenberg, and AG Yodh. In vivo cerebrovascular measurement combining diffuse near-infrared absorption and correlation spectroscopies. *Physics in medicine and biology*, 46(8):2053, 2001. (see pp. 39, 45, and 63)

[80] Martin Schweiger, Ilkka Nissilä, David A Boas, and Simon R Arridge. Image reconstruction in optical tomography in the presence of coupling errors. *Applied optics*, 46(14):2743–2756, 2007. (see p. 42)

[81] John Nolte. *The human brain*. Mosby-Year Book Inc. St. Louis, 1993. (see p. 43)

[82] Yee Sien Ng, Joel Stein, MingMing Ning, and Randie M Black-Schaffer. Comparison of clinical characteristics and functional outcomes of ischemic

stroke in different vascular territories. *Stroke*, 38(8):2309–2314, 2007. (see p. 44)

[83] Elizabeth MC Hillman. Coupling mechanism and significance of the bold signal: A status report. *Annual Review of Neuroscience*, 37(1), 2014. (see p. 44)

[84] Helene Girouard and Costantino Iadecola. Neurovascular coupling in the normal brain and in hypertension, stroke, and alzheimer disease. *Journal of Applied Physiology*, 100(1):328–335, 2006. (see p. 44)

[85] Ernst Niedermeyer and FH Lopes da Silva. *Electroencephalography: basic principles, clinical applications, and related fields*. Lippincott Williams & Wilkins, 2005. (see p. 44)

[86] SP Layne, G Mayer-Kress, and J Holzfuss. Problems associated with dimensional analysis of electroencephalogram data. In *Dimensions and entropies in chaotic systems*, pages 246–256. Springer, 1986. (see p. 44)

[87] Kristy S Hendrich, Patrick M Kochanek, John A Melick, Joanne K Schiding, Kimberly D Statler, Donald S Williams, Donald W Marion, and Chien Ho. Cerebral perfusion during anesthesia with fentanyl, isoflurane, or pentobarbital in normal rats studied by arterial spin-labeled mri. *Magnetic resonance in medicine*, 46(1):202–206, 2001. (see p. 44)

[88] SA Masino, MC Kwon, Y Dory, and RD Frostig. Characterization of functional organization within rat barrel cortex using intrinsic signal optical

imaging through a thinned skull. *Proceedings of the National Academy of Sciences*, 90(21):9998–10002, 1993. (see pp. 44 and 63)

[89] Amiram Grinvald, Edmund Lieke, Ron D Frostig, Charles D Gilbert, and Torsten N Wiesel. Functional architecture of cortex revealed by optical imaging of intrinsic signals. 1986. (see pp. 44 and 63)

[90] J David Briers. Laser doppler, speckle and related techniques for blood perfusion mapping and imaging. *Physiological measurement*, 22(4):R35, 2001. (see pp. 45 and 63)

[91] A Villringer, J Planck, C Hock, L Schleinkofer, and U Dirnagl. Near infrared spectroscopy (nirs): a new tool to study hemodynamic changes during activation of brain function in human adults. *Neuroscience letters*, 154(1):101–104, 1993. (see p. 45)

[92] Jun Li, Gregor Dietsche, Diana Iftime, Sergey E Skipetrov, Georg Maret, Thomas Elbert, Brigitte Rockstroh, and Thomas Gisler. Noninvasive detection of functional brain activity with near-infrared diffusing-wave spectroscopy. *Journal of Biomedical Optics*, 10(4):044002–044002, 2005. (see p. 45)

[93] C Terborg, S Bramer, S Harscher, M Simon, and OW Witte. Bedside assessment of cerebral perfusion reductions in patients with acute ischaemic stroke by near-infrared spectroscopy and indocyanine green. *Journal of Neurology, Neurosurgery & Psychiatry*, 75(1):38–42, 2004. (see p. 45)

[94] Guoqiang Yu, Turgut Durduran, Daisuke Furuya, Joel H Greenberg, and Arjun G Yodh. Hemodynamic measurements in rat brain combining diffuse near-infrared absorption and correlation spectroscopies. In *Photonics Asia 2002*, pages 1–8. International Society for Optics and Photonics, 2002. (see p. 45)

[95] H McIlwain. Metabolic response in vitro to electrical stimulation of sections of mammalian brain. *Biochemical Journal*, 49(3):382, 1951. (see p. 45)

[96] Beau M Ances, Joel H Greenberg, and John A Detre. Laser doppler imaging of activation-flow coupling in the rat somatosensory cortex. *Neuroimage*, 10(6):716–723, 1999. (see p. 45)

[97] Beau M Ances, Eric Zarahn, Joel H Greenberg, and John A Detre. Coupling of neural activation to blood flow in the somatosensory cortex of rats is time-intensity separable, but not linear. *Journal of Cerebral Blood Flow & Metabolism*, 20(6):921–930, 2000. (see pp. 45, 55, 58, and 63)

[98] John A Detre, Beau M Ances, Kazushi Takahashi, and Joel H Greenberg. Signal averaged laser doppler measurements of activation–flow coupling in the rat forepaw somatosensory cortex. *Brain research*, 796(1):91–98, 1998. (see pp. 45, 55, 58, and 63)

[99] Andrew M Siegel, Joseph P Culver, Joseph B Mandeville, and David A Boas. Temporal comparison of functional brain imaging with diffuse optical tomography and fmri during rat forepaw stimulation. *Physics in medicine and biology*, 48(10):1391, 2003. (see pp. 45 and 65)

[100] M Ueki, F Linn, and K-A Hossmann. Functional activation of cerebral blood flow and metabolism before and after global ischemia of rat brain. *Journal of Cerebral Blood Flow & Metabolism*, 8(4):486–494, 1988. (see p. 45)

[101] J Silverman and WW Muir 3rd. A review of laboratory animal anesthesia with chloral hydrate and chloralose. *Laboratory animal science*, 43(3):210–216, 1993. (see p. 46)

[102] Ralph Weber, Pedro Ramos-Cabrer, Dirk Wiedermann, Nadja van Camp, and Mathias Hoehn. A fully noninvasive and robust experimental protocol for longitudinal fmri studies in the rat. *Neuroimage*, 29(4):1303–1310, 2006. (see pp. 46, 63, and 64)

[103] Fatima A Nasrallah, Jolena Tan, and Kai-Hsiang Chuang. Pharmacological modulation of functional connectivity: α¡ sub¿ 2¡/sub¿-adrenergic receptor agonist alters synchrony but not neural activation. *Neuroimage*, 60(1):436–446, 2012. (see p. 46)

[104] Tiny Boumans, Frédéric E Theunissen, Colline Poirier, and Annemie Van Der Linden. Neural representation of spectral and temporal features of song in the auditory forebrain of zebra finches as revealed by functional mri. *European Journal of Neuroscience*, 26(9):2613–2626, 2007. (see pp. 46 and 64)

[105] Nadja Van Camp, Marleen Verhoye, Chris I De Zeeuw, and Annemie Van der Linden. Light stimulus frequency dependence of activity in the

rat visual system as studied with high-resolution bold fmri. *Journal of neurophysiology*, 95(5):3164–3170, 2006. (see pp. 46 and 64)

[106] Fuqiang Zhao, Tiejun Zhao, Lei Zhou, Qiulin Wu, and Xiaoping Hu. Bold study of stimulation-induced neural activity and resting-state connectivity in medetomidine-sedated rat. *Neuroimage*, 39(1):248–260, 2008. (see pp. 46 and 64)

[107] John Strupp et al. Stimulate: a gui based fmri analysis software package. *Neuroimage*, 3(3):S607, 1996. (see p. 49)

[108] Gary Strangman, Maria Angela Franceschini, and David A Boas. Factors affecting the accuracy of near-infrared spectroscopy concentration calculations for focal changes in oxygenation parameters. *Neuroimage*, 18(4):865–879, 2003. (see p. 64)

[109] George Paxinos, Charles Watson, Michael Pennisi, and Ann Topple. Bregma, lambda and the interaural midpoint in stereotaxic surgery with rats of different sex, strain and weight. *Journal of neuroscience methods*, 13(2):139–143, 1985. (see p. 65)

[110] J-O Coq and Christian Xerri. Sensorimotor experience modulates age-dependent alterations of the forepaw representation in the rat primary somatosensory cortex. *Neuroscience*, 104(3):705–715, 2001. (see p. 65)

[111] Akira Sumiyoshi, Jorge J Riera, Takeshi Ogawa, and Ryuta Kawashima. A mini-cap for simultaneous eeg and fmri recording in rodents. *Neuroimage*, 54(3):1951–1965, 2011. (see p. 65)

[112] Ralph Weber, Pedro Ramos-Cabrer, Carlos Justicia, Dirk Wiedermann, Cordula Strecker, Christiane Sprenger, and Mathias Hoehn. Early prediction of functional recovery after experimental stroke: functional magnetic resonance imaging, electrophysiology, and behavioral testing in rats. *The Journal of Neuroscience*, 28(5):1022–1029, 2008. (see p. 65)

[113] G Crosby, AM Crane, J Jehle, and L Sokoloff. The local metabolic effects of somatosensory stimulation in the central nervous system of rats given pentobarbital or nitrous oxide. *Anesthesiology*, 58(1):38–43, 1983. (see p. 66)

[114] Kazuto Masamoto and Iwao Kanno. Anesthesia and the quantitative evaluation of neurovascular coupling. *Journal of Cerebral Blood Flow & Metabolism*, 32(7):1233–1247, 2012. (see p. 66)

[115] Maria Angela Franceschini, Harsha Radhakrishnan, Kiran Thakur, Weicheng Wu, Svetlana Ruvinskaya, Stefan Carp, and David A Boas. The effect of different anesthetics on neurovascular coupling. *Neuroimage*, 51(4):1367–1377, 2010. (see p. 66)

[116] John S Meyer, F Nomura, K Sakamoto, and A Kondo. Effect of stimulation of the brain-stem reticular formation on cerebral blood flow and

oxygen consumption. *Electroencephalography and clinical neurophysiology*, 26(2):125–132, 1969. (see p. 66)

[117] Pamela W Duncan. Stroke disability. *Physical Therapy*, 74(5):399–407, 1994. (see p. 70)

[118] Bruce Dobkin. The economic impact of stroke. *Neurology*, 45(2 Suppl 1):S6–9, 1995. (see p. 70)

[119] Vladimir Hachinski, Costantino Iadecola, Ron C Petersen, Monique M Breteler, David L Nyenhuis, Sandra E Black, William J Powers, Charles DeCarli, Jose G Merino, Raj N Kalaria, et al. National institute of neurological disorders and stroke–canadian stroke network vascular cognitive impairment harmonization standards. *Stroke*, 37(9):2220–2241, 2006. (see p. 70)

[120] JC Van Swieten, PJ Koudstaal, MC Visser, HJ Schouten, and J Van Gijn. Interobserver agreement for the assessment of handicap in stroke patients. *Stroke*, 19(5):604–607, 1988. (see p. 70)

[121] Suzanne L Dawson, Ronney B Panerai, and John F Potter. Serial changes in static and dynamic cerebral autoregulation after acute ischaemic stroke. *Cerebrovascular diseases*, 16(1):69–75, 2003. (see p. 70)

[122] Jeffrey L Saver. Time is brain—quantified. *Stroke*, 37(1):263–266, 2006. (see p. 70)

[123] Joanna M Wardlaw, Veronica Murray, Eivind Berge, Gregory del Zoppo, Peter Sandercock, Richard L Lindley, and Geoff Cohen. Recombinant tissue plasminogen activator for acute ischaemic stroke: an updated systematic review and meta-analysis. *The Lancet*, 379(9834):2364–2372, 2012. (see p. 71)

[124] Valery N Kornienko and Igor Nicolaevich Pronin. Diagnostic neuroradiology, 2009. (see p. 71)

[125] Marcel JH Aries, Jan W Elting, Jacques De Keyser, Berry PH Kremer, and Patrick CAJ Vroomen. Cerebral autoregulation in stroke a review of transcranial doppler studies. *Stroke*, 41(11):2697–2704, 2010. (see pp. 71 and 92)

[126] Stefan Schwarz, Dimitrios Georgiadis, Alfred Aschoff, and Stefan Schwab. Effects of body position on intracranial pressure and cerebral perfusion in patients with large hemispheric stroke. *Stroke*, 33(2):497–501, 2002. (see pp. 71 and 92)

[127] Anne W Wojner-Alexander, Zsolt Garami, Oleg Y Chernyshev, and Andrei V Alexandrov. Heads down flat positioning improves blood flow velocity in acute ischemic stroke. *Neurology*, 64(8):1354–1357, 2005. (see pp. 71 and 92)

[128] José C Pinheiro and Douglas M Bates. *Mixed-effects models in S and S-PLUS*. Springer, 2000. (see pp. 77 and 101)

[129] R De Haan, J Horn, MMDP Limburg, JMDP Van Der Meulen, and P Bossuyt. A comparison of five stroke scales with measures of disability, handicap, and quality of life. *Stroke*, 24(8):1178–1181, 1993. (see p. 86)

[130] Terry Young, Mari Palta, Jerome Dempsey, James Skatrud, Steven Weber, and Safwan Badr. The occurrence of sleep-disordered breathing among middle-aged adults. *New England Journal of Medicine*, 328(17):1230–1235, 1993. (see p. 89)

[131] Terry Young, Paul E Peppard, and Daniel J Gottlieb. Epidemiology of obstructive sleep apnea: a population health perspective. *American journal of respiratory and critical care medicine*, 165(9):1217–1239, 2002. (see p. 89)

[132] Nayef AlGhanim, Vikram R Comondore, John Fleetham, Carlo A Marra, and Najib T Ayas. The economic impact of obstructive sleep apnea. *Lung*, 186(1):7–12, 2008. (see p. 89)

[133] Amy Atkeson, Susie Yim Yeh, Atul Malhotra, and Sanja Jelic. Endothelial function in obstructive sleep apnea. *Progress in cardiovascular diseases*, 51(5):351–362, 2009. (see p. 90)

[134] Rohit Budhiraja, Sairam Parthasarathy, and Stuart F Quan. Endothelial dysfunction in obstructive sleep apnea. *Journal of clinical sleep medicine: JCSM: official publication of the American Academy of Sleep Medicine*, 3(4):409, 2007. (see p. 90)

[135] Silke Ryan, Cormac T Taylor, and Walter T McNicholas. Selective activation of inflammatory pathways by intermittent hypoxia in obstructive sleep apnea syndrome. *Circulation*, 112(17):2660–2667, 2005. (see p. 90)

[136] Markku Partinen and C Guilleminault. Daytime sleepiness and vascular morbidity at seven-year follow-up in obstructive sleep apnea patients. *CHEST Journal*, 97(1):27–32, 1990. (see p. 90)

[137] Susan Redline, Gayane Yenokyan, Daniel J Gottlieb, Eyal Shahar, George T O'Connor, Helaine E Resnick, Marie Diener-West, Mark H Sanders, Philip A Wolf, Estella M Geraghty, et al. Obstructive sleep apnea–hypopnea and incident stroke: the sleep heart health study. *American journal of respiratory and critical care medicine*, 182(2):269–277, 2010. (see p. 90)

[138] F Javier Nieto, Terry B Young, Bonnie K Lind, Eyal Shahar, Jonathan M Samet, Susan Redline, Ralph B D'Agostino, Anne B Newman, Michael D Lebowitz, Thomas G Pickering, et al. Association of sleep-disordered breathing, sleep apnea, and hypertension in a large community-based study. *JAMA: the journal of the American Medical Association*, 283(14):1829–1836, 2000. (see p. 90)

[139] Jose M Marin, Santiago J Carrizo, Eugenio Vicente, and Alvar GN Agusti. Long-term cardiovascular outcomes in men with obstructive sleep apnoea-hypopnoea with or without treatment with continuous positive airway

pressure: an observational study. *The Lancet*, 365(9464):1046–1053, 2005. (see p. 90)

[140] JF Garvey, CT Taylor, and WT McNicholas. Cardiovascular disease in obstructive sleep apnoea syndrome: the role of intermittent hypoxia and inflammation. *European Respiratory Journal*, 33(5):1195–1205, 2009. (see p. 90)

[141] SS Derderian, RH Bridenbaugh, and KR Rajagopal. Neuropsychologic symptoms in obstructive sleep apnea improve after treatment with nasal continuous positive airway pressure. *CHEST Journal*, 94(5):1023–1027, 1988. (see p. 90)

[142] Murray W Johns et al. A new method for measuring daytime sleepiness: the epworth sleepiness scale. *sleep*, 14(6):540–545, 1991. (see p. 91)

[143] Patricia Lloberes, Joaquín Durán-Cantolla, Miguel Ángel Martínez-García, José María Marín, Antoni Ferrer, Jaime Corral, Juan Fernando Masa, Olga Parra, Mari Luz Alonso-Álvarez, and Joaquín Terán-Santos. Diagnosis and treatment of sleep apnea-hypopnea syndrome. *Archivos de Bronconeumología ((English Edition))*, 47(3):143–156, 2011. (see pp. 91 and 122)

[144] Hans W Duchna, Christian Guilleminault, Riccardo A Stoohs, John L Faul, Heitor Moreno, Brian B Hoffman, and Terence F Blaschke. Vascular reactivity in obstructive sleep apnea syndrome. *American journal of respiratory and critical care medicine*, 161(1):187–191, 2000. (see p. 91)

[145] Sebastian F Ameriso, John G Mohler, Manuel Suarez, and Mark Fisher. Morning reduction of cerebral vasomotor reactivity. *Neurology*, 44(10):1907–1907, 1994. (see p. 91)

[146] Marcel J Aries, Jan Willem Elting, Roy Stewart, Jacques De Keyser, Berry Kremer, and Patrick Vroomen. Cerebral blood flow velocity changes during upright positioning in bed after acute stroke: an observational study. *BMJ open*, 3(8), 2013. (see p. 92)

[147] Frank M Faraci and Donald D Heistad. Regulation of the cerebral circulation: role of endothelium and potassium channels. *Physiological Reviews*, 78(1):53–97, 1998. (see p. 122)

[148] Sanja Jelic, Margherita Padeletti, Steven M Kawut, Christopher Higgins, Stephen M Canfield, Duygu Onat, Paolo C Colombo, Robert C Basner, Phillip Factor, and Thierry H LeJemtel. Inflammation, oxidative stress, and repair capacity of the vascular endothelium in obstructive sleep apnea. *Circulation*, 117(17):2270–2278, 2008. (see p. 122)

[149] Masahiko Kato, Philip Roberts-Thomson, Bradley G Phillips, William G Haynes, Mikolaj Winnicki, Valentina Accurso, and Virend K Somers. Impairment of endothelium-dependent vasodilation of resistance vessels in patients with obstructive sleep apnea. *Circulation*, 102(21):2607–2610, 2000. (see p. 122)

[150] Virginia A Imadojemu, Zubina Mawji, Allen Kunselman, Kristen S Gray, Cynthia S Hogeman, and Urs A Leuenberger. Sympathetic chemoreflex

responses in obstructive sleep apnea and effects of continuous positive airway pressure therapy. *CHEST Journal*, 131(5):1406–1413, 2007. (see p. 122)

[151] JT Carlson, Jan Hedner, Mikael Elam, H Ejnell, JBGW Sellgren, and BG Wallin. Augmented resting sympathetic activity in awake patients with obstructive sleep apnea. *CHEST Journal*, 103(6):1763–1768, 1993. (see p. 122)

[152] Virend K Somers, Mark E Dyken, Mary P Clary, and Francois M Abboud. Sympathetic neural mechanisms in obstructive sleep apnea. *Journal of Clinical Investigation*, 96(4):1897, 1995. (see p. 122)

[153] Frank M Faraci. Oxidative stress the curse that underlies cerebral vascular dysfunction? *Stroke*, 36(2):186–188, 2005. (see p. 122)

[154] Jose-Luis Garcia-Roldan and John A Bevan. Flow-induced constriction and dilation of cerebral resistance arteries. *Circulation research*, 66(5):1445–1448, 1990. (see p. 122)

[155] Harm J Knot and Mark T Nelson. Regulation of arterial diameter and wall [ca2+] in cerebral arteries of rat by membrane potential and intravascular pressure. *The Journal of Physiology*, 508(1):199–209, 1998. (see p. 122)

[156] Gerrit J Bouma, J Paul Muizelaar, Kuniaki Bandoh, and Anthony Marmarou. Blood pressure and intracranial pressure-volume dynamics in severe

head injury: relationship with cerebral blood flow. *Journal of neurosurgery*, 77(1):15–19, 1992. (see p. 123)

[157] E Bernd Ringelstein, Carsten Sievers, Sara Ecker, Peter A Schneider, and Shirley M Otis. Noninvasive assessment of co2-induced cerebral vasomotor response in normal individuals and patients with internal carotid artery occlusions. *Stroke*, 19(8):963–969, 1988. (see p. 123)

[158] Fabio Placidi, Marina Diomedi, LETIZIA CUPINI, Giorgio Bernardi, and Mauro Silvestrini. Impairment of daytime cerebrovascular reactivity in patients with obstructive sleep apnoea syndrome. *Journal of sleep research*, 7(4):288–292, 1998. (see p. 124)

[159] David S Celermajer, Keld E Sorensen, Catherine Bull, Jacqui Robinson, and John E Deanfield. Endothelium-dependent dilation in the systemic arteries of asymptomatic subjects relates to coronary risk factors and their interaction. *Journal of the American College of Cardiology*, 24(6):1468–1474, 1994. (see p. 125)

[160] Sissel Vorstrup, Leif Henriksen, and Olaf B Paulson. Effect of acetazolamide on cerebral blood flow and cerebral metabolic rate for oxygen. *Journal of Clinical Investigation*, 74(5):1634, 1984. (see p. 125)

[161] Hideo Saito, Kuniaki Ogasawara, Taro Suzuki, Hiroki Kuroda, Masakazu Kobayashi, Kenji Yoshida, Yoshitaka Kubo, and Akira Ogawa. Adverse effects of intravenous acetazolamide administration for evaluation of cerebrovascular reactivity using brain perfusion single-photon emission com-

puted tomography in patients with major cerebral artery steno-occlusive diseases. *Neurologia medico-chirurgica*, 51(7):479–483, 2011. (see p. 125)